THE EFFECTS OF DESIGN AND ENVIRONMENTAL FACTORS ON THE RELIABILITY OF ELECTRONIC PRODUCTS

Wayne Lawson

B.Eng.(Hon)., M.Sc., C.Eng.

Ph.D. Thesis 2007

The Effects of Design and Environmental Factors on the Reliability of Electronic Products

Wayne LAWSON

B.Eng., M.Sc., C.Eng.

Materials Research Institute (MRI)
School of Computing, Science and Engineering
University of Salford, Salford, UK

Submitted in Partial Fulfilment of the Requirements of the Degree of Doctor of Philosophy, December 2007

TABLE OF CONTENT

ACKNOWLEDGEMENTS

This research could never have been completed if it had not been for the support of my family, especially for Catherine's compassion and patience in light of our recent addition, Amelia.

I am indebted to my project supervisor, Dr Richard Pilkington, who provided vital support and help through his encouragement and compassion.

I would like to give my sincere thanks to Delphi for funding this PhD and the support over my years of study. I would especially like to thank John McColl, who now has left Delphi, for providing the opportunity to pursuit this line of study. Not forgetting, Bob Schofield and Ian Gaskell for continuing this support. Even more so to Bob for his steady guidance and the use of his red pens!

I would also like to give a heartfelt thank you to the following people for their support on various aspects of my studies: Professor Ndy Ekere (Greenwich University), Jay Smith (help in alchemy, chemistry and electronics: University of Salford), Keith Jordan and Ann Rushton (For their expertise and use of the SEM/EDX: Delphi), Mike Riley (for his support in Industrial Statistics: Delphi) and Steve Graham (for the acquisition of test combs: Delphi).

ABSTRACT

The reliability of electronic products is fast becoming of major importance with the demand for increased safety, especially in the automotive industry. Tracks, pads and vias on printed circuit boards can suffer a variety of problems if circuits are contaminated with electrical-conducting substances.

Electrochemical migration, especially dendrite growth, has long been a concern in safety critical and durable systems, and current preventative methods tend to focus on various styles of printed circuit board protective coatings. These measures have a number of disadvantages, mainly process and material costs with extreme scepticism on their overall efficacy. Any design related developments that can minimise the impact of dendrite growth on reliability can lead to a more economic, durable and safer product.

The work in this thesis provides a thorough literature search of the field of electrochemical migration on printed circuit boards. This study then develops a novel circuit-design-orientated model, based on a multilevel full-factorial design, to study the effects of temperature, voltage and electrode gap on dendritic growth under saturated conditions. Preparation of several DC-biased copper-comb patterned printed circuit boards placed in temperature-controlled water-filled cuvettes enables the specific monitoring of dendrite activity, and detects a sharp current increase that accompanies a dendritic short circuit condition.

A high R^2 polynomial correlation-model is derived and it is noted that increased voltage and temperature and reduced track spacing increases the impact of dendritic growth on reliability. At voltages between 3 and 4V, gas bubble formation at the electrodes has the effect of increasing reliability by destroying the dendrite fuses. It is shown that dendrites may not grow below 1.25V, which coincides with the theoretical onset voltage for the decomposition of water. It was also demonstrated that electrically biased, water-contaminated printed circuit boards form extreme acid and alkaline regions close to the anode and cathode terminations, respectively, which can cause corrosion.

The thesis proposes a novel approach, termed ‘design contingency’, for preventing dendritic growth through design optimisation.

GLOSSARY

Adsorption:	The take-up of a substance at the surface of another material
Anode and cathode:	Anode and cathode are the positive and negative polarities of an electrochemical system, respectively.
CAF:	Conductive Anodic Filaments are electrochemical growths between the laminates of printed circuit boards, which are usually formed from copper.
Copper-clad:	Printed circuit board before the etching process. This is usually thin copper bonded to a fibre glass substrate.
Corrosion:	The decomposition of a metal due to the exchange of electron and the formation of ionic species usually in an aqueous solution.
Dendrite:	Electrochemical growths with a fractal-like structure
Dendrite fusing:	The point when a dendrite shorts between two electrically biased electrodes causing a reduction in resistance.
Double-layer capacitance:	A capacitance created by the charge of molecules between metal-liquid interfaces below the overvoltage potential.
EDX:	Energy-dispersive X-ray spectroscopy, used to analyse the atomic composition of a material.
Factors:	A parameter under consideration that can influence the response variable
Field Life:	The expected working operation of an electronic system

Flux:	A liquid substance use to clean metallic surface before a solder wets
Halide:	The ionised form of halogens
Halogens :	A series of non-metal elements from the periodic table, comprising fluorine, chlorine, bromine, iodine, and astatine.
Hydroscopic :	A material's ability to absorb moisture from the atmosphere
Hydroxide:	The ion form of OH
Interaction:	Two or more variables that interact with each other and hence the response
Migration:	The movement of ions through an electrolyte
Nernst diffusion-layer:	A linear diffusion region adjacent to an electrode where the species concentration remains stagnant and is unchanged by time when electrolysis occurs.
Noble metal:	Metal that is more resistant to corrosion or oxidation.
Overvoltage:	The additional potential added to the theoretical activation energy required for electrolysis to occur.
Pad:	The metallic area of a printed circuit board where electronic component leads are soldered
PCB:	Printed Circuit Board
Point source:	A nucleation point that can experience high current concentrations.

Pourbaix Diagram:	A diagram used to plot electrochemical reaction relative to potential and pH, named after it creator Marcel Pourbaix (1904-1998), also known as Potential-pH diagram.
p-value:	The probability of the event happening.
Redox:	Reduction and Oxidation
Reflow soldering:	A method of forming a solder joint between component and circuit board by heating solder paste to its alloy liquidus temperature
Regression:	A method of determining the next response from historical data.
RH	Relative Humidity (scale 0-100%)
RMA	Flux activation level. Rosin Mildly Activated.
Rosin:	A natural product from the sap of pine trees and the main ingredient in solder fluxes.
R-square:	The difference between the observed data and the model. A high percentage value indicates that the model closely represents the observed data.
SEM:	Scanning Electron Microscope used for producing high-resolution images
SHE	Standard Hydrogen Electrode
SIR:	Surface Insulation Resistance
Via:	A connection between layers on a printed circuit board (also known as PTH - plated through holes)

LIST OF FIGURES

LIST OF TABLES

Chapter One: Introduction

Satellite failures are rare and very costly when they occur, with interconnection failures accounting for over 15% of satellite malfunctions[1]. In May 1998 a Boeing 601 telecommunications satellite, Galaxy 4, failed with drastic results[2]. The failure, which disabled telephone networks across the United States, was unexplained for many years although the failure mechanism was later believed to be the formation of tin growths.

The earliest account of metal migration was a report on a telephone-switchboard by Kohman in 1955[3] who found an electrical field and water were needed for migration to occur through an electrochemical process.

Reliability of electronics is of paramount importance and failures can cause serious, if not disastrous, consequences. In the manufacture of electronic goods the drive towards longer field life and increased reliability is an ongoing trend, driven by a demand for improved reliability, durability and safety.

In the manufacture and assembly of printed circuit boards (PCB), residues produced by the process can be deposited on a PCB. When PCBs are energised by electronic signals, these residues can produce parasitic growths, potentially causing short circuits and the failure of the PCB. The occurrences of electrochemical migration failure modes, such as dendrites and conductive anodic filaments (CAF), are problems which can bring catastrophic failure and lead to the malfunction of mission critical systems[4].

1.1 Electrochemical Degradation of Printed Circuit Boards

The conductive lands on a printed circuit board can suffer a variety of problems if metallic surfaces are contaminated with electrically-conductive substances. When contamination is combined with moisture it can result in the lowering of resistance between the tracks and pads and lead to the galvanic corrosion of metals. It can also lead to the formation of dendrites and/or CAFs between the conductors.

Electronic equipment used under very dry conditions may not have such problems, unless there are large temperature fluctuations that result in dew condensation occurring on the surface of the circuitry or if the contaminants are hygroscopic and adsorb enough moisture to provide a liquid film on the surface. With high relative humidity conditions, a thin layer of moisture can occur on the surface which may be sufficient to decrease surface insulation resistance, cause corrosion or form metallic dendrites. Higher humidity can cause a thicker moisture layer and a faster corrosion or dendrite growth can then take place[5].

The problem of electrochemical degradation in electronic systems has long been recognized. The first dendritic failure was reported in 1955[3, 6], with further publications later[7-10]. CAF failure modes were first reported by Bell Laboratories in 1976[11].

More recently there has been an increase in reliability concerns arising from electrochemical degradation for three main reasons:

- Increased use of electronics in safety critical applications in harsh environments, such as in automotive, aviation and medical fields.
- Integration and the trend towards smaller multi-layer printed circuit board geometries.
- Increased use of lower operating currents and voltages (dendrite bridges will often self-heal if the current is large enough to blow the short).

1.2 Electrochemical Migration (ECM)

Electrochemical migration can be defined as the movement of metal or metal-salt ions under the influence of a voltage bias. This can occur on the surface of a printed circuit board or through the bulk of the printed circuit board fibre glass[12]. The growths occur through electrolysis of an aqueous solution containing metal ions dissolved from the complementary metal conductor i.e. tracks, pad or via. This can occur on the surface of a printed circuit board, potentially resulting in dendrites, or through the bulk of the printed circuit board fibre glass, potentially resulting in CAFs[12].

There are two distinct electrochemical migration failure phenomena that can occur on printed circuit boards. The first form is conductive anodic filament (CAF) formations. CAF failures in printed circuit boards occur under conditions of high humidity and high voltage gradients, with the filament composed of copper salts that grow from the anode towards the cathode along the fibres of the epoxy/glass interface. As CAFs are formed within the fibres it is not possible to see the failures on the surface of the substrate, as in the case of a dendrite, and substrate sectioning and polishing is required to expose the growth. An example section of a CAF is shown in Figure 1. Note the black CAFs spikes from the positive terminal, anode, emanating towards the ground plane, cathode.

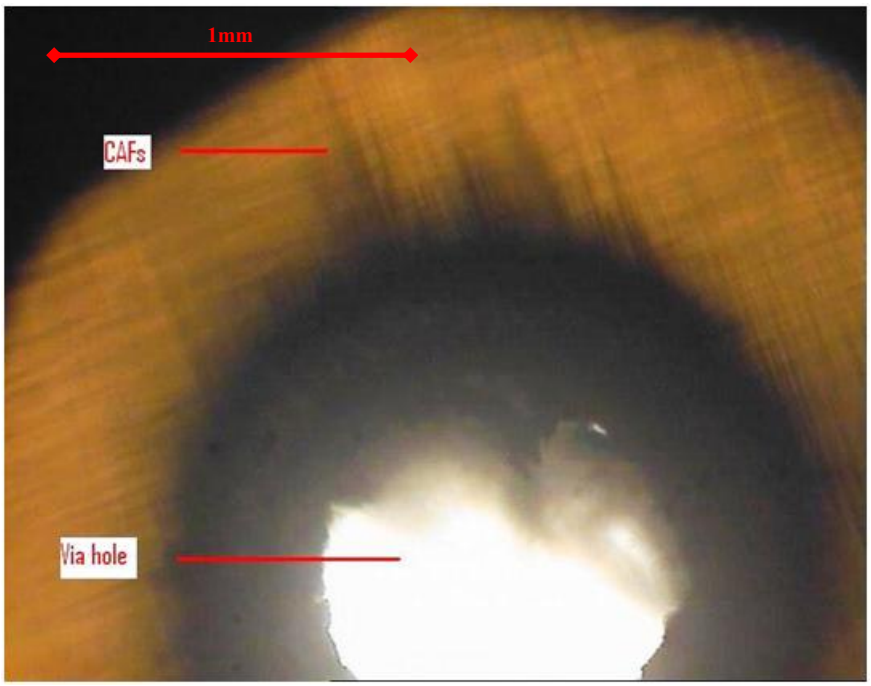

Figure 1 – Cross-section of a PCB Via Showing Evidence of CAF

The second form of electrochemical migration failures and the focus of this thesis are surface dendrites. Dendrites can grow from the cathode to the anode under an applied voltage bias when aqueous contamination is present. These dendrites are fractal in shape, as in Figure 2, and can bridge the conductors (cathode-anode).

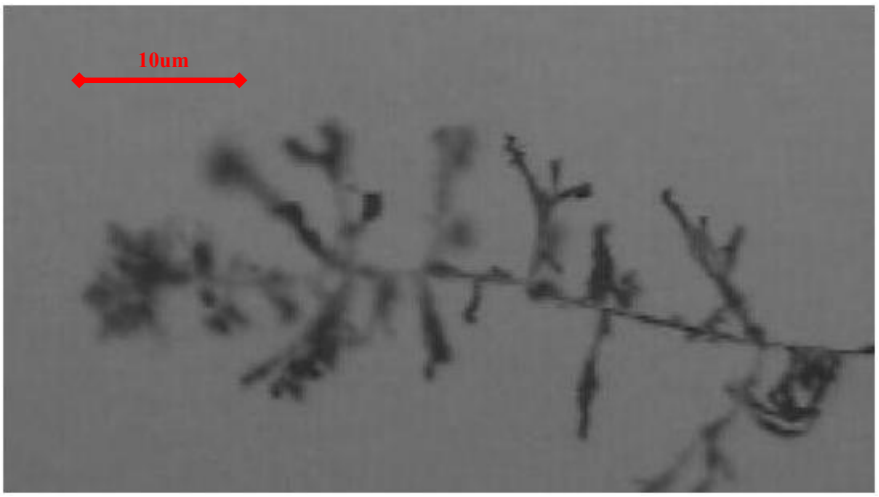

Figure 2 – Example of a Dendrite

In the presence of low currents (μA) dendrite shorts can be maintained. However, if the currents are sufficiently high they can blow, similar to a fuse. Dendrites differ from CAFs for a number of reasons as follows[13]:

- Dendrite growth usually occurs on the surface of a substrate/contact and not internally as in CAF growth.
- A dendrite can be formed from various metals such as copper, lead or tin, whereas in CAF growth, the migrating metal is usually copper.
- The direction of a dendrite's filament growth is from the cathode to anode and not from the anode to the cathode as observed in CAF growth.
- The composition of a dendrite filament is understood to be neutral metal and not a metallic salt as found in CAF growth.

A full description of these aspects is given in Chapter 2.

1.3 Aims and Objectives

To better understand the problem contacts were established with Delphi Automotive Systems, The Test Lab (USA), National Physics Laboratories (NPL - UK) and Heraeus Circuit Materials (USA).

From discussions with these links, the broad aims and objectives of this research were established. The sponsoring company, Delphi Electronics Systems, has a particular interest in the following areas:

- Operating temperatures for automotive electronic engine controllers are extreme from -40ºC to 125ºC. However, whilst most of the validation for controllers operate at either end of these extremes the mechanisms of failures such as dendrites at normal ambient temperatures (5-50ºC) is assumed to be similar. Gaining an understanding of the operating parameters of typical failure mechanisms, such as dendrites, would benefit overall automotive electronic controller reliability.
- Further understanding of dendrite growth relative to the design parameters required to minimise or even eliminate their formation.
- Designing and developing a system to conduct analysis of typical ionic and dendritic formations on PCBs, whilst eliminating external factors that hinder experiments of parametric identification.
- Understanding mechanisms of dendritic growth under DC and AC conditions.

Based on these requirements this research project investigates factors that enhance dendrite formation between printed circuit board (PCB) tracks. The main parameters studied are (1) conductor track spacing, (2) temperature, (3) operating voltage and (4) effect of pH.

The purpose of this project is to further the understanding of electrochemical migrations on printed circuit boards, especially dendrite growth, to prevent field failures. And to then develop a model and subsequently new design guidelines for improving the reliability of electronic automotive products.

The motivation for this research is to determine improved methods for assessing printed circuit board (PCB) reliability of current surface insulation resistance (SIR) failures.

The author bases part of this study on his M.Sc – 'Investigation into a modified area-of-spread method to monitor the effect of oxygen levels in a reflow oven'[14, 15] and, to a degree, on his B.Eng project 'The effects of hydrogen/nitrogen mixtures on Soldering in Electronics of copper and tin/lead surfaces for PCB assemblies'[16].

In some fields, such as AC formation, there is very little literature. In these cases, additional experimentation has been conducted to remove gaps in the background information, allowing continuity and a more complete description of the current area.

1.4 Thesis Outline

This thesis is divided into seven Chapters and three appendices. ***Chapter 1*** covers the project background and the problem description. It also reviews the research objectives and gives an overview of the thesis. ***Chapter 2*** presents the background and literature review on electrochemical failures. The first part of this Chapter outlines materials used in the electronics industry and then develops an understanding of electrochemical migration before moving on to mechanisms associated with electrochemical failures. ***Chapter 3*** explains the methods and equipment used for the experiment outlined in Chapters 4 and 5. ***Chapter 4*** presents the initial work on dendrite growth that forms the basic understanding for experimental methods used in Chapter 5. ***Chapter 5*** is devoted to understanding the parameters that augment the growth of dendrites, which aids the development of a factorial design used in Chapter 6. ***Chapter 6*** presents a multilevel factorial experiment as the basis for modelling three main parameter, temperature, voltage and track spacing. ***Chapter 7***, the final Chapter presents the conclusion of the thesis and proposes areas for further investigation.

Appendix 1 contains three publications as a result of this work. Appendix 1a is a copy of a paper on the work conducted in Chapter 6 and accepted for publication in Microelectronics International in May 2007. Appendix 1b is a white paper, requested by Delphi, published internally to help employees understand the differences between Dendrites and CAF. Appendix 1c presents a poster proposed at an early material conference, April 2006, which identifies dendrite fusing and suggests AC as an alternative for surface insulation resistance testing.

Chapter Two: Background and Literature Review

Much work has been conducted on the reliability impact of metallic and slat deposits formed by an electrochemical process when a printed circuit board is contaminated with an aqueous solution[3, 17-23]. The earliest citation on electrochemical migration on printed circuit boards was published by Bell Systems[7], with most of the relevant subsequent publications, up to 1977, focussing on silver migration[7-9, 24].

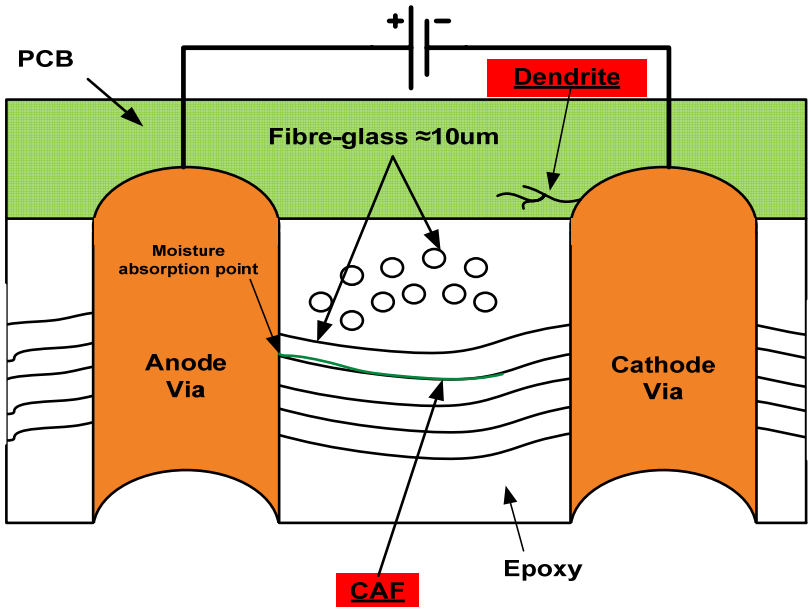

Figure 3 – Two Types of Electrochemical Migration
Dendrites and CAF

Electrochemical migration in the field of printed circuit board reliability can be classified as either dendrite or conductive anodic filament (CAF) depending on the shape of the deposits and the conditions leading to the occurrence, as in Figure 3. The term dendrite refers to the tree-like shape formed on the surface of the PCB insulation and emanating from the cathode. The term CAF refers to metal-salt deposits in the shape of elongated fibres deposited along the glass fibres of the interior of the printed circuit board insulation panel emanating from the anode. Figure 4 shows the established formation of a dendrite between two components leads created in a laboratory.

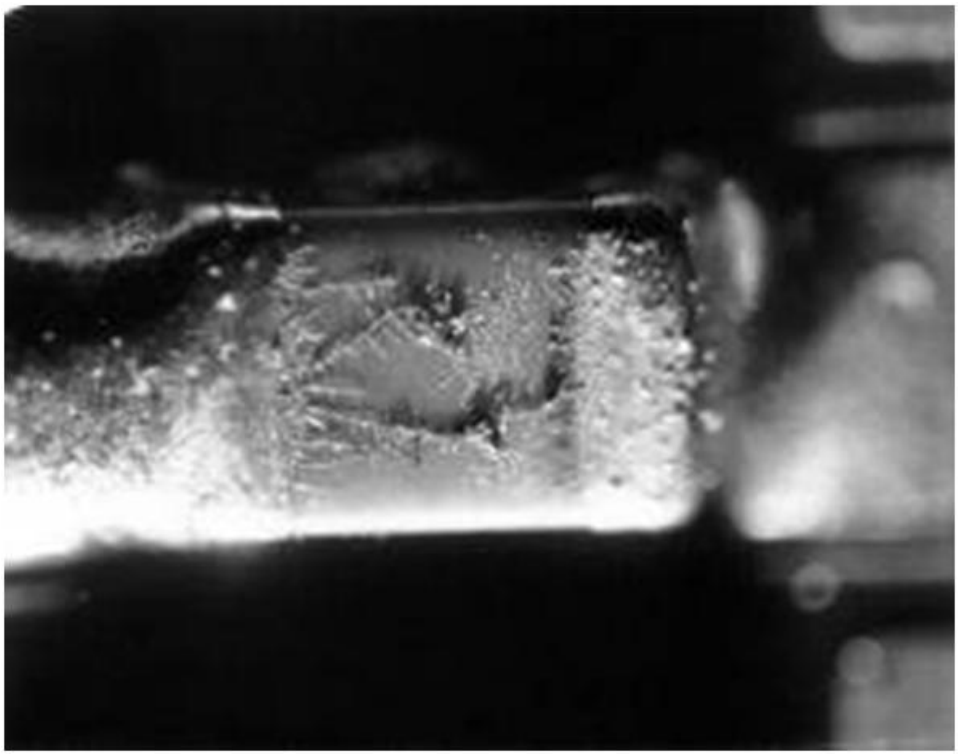

Figure 4 – Formations of tin/lead Dendrites on a SMD Capacitor (Delphi, 2005)

Figure 5 show the growth of a dendrite between two copper tracks.

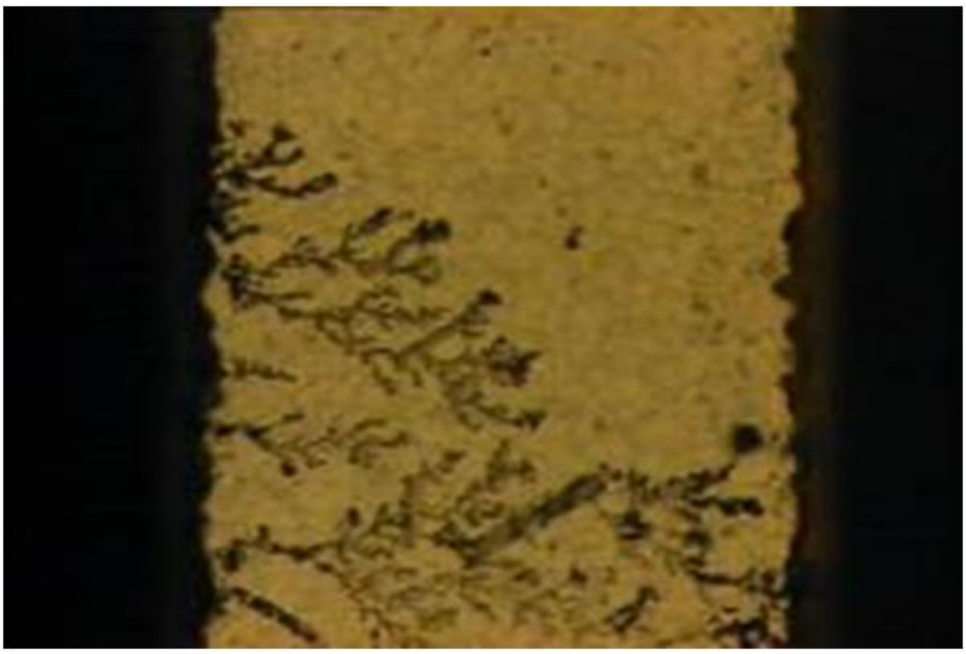

Figure 5 – Example of a Dendrite between Two Copper Tracks

To understand the nature of the electrochemical failure mode of electronic products it is important to review the construction of printed circuit boards, the metals used in the industry, flux and its removal, and electrochemistry.

2.1 Materials Used in the Electronics Industry

2.1.1 Printed Circuit Boards

Printed circuit boards (PCB) or printed wiring boards (PWB) were commercially introduced after World War II, usually credited to Paul Eisler[25, 26], and were primarily used for airborne instruments and for telecommunications. However, the substantial production of printed circuit boards did not start until the 1950s. Since its introduction, the printed circuit board has been used in most applications from communication satellites to the humble transistor radio.

The printed circuit board is constructed of conductors, also called tracks, consisting of copper strips adhered to an insulating substrate. There are four major printed circuit board constructs:

1) Single-sided boards: The copper is only present on one side of the insulating material.
2) Double-sided boards: The copper is present on both side of the insulating material and connections between the two sides are usually made by plated tin-lead alloy, commonly known as plated through hole (PTH) or vias.
3) Multilayer boards: The copper is present on both sides of the insulating material with additional conductor layers inside the boards. Typical constructs are of four, six and eight layers, with the outer layer (top and bottom) used for power i.e. ground and other voltage levels. Figure 6 shows a cross-section of an eight-layer board with a component lead soldered at both ends of the board to a through-hole via.
4) Flexible circuit: These circuits use any of the above configurations although normally using a flexible insulating material. These are typically used in digital cameras or application where greater density is required.

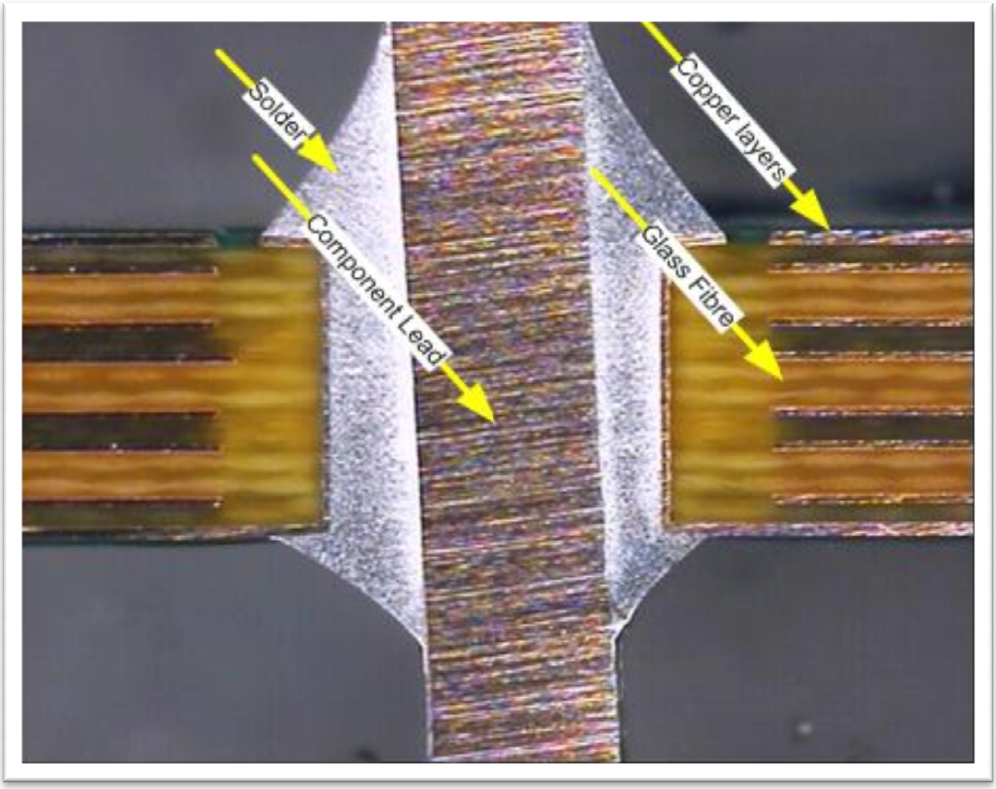

Figure 6 – Cross-section of a Multilayer Board

The two outer sides (top and bottom) of the printed circuit board are typically known as the solder side and component side. Using surface mounted components the solder side and component side exist on both sides i.e. components and soldering can be placed on a single surface.

The printed circuit board patterns are usually formed by a selective etching process of removing unwanted copper from a copper-clad substrate, with copper thickness typically 35µm and 70µm[26]. Common chemicals used for copper etching are ferric chloride, ammonium persulphate, sodium persulphate and acid cupric chloride.

The insulating material is indicated by the NEMA (National Electrical Manufacturers Association) grade. Commonly used substrates are[26]:

- FR-2, FR3 – phenolic paper laminate, used mostly for single sided PCBs.
- FR-4, FR-5, G-10, G-11 – epoxy glass fibre reinforced laminate, used mostly for double-sided and multilayer boards.

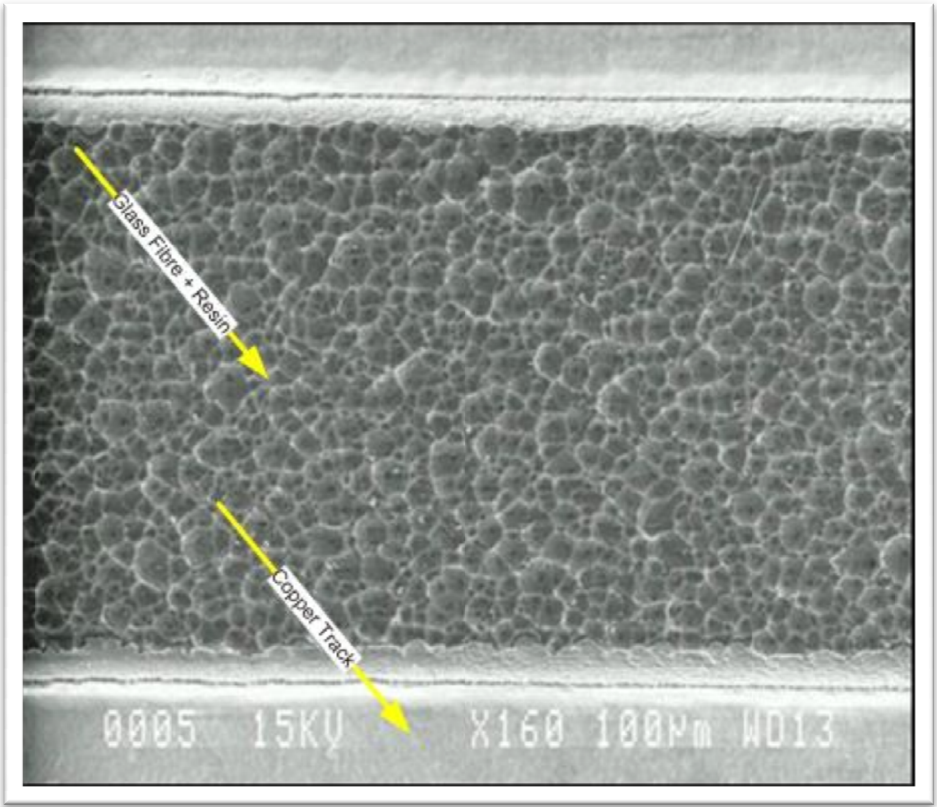

Figure 7 – SEM of FR4 substrate

Most of these substrates contain additional compounds, namely bromide, to act as a flame-retardant. Whilst halide ions can act as catalysts in localised corrosion[27] reports on the impact of bromide on printed circuit boards demonstrate that it has virtually no effect on migration potential on FR-4 circuit boards[28, 29]. Figure 7 shows a SEM of the FR4 substrate used in the experiments for this thesis; typical of substrate used in automotive assemblies. Figure 8 shows an EDX of the FR4 image, in Figure 7, demonstrating the bromine peaks.

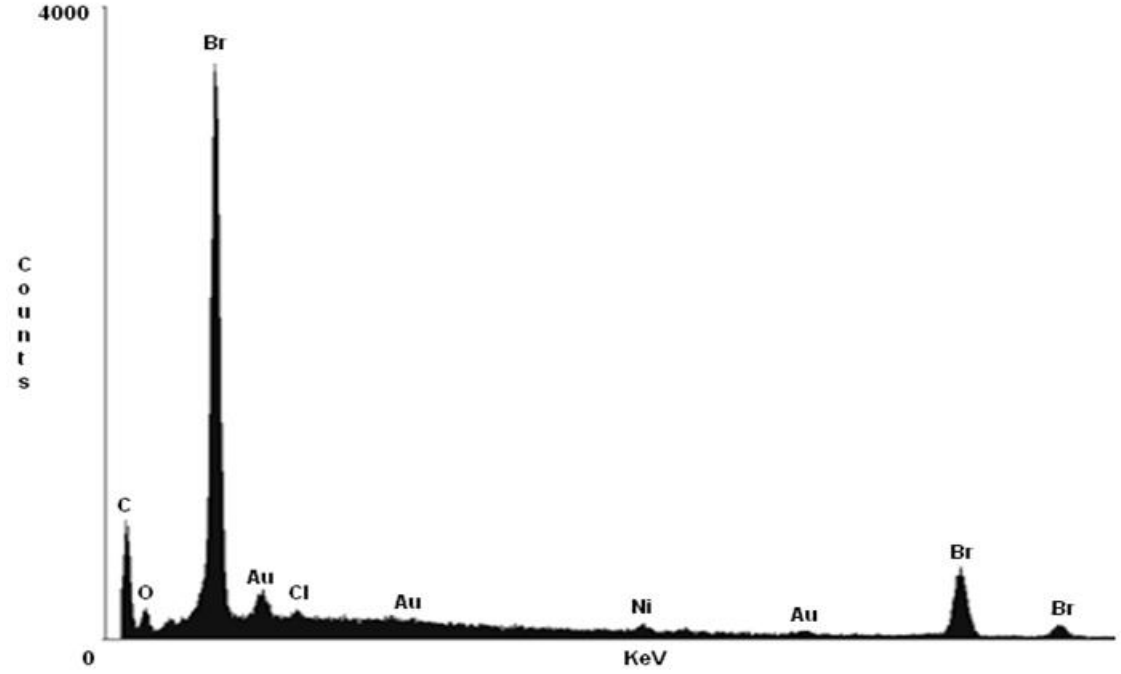

Figure 8 – EDX of FR4 Image

2.1.2 Metals

From the electronics manufacturing point of view, the most important metals for interconnection systems include at least three elements; copper, tin and nickel. Copper is the main metal used for printed circuit board tracks and therefore constitutes the main base interconnect material. Tin, copper, nickel or nickel-based alloys with protective coatings such as gold are used for other contact metallization. Electrochemical migration failures experienced in electronic products usually involves the copper or tin parts of the printed circuit board in the form of dendrites, CAFs or even current leakages. Although it is noted[13, 30] that the formation of CAFs only occurs with copper.

Copper is also used for high grade and high density interconnects on integrated circuits, replacing the nickel/iron alloy lead-frames and aluminium wirebonds. The reason for changing to copper is due to its superior thermal conductivity, coefficient of thermal expansion (CTE) and electrical conductivity[31]. However, there has been a reported disadvantage[32] in using copper for die wirebonds due to a greater electrochemical migration susceptibility than its aluminium predecessor.

Under relatively high humidity, electronic components with metal content respond to applied voltages by electrochemical migration of metal ions and the formation of a filament that can lead to short-circuit failure, termed electrochemical migration (ECM) [30, 32-35]. A metal which, in the presence of moisture, can form ions with reasonable mobility under electrical potential can exhibit electrochemical migration[36]. The transfer occurs between the electrodes of devices when exposed to both moisture and an electric field. An example is dew condensation adhering between two electrodes.

2.1.3 Flux

Component leads, terminations and pads are normally covered in a layer of oxide before they are soldered, and therefore a flux is required. The chemical function of flux is to remove oxide films from the surface and to protect the clean surface from re-oxidising. There are two main types of flux used in electronic manufacturing; water soluble fluxes that require removal after the reflow process and no-clean flux that can be left on the printed circuit board with no, or very little, impact on reliability, with both types containing tree rosins.

The flux in a typical solder paste contains up to 60% by weight of rosin, 7-10% thickeners, 5-10% viscosity agents and up to 2% actuators. The rest of the flux contains a variety of solvents such as alcohols (isopropyl, butyl alcohol and polyethylene glycol) to form the solution. Rosin is a natural product that is extracted from pine tree and therefore its constituents depend on where it originates. Rosin consists of several rosin acids and the typical composition is listed in Table 1.

Rosin Acid	% Composition
Levopimaric	Trace
Neoabietic	10-20
Abietic	30-40
Isodextropimaric	8
Dextropimaric	8
Dehydroabietic	5
Dihydroabietic	16
Tetra-abietic	16

Table 1 – Typical Composition of Rosin[14, 36, 37]

Hunt et al. report[38, 39] on the impact of flux on circuit board contamination where, in the presence of high humidity conditions, flux can cause a decreases in surface insulation resistance, Figure 9. Figure 9 shows three levels of contamination levels;

clean (no flux), 30µl and 100µl. The measured flux volumes were applied to a combed test pattern, similar to the one shown in Figure 35, using a pipette.

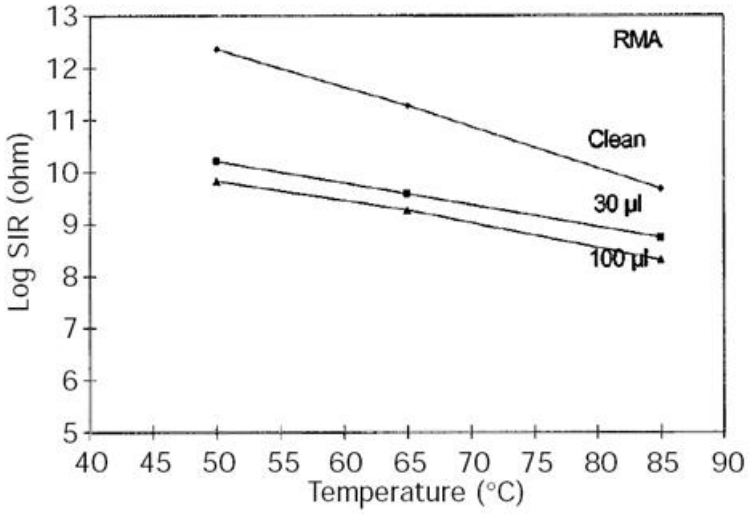

Figure 9 – Effect of Temperature on SIR at 85% RH[38]

Flux can be the source of various anions such as chlorine ions, bromine ions and other ions that originate from rosin and organic acids[40]. This increases the number of ions and hence increases the number of charge carriers, which leads to a reduction in surface resistance. For circuit reliability the presence of flux residues combined with surface water leads to a stray current, causing dendrites and leading to circuit failure.

2.1.3.1 Flux Removal

In applications requiring a high degree of reliability, such as military applications, the flux is commonly removed. The flux used for these applications is usually water soluble and is removed using saponifiers, as opposed to environmentally aggressive alternatives, such as Trichloroethane and other CFCs, the use of which is now forbidden under the 1987 Montreal Protocol[41].

In a typical surface mount process flow the flux cleaning process, shown in Figure 10 highlighted in blue, is commonly located immediately after the reflow oven, i.e. after the component leads are soldered. It is commonly believed that removing the flux using water based methods provides the safest means of cleaning[39]. However, as processes used for removing water-based flux involve the use of high pressure deionised water,

problems can occur if the cleaning processes are not strictly controlled, as water contamination may be left on the PCBs after the operation.

The use of no-clean fluxes provides a lower cost alternative to expensive water-based cleaning processes. However, whilst the commercial literature for no-clean fluxes tends to indicate that the contaminates left behind after the reflow process will not cause electromigration problems, it has been reported[42] that when water contaminates an electrically-biased PCB with no-clean residues, dendrites can still occur.

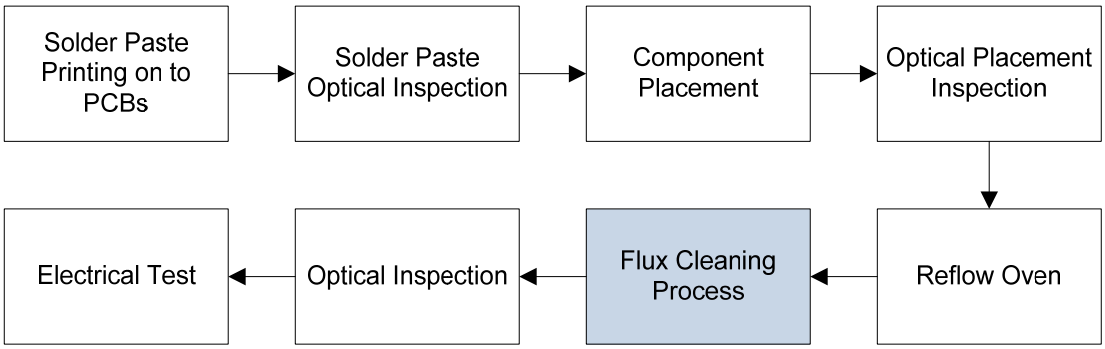

Figure 10 – A Typical Surface Mount Process Flow

2.2 Electrochemical Migration

Various failure modes can be further understood by the use of electrochemistry. Examples include migration potentially leading to dendrite growth and pH diffusion potentially leading to corrosion and CAF formation[13]. This Section focuses on the specific aspects of electrochemistry applicable to copper and water electrolyte.

When electrically-biased copper, such as a track on a printed circuit board, is exposed to water a resistive pathway is created through the water electrolyte, allowing current to flow, see Figure 11.

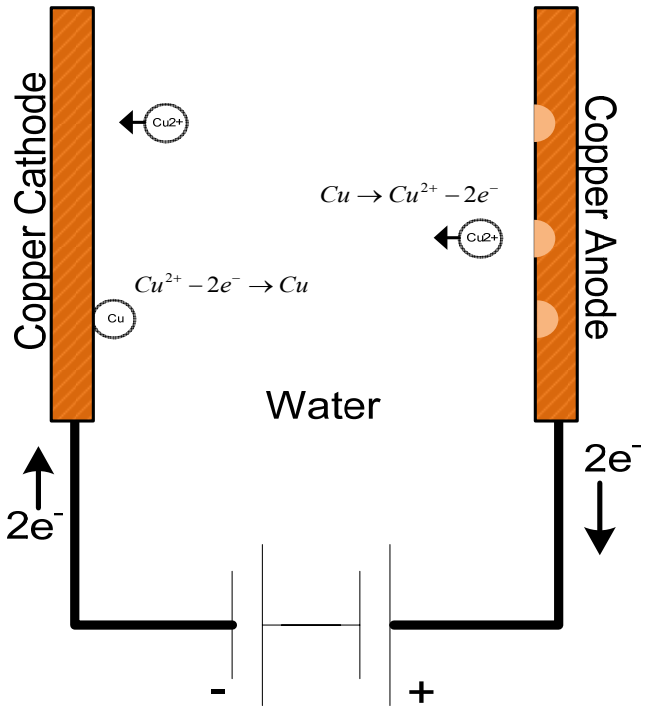

Figure 11 – Copper Migration of PCB Tracks

The mechanism at the anode and the cathode involves oxidation and reduction of the copper. There are three species of copper present in a copper-water based electrolytic system. They are neutral metal copper, cuprous ion copper(I) Cu^{1+} and cupric ion copper(II) Cu^{2+}. These evolve from two electrochemical reactions[43, 44], as in Equation 1 and Equation 2.

$$Cu^{2+} - e^- \leftrightarrow Cu^{1+} \qquad \textbf{Equation 1}$$

$$Cu^{1+} - e^- \leftrightarrow Cu \qquad \textbf{Equation 2}$$

$$Cu^{2+} - 2e^- \leftrightarrow Cu \qquad \textbf{Equation 3}$$

However, copper(I) only evolves when the copper is not biased (as in corrosion processes) or if other contaminates are present, such as chloride. As neutral copper is not a charged ion, copper deposition is produced when copper(II) migrates from the anode depositing copper onto the cathode, as shown in Equation 3[43].

2.2.1 Anode and Cathode

There is a great deal of confusion in some literature on the understanding of electrode polarity. The general perception is that the anode corresponds to the positive polarity and the cathode corresponds to the negative polarity. International convention[45, 46] calls the electrode where oxidation occurs the anode and the electrode where reduction occurs the cathode. The polarity on the electrodes depends on whether the cell converts electricity into chemical energy or *vice versa*[47, 48]. If the electrical energy is converted to chemical energy (reaction is not spontaneous), i.e. electrolysis of water to produce hydrogen and oxygen, then the anode is positive and the cathode is negative, i.e. electrons flow into the cathode. However, if chemical energy is converted to electrical energy (reaction is spontaneous), i.e. non-rechargeable battery or the phenomenon of corrosion (where no useful electrical energy is produced as it is internally converted to heat), then the anode is negative and the cathode is positive, i.e. electrons flow out of the cathode, Figure 12.

However, to reduce confusion and maintain continuity the general perception of polarity is used throughout this thesis, i.e. anode equates to positive and cathode equates to negative.

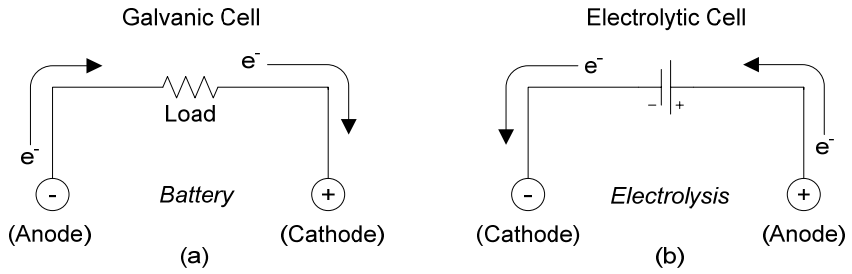

Figure 12 – International Convention of Electrode Polarity

2.2.2 Electrolysis of Water

The electrolysis of water is an electrochemical process in which water decomposes into oxygen and hydrogen caused by the flow of electrons, according to the reaction shown in Equation 4.

$$2H_2O(liquid_{electrolyte}) \rightarrow 2H_2 \uparrow (gas_{cathode}) + O_2 \uparrow (gas_{anode}) \qquad \textbf{Equation 4}$$

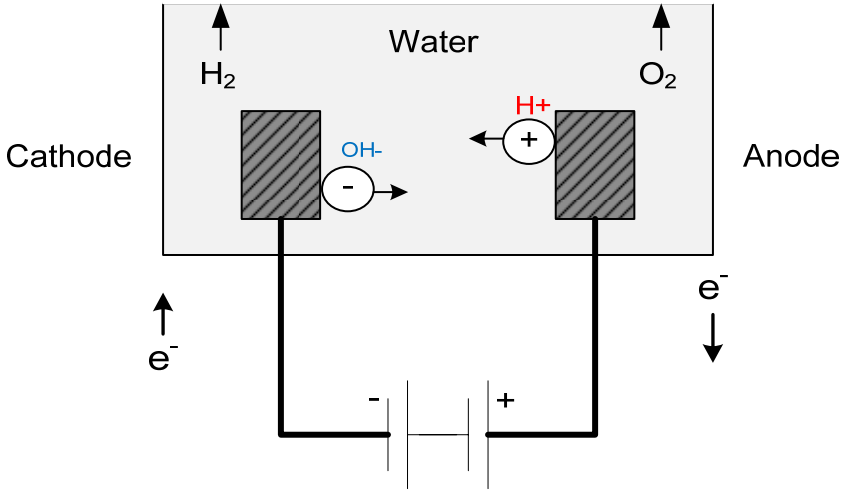

Figure 13 – A Typical Aqueous Electrochemical Cell

Figure 13 shows a typical electrolytic cell consisting of two inert electrodes, such as platinum, with a water electrolyte, which is representative of either a large volume of water or a water drop. A potential difference is applied between the electrodes, with the anode connected to the positive terminal attracting the negative ions (anions) in the electrolyte. Similarly, the cathode is connected to the negative terminal attracting the positive ions (cations). The velocity of the ions migrating from the anode is typically a function of the viscosity of the bulk fluid, the ion radius and the electric field. For this reason it can be difficult to calculate the velocity, theoretically, for an unknown contaminate without experimentation.

On the surface of the electrodes a reaction occurs that leads to the release or incorporation of electrons by the ions with the creation of a large pH gradient. At the anode water is oxidised to form oxygen gas and hydrogen ions (H+) and at the cathode water is reduced to form hydrogen gas and hydroxide ions (OH-).

Figure 14 demonstrates the large pH gradients produced at the interface of the electrodes due to the creation of the H+ and OH- ions, shown in red and blue in Equation 5 and Equation 6, respectively. At the anode the pH gradient is more acidic (pH<7) with the creation of H+ ions, while the creation of OH- at the cathode leads to a more basic pH gradient (pH >7). These pH gradients can strongly affect the corrosive properties of the metal[49]. The reaction involved for a metal exposed to moisture under a range of electric potentials and solution pH conditions are portrayed in a pH-potential (usually referred to as Pourbaix diagrams[50]), see Section 2.2.3.

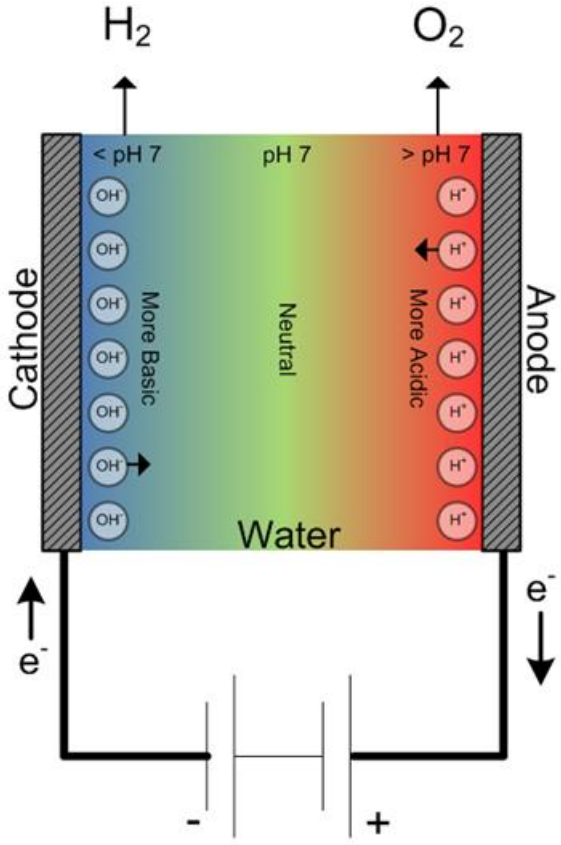

Figure 14 – Demonstration of pH Gradients at the Metal Interfaces

An electrolytic cell, shown in Figure 13, consists of a redox reaction composed from two half-reactions (anode-cathode).

$2H_2O \rightarrow O_2 \uparrow +4H^+ + 4e^-$ $E^{\theta,O_2}_{Anode} = -1.23V$ Oxidation (Anode) **Equation 5**

$2H_2O + 2e^- \rightarrow H_2 \uparrow +2OH^-$ $E^{\theta,H_2}_{Cathode} = -0.83V$ Reduction(Cathode) **Equation 6**

or

$O_2 + 2H_2O + 4e^- \rightarrow 4OH^-$

Equation 5 and Equation 6 shows the half-reactions for the anode and cathode, respectively[51]. The E^{θ,O_2}_{Anode} and $E^{\theta,H_2}_{Cathode}$ values, shown to the right of the equations, are known as the electrochemical series or standard electrode potentials (E^{θ}), Section 2.2.2.1. Under ideal conditions a potential of 1.23V is required to oxidise water to form oxygen gas and 0.83V to form hydrogen gas. Therefore, biasing the cell with a voltage of 1.23V would initiate redox (reduction-oxidisation). However, under real conditions decomposition of water requires larger voltages to initiate the redox reaction. This is due to a phenomenon called overvoltage, see Section 2.2.2.2, which is the additional potential required to initiate the reaction to the rate it would occur in an ideal system. The minimum practical voltage required to initiate redox of water needs to be at least 0.5V greater than the ideal voltage[51]. However, depending on material used for the electrode, the overvoltage potential can be up to 1V greater than the ideal voltage.

2.2.2.1 Standard Electrode Potentials

The standard electrode potentials are individual thermodynamic voltages of any electrode material at a temperature of 298.15K (25ºC) and at a pressure of 1 atmosphere, that are referenced to a hydrogen electrode, with an E^{θ} potential of 0V. The values are produced from an electrochemical cell that consists of two electrodes, a hydrogen electrode (hydrogen over platinum) and a test metal, in an acidic solution with an activity of H^+ = 1 mol/dm^{-3}, at a temperature of 298K[52]. Metals that have a standard electrode potential higher than that of the standard hydrogen electrode (SHE) are considered ‘noble’ and the E^{θ} value is positive, whilst the E^{θ} value of ‘ignoble’ metals is negative Noble metals tend not to corrode with the release of hydrogen in a solution with a zero pH value, whereas, ignoble metals tend to corrode with the release of hydrogen in a solution[50].

The standard electrode potentials are also derived from thermodynamic data and are calculated using the Nernst equation, Equation 7, with the Gibbs energy (ΔG) sourced from standard tables[52, 53].

$$\Delta G = -nFE^{\theta} \qquad \textbf{Equation 7}$$

Where n is the number of electrons transferred for one step of the overall reaction; F is the Faraday Constant (96,487 C mol^{-1}) and E^{θ} is the electrode potential. Thus for water, n = 2 and for ΔG = -237,100 J/mol at 25ºC, which gives the electrode potential of 1.229V.

Table 2 lists the relative electrochemical potentials of metals commonly used in electronics, listed in order of their chemical reactivity, the less active at the top and the more active, or nobler at the bottom of the table. The scale of electrochemical series is used to give the degree of nobility of various electrode processes and thus is used to indicate the ability of material to 'resist' an electrochemical redox process, such as the corrosion process.

Metal	Reaction			E0 (V)
Gold	Au+ + e-	=	Au	1.692
Gold	Au3+ + 3 e-	=	Au	1.498
Platinum	Pt2+ + 2 e-	=	Pt	1.18
Palladium	Pd2+ + 2 e-	=	Pd	0.951
Silver	Ag+ + e-	=	Ag	0.7996
Copper	Cu+ + e-	=	Cu	0.521
Copper	Cu2+ + 2 e-	=	Cu	0.3419
Hydrogen	2H+ +2e-	=	H	0.00
Iron	Fe3+ + 3 e-	=	Fe	-0.037
Lead	Pb2+ + 2 e-	=	Pb	-0.1262
Tin	Sn2+ + 2 e-	=	Sn	-0.1375
Indium	In+ + e-	=	In	-0.14
Nickel	Ni2+ + 2 e-	=	Ni	-0.257
Cadmium	Cd2+ + 2 e-	=	Cd	-0.403
Iron	Fe2+ + 2 e-	=	Fe	-0.447
Bismuth	Bi+ + e-	=	Bi	-0.5
Tantalum	Ta3+ + 3e-	=	Ta	-0.6
Chromium	Cr3+ + 3 e-	=	Cr	-0.744
Zinc	Zn2+ + 2 e-	=	Zn	-0.7618
Chromium	Cr2+ + 2 e-	=	Cr	-0.913
Aluminium	Al3+ + 3 e-	=	Al	-1.662

Table 2 – Electrochemical Series of Metals Used in the Electronics Industry[52]

The degree of standard electrode's potential nobility can differ considerably from the 'practical nobility' established experimentally i.e. in situ experiments as opposed to

absolute values of quantitative evaluations. The differences may be due to the following[50]:

1. Some metals dissolve in the form of two simple ions (Cu^{+} and Cu^{2+}) and in the form of a complex ion ($CuCl^{2-}$) as opposed to the single form (Cu^{+}), thus compounding the E^{θ} value and producing a misleading result.
2. Some metals may become coated with a passivating film. Yielding, for example the E^{θ} value for the complex $Cu(OH)_2$ rather than the correct E^{θ} value for copper.
3. The additional potential added to the theoretical activation energy required for electrolysis to occur; known as the overvoltage.

2.2.2.2 Overvoltage

Overvoltage (η), in Equation 8, is the difference between thermodynamic potential, E^{θ}, and the practically measured potential (E) at which a noticeable current flows, i.e. the potential at which bubbles of gas appear[54]. It is the potential at which hydrogen and oxygen evolves at the cathode and anode, respectively.

$$\eta = E^{\theta} - E \qquad \textbf{Equation 8}$$

The overvoltage potential is influenced by pH, temperature and other ion species in the solution, although it varies considerable with different electrode materials[55].

Material	Overvoltage (V)	Periodic Block	Material	Overvoltage (V)	Periodic Block
Platinum	0.03	d	Copper	0.67	d
Tungsten	0.27	d	Iron	0.71	d
Smooth platinum	0.29	d	Graphite	0.77	p
Antimony	0.43	p	Aluminium	0.80	p
Gold	0.48	d	Mercury	0.89	d
Nickel	0.56	d	Tin	0.92	p
Palladium	0.59	d	Zinc	0.94	d
Silver	0.62	d	Lead	1.00	p
Carbon	0.64	p	Cadmium	1.22	d

Table 3 – Average Overvoltage of Hydrogen on Various Metal Cathodes[54, 56]

Table 3 [54, 56] tabulates a number of experimentally gained overvoltage values for various electrode materials. The list is compiled from various literature values and is aimed at demonstrating the affinity of overvoltage between the different materials. However, overvoltage values are normally only obtained through experimentation, because of the number of factors involved for a given system.

The highest values of overvoltage tend to be observed from s- and p-block metals such as lead and mercury, whilst the lowest tend to be observed for transition metals (d-block) such as platinum[57].

For an aqueous cell with platinum electrodes, as in Figure 13, the voltage applied to form gas bubbles is in the order of 1.7V[54], demonstrating an overvoltage of 0.47V above the thermodynamic potential of water (E^{θ}), which is 1.23V.

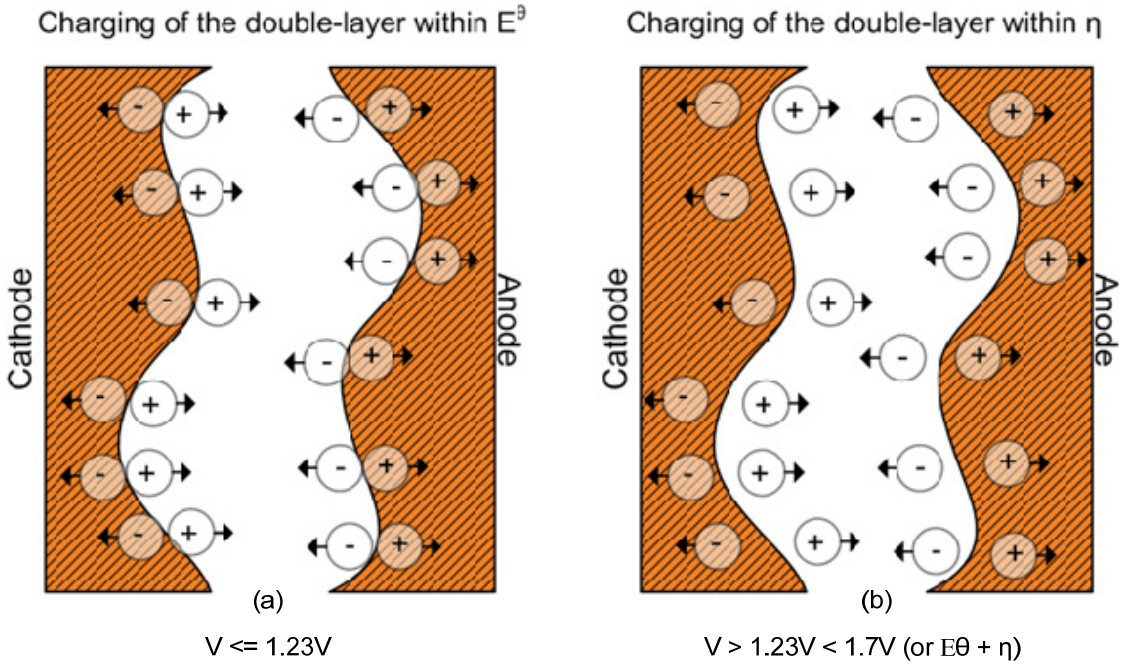

Figure 15 – Charging of the Double-Layer within Decomposition Voltage

If the applied voltage varies with E^{θ}, i.e. below 1.23V, then no decomposition will initiate although charging of the double layer will occur, as in Figure 15(a). If the applied voltage varies within the overvoltage, η, e.g. between 1.23-1.7V, it may only alter the charge characteristics of the double layer capacitance[58], i.e. increase the electrostatic distance between the molecules and reduce the capacitance of the double-

layer at the metal interface, as in Figure 15(b). However, beyond E (i.e. $E^{\theta}+\eta$) the effective capacitance at the double layer significantly reduces as the water molecules decompose and effectively reducing the resistance.

2.2.3 Pourbaix Diagrams

Pourbiax diagrams, named after the originator Marcel Pourbaix (1904-1998), or E-pH diagrams are plots for viewing the interrelationships between pH and potential[50].

On a Pourbaix diagram there are two axes, the Y-axis labelled E for the voltage and the X-axis labelled pH. Within the graph there are several regions that describe the function relative to pH and potential.

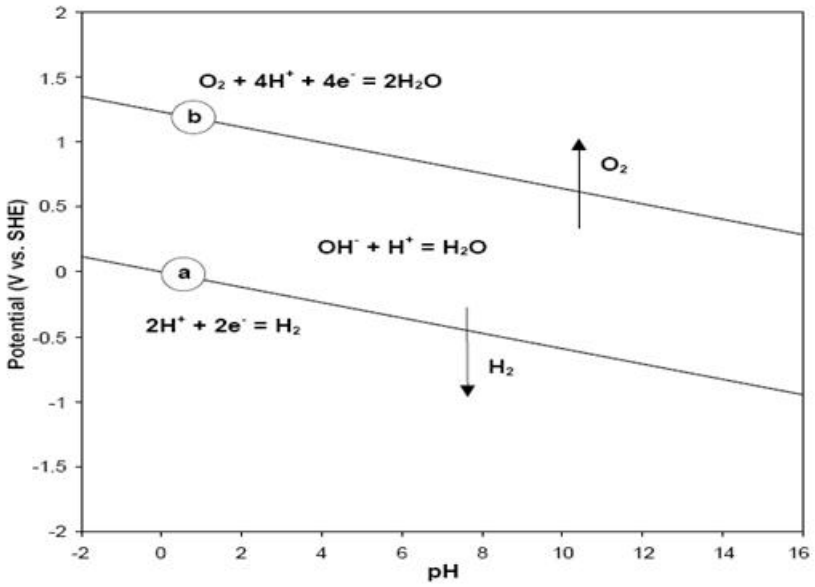

Figure 16 – Outline of a Pourbaix Diagram for an Aqueous Systems [50]

In the Pourbaix diagram in Figure 16 the lines (a) and (b) indicate the decomposition of water and the regions inside these lines are explained as follows:[50]

- In the region below line (a) water is unstable and will decompose to hydrogen by electrolysis at the cathode.
- In the region above line (b) water is unstable and will oxidise to oxygen by electrolysis at the anode.

- In the region between lines (a) and (b) water is stable. Hydrogen is oxidised to water and any oxygen dissolved is reduced to water.

Figure 17 shows a calculated Pourbaix diagram at 25°C for copper[60] in water. These metals are commonly used in electronic manufacture with silver and gold used for connector contacts, platinum and palladium used for relay contacts, and tin and lead as the main constituents of solder.

Pourbaix diagrams are useful indicators for electrochemical failure modes, but are limited to pure elements and pure water. Therefore such diagrams may not reveal the true condition of a specific failure mode.

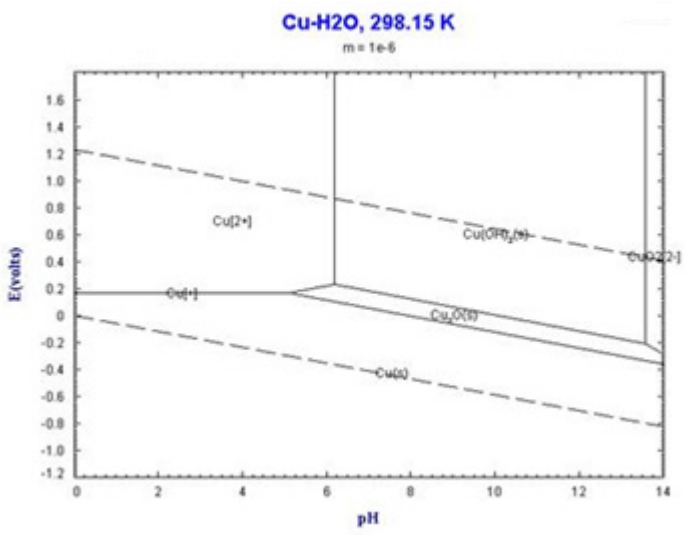

Figure 17 – Copper Pourbaix Diagram at 25°C[60]

2.2.4 Metal Migration Potential on Electronic Products

Some metals are more susceptible than others to migrating and thus forming deposits that affect the resistance between circuit tracks. Table 4 lists a number of commonly used metals in the electronics industry[61]. The metals are categorised into three groups in terms of susceptibility for electrochemical migration (ECM). The electrochemical migration of the first group can occur in the presence of water and an electric field. The second group requires the addition of halogen-containing contaminants. The final group is quite passive in a normal environment [36].

Metals that migrate with deionised water	Metals that migrate with deionised water and halogen contaminant	Metals that may need other conditions to migrate
Bismuth	Gold	Aluminium
Cadmium	Indium	Antimony
Copper	Palladium	Chromium
Lead	Platinum	Iron
Silver		Nickel
Tin		Rhodium
Zinc		Tantalum
		Titanium
Bias* 1-45 volts		

Table 4 – ECM Condition for Different Metals Used in Electronics [61]

Figure 18, Figure 19 and Figure 20 show the Pourbaix diagrams of the metal groups in Table 4.

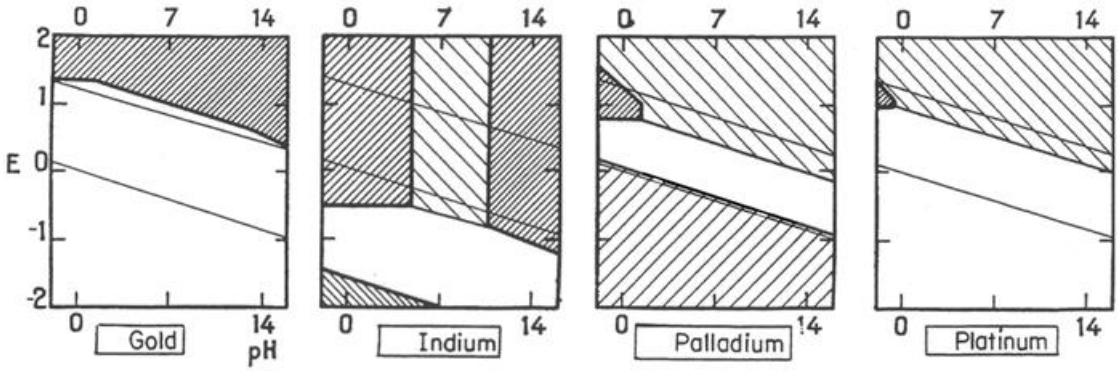

Figure 18 – Pourbaix Diagrams of Metals that Migrate with Deionised Water and Halogen Contamination[50]

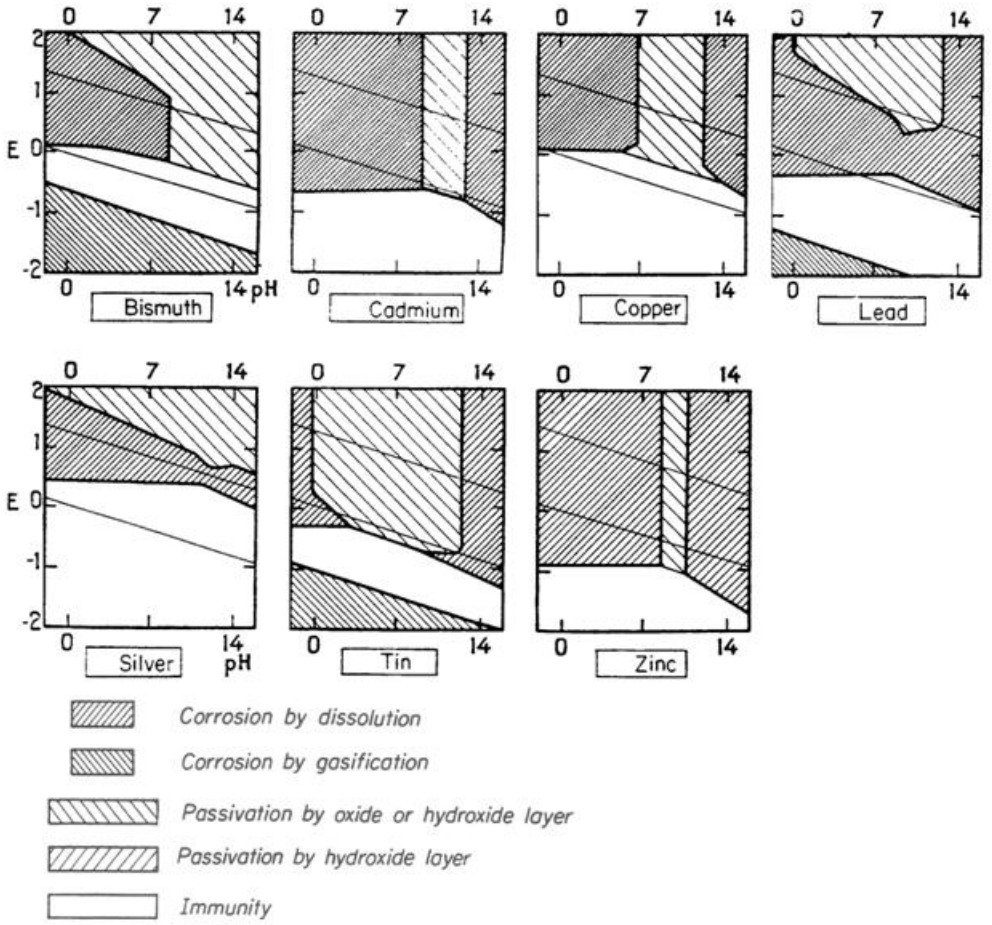

Figure 19 – Pourbaix Diagrams of Metals that Migrate with Deionised Water[50]

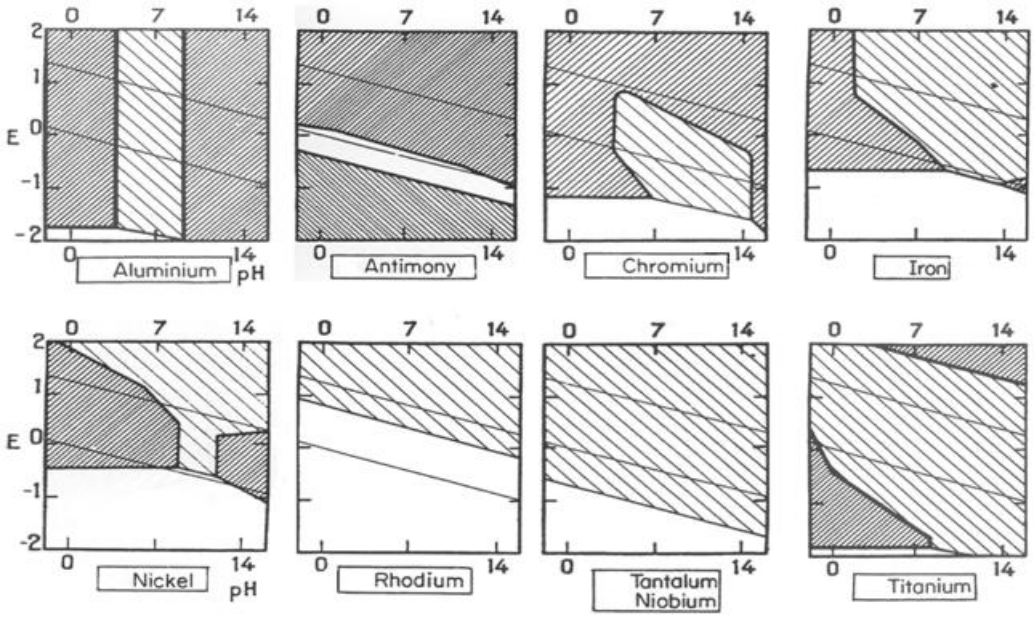

Figure 20 – Pourbaix Diagrams of Metals that may need other Conditions to Migrate[50]

When two oppositely polarized metal electrodes on a circuit, for example two copper tracks, are contaminated with water then electrolysed mass migration only occurs at redox, or above 1.23V. Below this voltage threshold any free ions within the contaminated-water solution will migrate to the opposite electrode and the current will decay to near zero and aid in the formation of the metal double-layer. Once the electrolysis threshold has been breached the electron flow will continue. Table 5 shows a number of Ea values of potential chemical species that may be present in a copper/water electrochemical system; such as a copper tracks contaminated by water. Note that the decomposition potential of water is 1.229V.

For all metals, electrolysis in water does not theoretically begin unless the voltage is greater than 1.23V. Below this voltage the capacitive charging effects can be observed due to the double-layer capacitance. This large capacitance occurs below 1.23V as the electrode interfaces are largely undisturbed by movement caused by water decomposing.

Species	ΔG (J/mol)	E_a (V)
H_2O	-237,100	1.229
Cu(s)	0	0
Cu^{+}(aq)	50,000	0.518
Cu^{2+}(aq)	65,000	0.337
CuO	-129,700	0.672
Cu_2O	-146,000	0.757
$OH^{-}_{(aq)}$	-157,000	1.627
$Cu(OH)_2$	-373,000	1.939

Table 5 – ΔG [52, 53] and calculated Ea values of Typical Ionic Species when Copper is Electrolysed in Water

It is worth noting that whilst certain other electrochemical reliability failure modes, such as dendrite growth and CAF formation, are well reported there seems to be no literature published on the potential failure effects of large capacitances caused by the double-layer on printed circuit board contamination.

2.3 Electrochemical Failures on Electronic Products

2.3.1 Dendrites

The process of dendrite growth begins with the oxidation of a metal, forming metal ions, at the anode, Equation 9, that migrate to the cathode where the metal ions then reduce back to their base metal, Equation 10[62]. This reaction is similar to the processes experienced in electroplating, although in electroplating the migrating metal ions usually plate a metal film on the cathode and tend not to form dendrites, such as shown in Figure 21.

$$Metal \rightarrow Metal^{n+} + ne^{-} \qquad \textbf{Equation 9}$$

$$Metal^{n+} + ne^{-} \rightarrow Metal \qquad \textbf{Equation 10}$$

When the metal ions migrate toward the cathode they can attach themselves to nucleation points on the cathode surface, producing localised sites in the form of needles or spikes[63]. At the tip of these nuclei the current densities, as in Figure 22, are at a maximum and this results in an increased possibility of further deposits or growths, shown as accelerated growth emanating from the tip in the form of fine black filaments growing from the cathode back towards the anode, as in Figure 23[34].

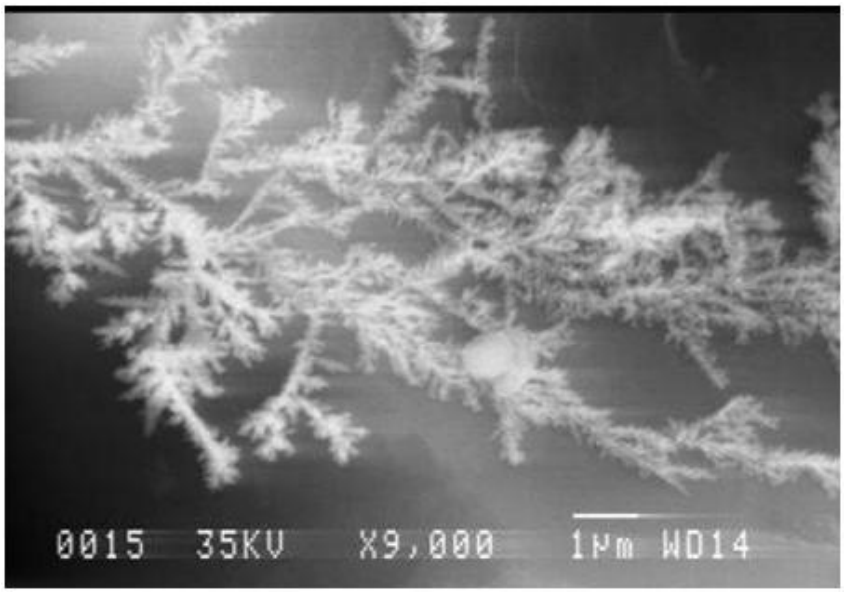

Figure 21 – 9K x Magnification of a Dendrite Showing Fractal-like Branching

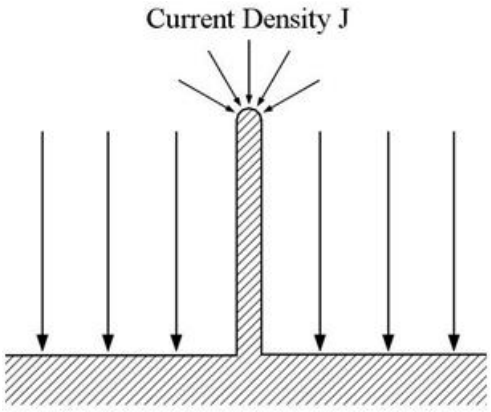

Figure 22 – Large Current Density at the Tip of a Nucleus

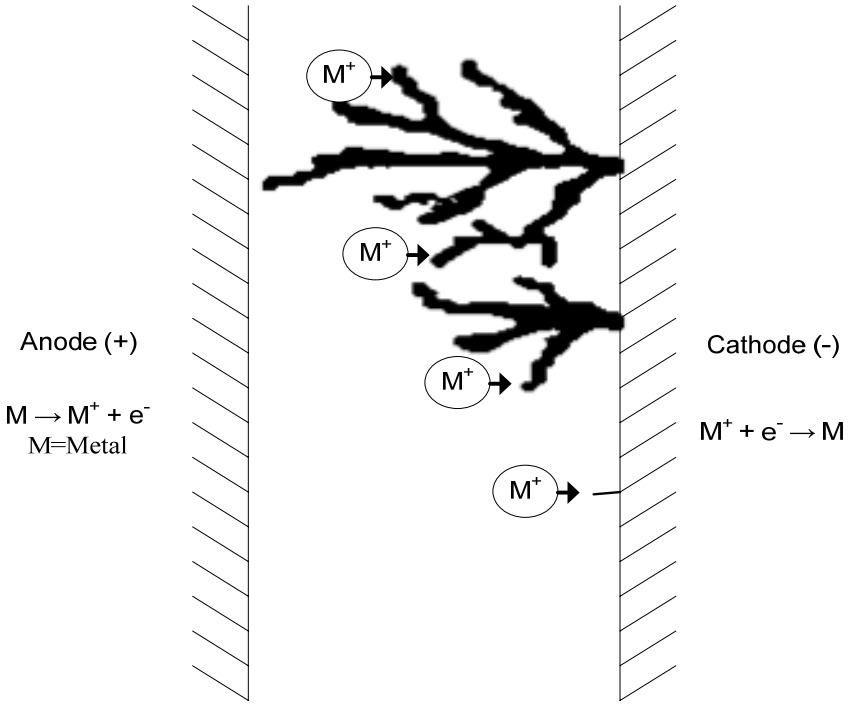

Figure 23 – Basic Mechanism of Dendrite Formation

Metal ions produced at the anode must be able to migrate to the cathode without forming other neutral insoluble compounds i.e. non-ionised species that do not dissolve in water. Copper(I) tends to precipitate with OH^- to form Cu(OH) and therefore may not form nucleation points, unlike Cu(II) which migrates from the anode without precipitation[62], and can form nuclei and start growth of a dendrite.

Most metals used as conductors can be electrochemically oxidised, including copper, gold, platinum and palladium, although gold, platinum and palladium usually require additional contaminants such as bromide, chloride and iodide ions[36, 62], as noted in Table 4. These contaminants are commonly found on printed circuit board, with bromide used as a fire retardant, and chloride and iodide used in copper etchants. Chloride and bromide are also found in solder fluxes.

The formation of a dendrite is accompanied by the decomposition of water which involves an oxidisation process at the anode and a reduction process at the cathode[64], with large pH gradients formed at the electrode interfaces. These steps are typically termed as a redox (reduction-oxidation) process. This is sometimes demonstrated by the production of gas at the electrodes. As noted in Section 2.2.2, the decomposition

process of water consist of two sets of reactions with the base reaction for the anode shown in Equation 5, with Equation 6 showing the base reactions for the cathode.

The pH of a solution is defined as the inverse log of the H^+ ion concentration, i.e. –log $[H^+]$, and thus the pH level experienced at each electrode differs as a function of H^+ production. This can be seen in the reactions in Equation 5 and Equation 6 with the production of H^+ at the anode forming a more acidic solution and at the cathode with the production of OH^- ions forming a more basic solution, i.e. more OH^- than H^+. However, the final pH at the electrode interface also depends on the contamination present such as sodium and potassium carbonate from the basic solder mask developer[65] and weak organic acids found in solder fluxes, shown in Table 1.

An experimental study[64] into the effects of pH on dendritic growth in saturated conditions indicates dendritic growth is accelerated by decreasing the pH below pH 5, with higher pH suppressing growth, although signs of solid corrosive products may be observed between the anode and cathode. The study explains that a fractal formation of a dendrite, i.e. shape, size and overall characteristics, changes notably if anionic contaminants, such as Cl^-, are added to the electrolyte, i.e. water. Another source[66] suggests a similar change to the dendrite shape, where an increase in the concentration gradient reduces the fractal nature of the dendritic growth, as in Figure 24.

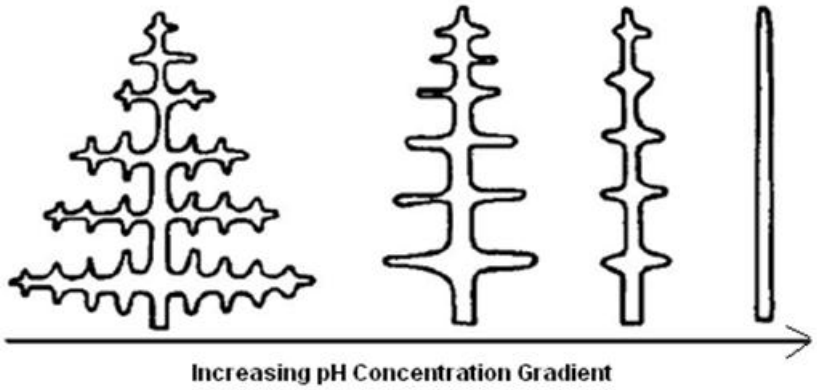

Figure 24 – Dendrite Shapes as a Function of Concentration Gradient[66]

Dendrites usually form a bridge between two electrodes effectively shorting the conductors and producing an increase in current. The cross-sectional area of a dendrite is typically only 0.5-2.5um diameter[67] and thus in high power circuits the bridges will

fuse and the current leakage is either reduced or disappears. However, over time the dendrite filament will thicken and the current may increase sufficiently to produce circuit failures [68, 69].

With lower current circuits, such as microprocessor data buses, these dendrite bridges can be problematic. The failures caused by the formation of dendrites are not normally intermittent, i.e. they are either fully open or fully short, and for this reason it can be difficult to detect dendrites especially if they have been blown-out.

Available papers dealing with the effects of dendrites at varying temperature within normal operating conditions of commercial electronics are limited. This is probably due to a combination of the long durations required for each experiment (at humidity less than saturation) and the emphasis on standard testing, i.e. 1800 hours,(rather than operating) conditions, with most electrochemical migration validation testing limited to comparatively high temperatures of 85°C/85% RH exposure[21, 23]. Wassink[26] generalised that the chance of dendrite growth is a function of the Arrhenius equation, which is shown in Section 2.5.

2.3.1.1 Electrochemical Growth Models

Theoretical growth models that reflect the behaviour of failure mechanisms such as dendritic growth tend not to reflect the failure conditions experienced in the field. The most accurate models are those produced from experimental data that determine the quality of fit, which is generally not perfect. The reason is the unseen variables that are not considered and which can play a significant role in the end result[70]. The quality of the data depends on the material quality and the experimental control.

Bockris[71] discusses two theories that may account for the formation of growths in an electrochemical system due to ion transport; he termed electro-growth. In the first theory he explains the deposition in terms of micro steps, where each subsequent micro step is the adsorption of a single ion. The single ‘flat’ face interpreted as the terrain of the electrode-electrolyte interface, may be valid as a starting condition although with continued deposition a number of reactions could take place, with one such reaction

shown in Figure 25[49]. Here positive metal ions are formed at the positively biased electrode (the anode), and migrate toward the negatively charged cathode.

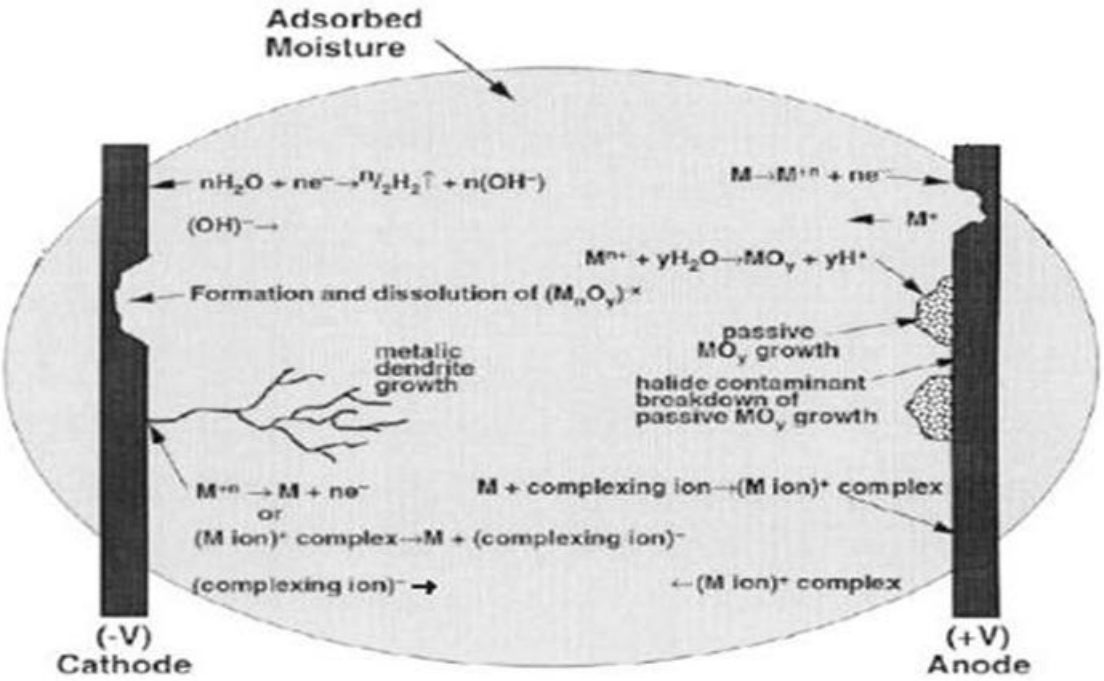

Figure 25 – Overview of Electrochemical Migration [49]

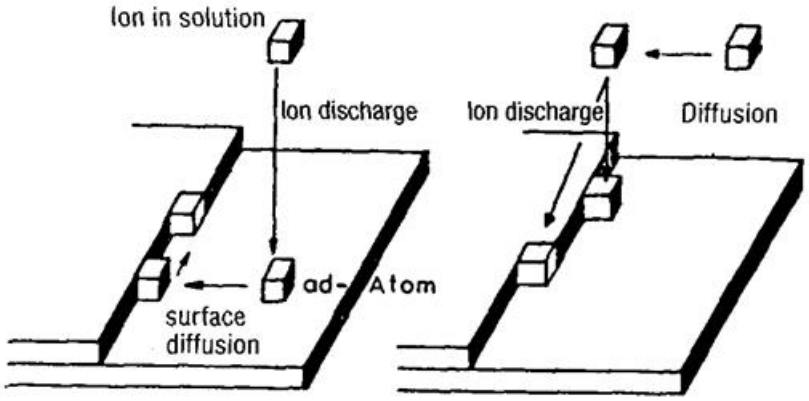

Figure 26 – Micro-steps [72]

The micro-steps, shown in Figure 26, cluster into irregularities and appear on the surface. At these projections the electric field becomes concentrated and results in faster growth, as displayed in Figure 27, which portrays a representation of the

concentrated electric field at a projection; producing a faster growth than on a flat surface.

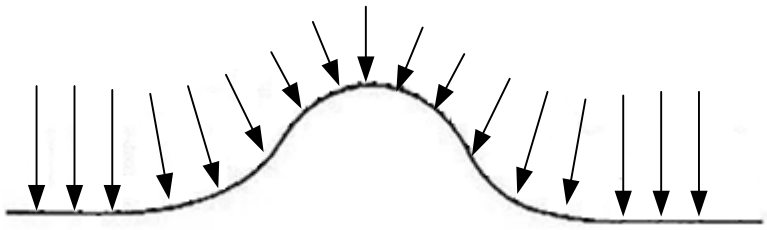

Figure 27 – Representation of a Concentrated Electrical Field [71]

In his second theory Bockris explains the mechanics of dendritic growth under the heading of dendrites; loosely termed the elementary theory of dendrite formation. This theory seems to complement the previous theory that under the 'right conditions' the next step, after the growth of a metal deposit, is to form a dendrite. However, Bockris does not make this connection obvious.

The tip of the growth has a small diameter of approximately 1um. In contrast to micro-step formation, this should not be considered a 'plane sink', Figure 27, that stimulates linear diffusion. It is virtually a 'point sink', as in Figure 22, or point source dependent on the polarity, with the radius of curvature being much less than the diffusion-layer thickness ($r<<\delta$). The linear concentration gradient can be considered as occurring over an effective distance of δ, the Nernst diffusion-layer thickness, obtained by extrapolating the linear portion of the concentration change (Ce –C) as in Figure 28. Under these conditions there is a spherical diffusion to the point-sink.

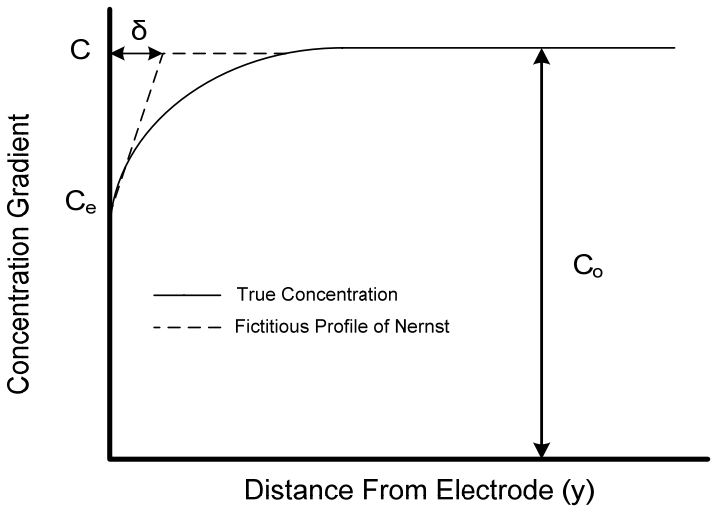

Figure 28 – The Nernst Diffusion-layer Thickness (δ)

Di Giacomo [73] explains that for the production of a metal dendrite, the current density at the whisker's tip must be several orders of magnitude higher than the average current. The growth is possible through spherical diffusion 'focusing' the ionic current on the dendrite tip, which can be expressed in terms of its radius of curvature.

The electric field can be calculated from the voltage bias, which, in turn, is directly proportional to the force applied on a charged particle (e.g. a metal ion) within the field[74]. The force applied on a charged particle may affect the time it takes an ion to move through the electrolyte. The electric field can be calculated from the applied voltage and electrode geometry under consideration. In its simplest form the field in a parallel plate capacitor is expressed by, E=V/d where E is the electric field, V is the applied voltage and d is the distance between the two oppositely biased plate electrodes[75].

2.3.2 Conductive Anodic Filaments (CAFs)

In the mid 1970s Bell laboratories first reported[76-78] electrical shorts due to conductive anodic filament (CAF) in epoxy-glass (FR-4) printed circuit boards which presented a major reliability problem in both the computer and telecommunications industry. The main characteristic of this failure mode is the abrupt and unpredictable loss of current flow between electrically biased conductors. The occurrence of CAF tends to be observed where fine pitched circuit layout and uncontrolled environments

are used. However, the chemical composition of the laminates and processing materials, humidity, and voltage bias are also understood to aid in their formation[79].

The formation of a CAF is the result of an electrochemical migration process that initiates at the anode. In contrast to dendrites forming from the cathode, CAF growths emanate from the anode inside the printed circuit board epoxy fibres and contain a combination of materials such as halide ions to form copper salts[22, 30, 79]. These growths tend to form between vias, also known as printed-through holes, and can potentially migrate to a more cathodic via and form a short circuit, shown in Figure 29.

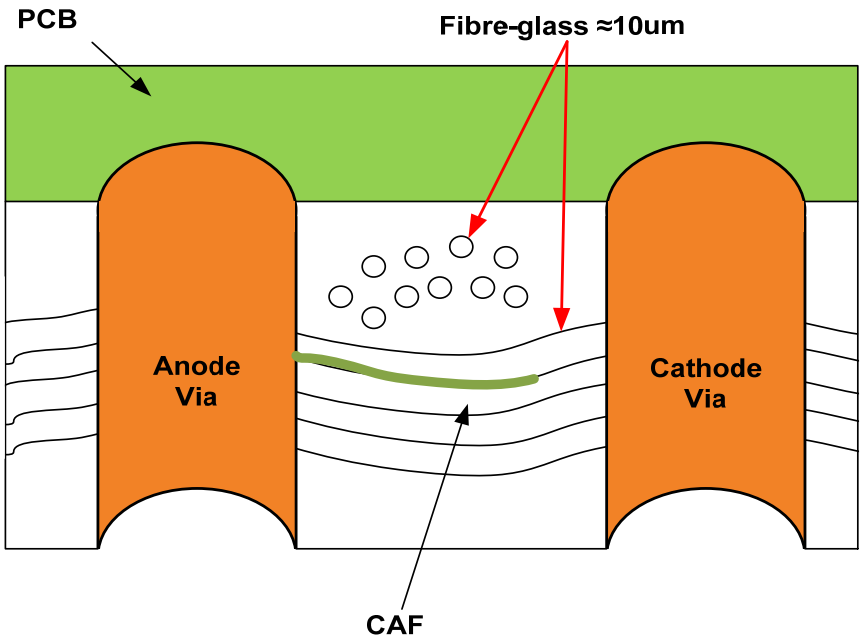

Figure 29 – Schematic of a CAF Pathway between Two Vias

Bell Laboratories[76, 77] published the mechanism by which CAF formations evolve in the form of several steps. In the first step the epoxy fibres degrade and moisture absorption occurs. This creates an aqueous channel through the separated epoxy fibre interfaces that provides a conductive path. These separated epoxy fibre interfaces are the result of laminating several layers to form a multilayer printed circuit board. The second step is the process of electrochemical corrosion from the absorbed water acting as an electrolyte. The two copper vias act as electrodes and the operating voltage drives the ion migration process. At each of the electrodes a pH gradient occurs with an acidic pH gradient (H^+) occurring at the anode and basic pH gradient (OH^-) occurring at the

cathode (Equation 5 and Equation 6). If these pH gradients either propagate or the pH diffusion regions are in close proximity, for example closely spaced vias, then essentially these extreme pH concentrations can form salts (i.e. base+acid = salt). The simplified copper Pourbaix diagram[50], in Figure 30, shows that with a pH below 7 and a potential greater than 0.2V copper corrosion can occur. In a CAF, as the anode produces copper ions (Cu^{2+}), migration occurs towards the cathode, which remains virtually stable at all pH levels. As the copper ions migrate they move towards the cathode, a more basic region, and the pH increases above 5 where the corrosion process starts to declines. At approximately pH 8.6 the copper product becomes insoluble[69], forming stable conductive copper salts that emanate from the anode acting as conductive paths and potentially electrically shorting the biased vias.

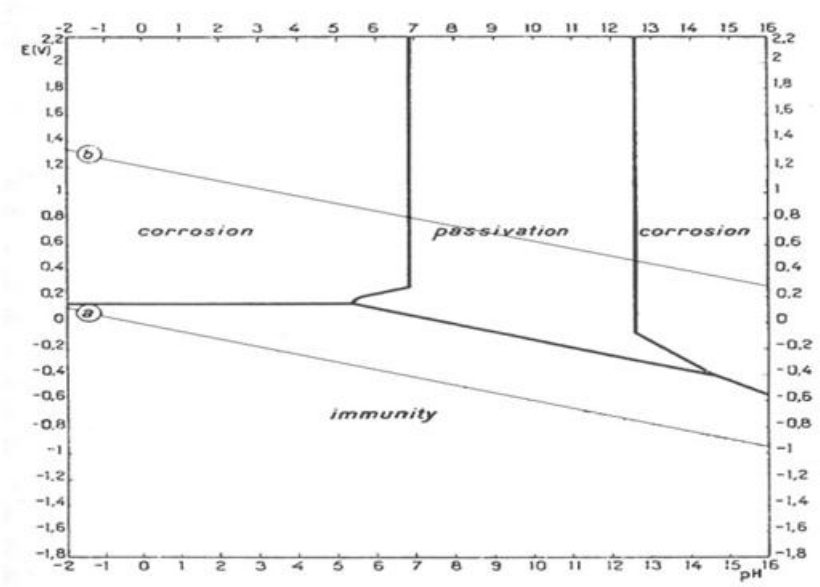

Figure 30 – Simplified Copper Pourbaix Diagram 25ºC [50]

2.3.3 AC Formations

Literature searches have not revealed any published work that directly cites results using AC (alternating current) ECM (electrochemical migration) testing or AC ECM reliability issues for printed circuit boards. This is clarified in a communication with Neves[80] and a meeting with NPL. Neves comments in one of his articles[81] that there are some movements in Europe towards the use of AC power sources in ECM testing.

In correspondence, Neves explains that his comments in the article are founded on general discussions on CAF testing with members of the IEC (International Electro-technical Commission), in his role as chairman of the working group for Test Methods for Printed Circuit Boards & Materials. Within this working group they discussed the creation of methods for the IEC 61189[82] standard. In this correspondence, Neves also clarifies that they too have not found published work in the field of AC in ECM testing. His group feels this may become an area that should be noted and thus his comments in his article.

In a further communication with Neves [83] he indicates an interest in understanding (empirically) how AC voltages influence ECM, both with, and without, a DC bias, and an interest in comparing the results with the present DC ECM test methods. The author later found the sole European interest was actually the NPL funded by the DTI (Department of Trade and Industry).

In its simplest form ECM using low frequency AC is similar to electroplating. When running a DC ECM test (Surface Insulation Resistance), the metal atoms on the most positive electrode experience oxidisation (lose electrons to become ions) and dissolve into the electrolyte (in this case a layer of water). They then begin to migrate from the anode to the cathode. If, however, the polarity abruptly reverses after say $1/50^{th}$ of a second (50Hz), the metal ions may migrate back to the electrodes where they originated and thus reduce back to a metal atom, shown in Figure 31, resulting in no net flow. However, it is possible the ion continues in the same direction immediately after the polarity of the cell reverses, due to inertia, shown at t_2 on Figure 31.

Examples of dendrites grown with an AC bias are shown in Figure 32, with the left image showing a dendrite grown at ±2v 0.0001Hz and the right image showing a double tailed dendrite grown at ±2v 0.1Hz. As these dendrites are grown at sub-hertz frequencies it could be said the bias used is pulse DC as opposed to AC, effectively operating as a DC electrochemical cell. However, formations grown at frequencies greater than 10Hz do not produce dendrite-like structures, but rather powder-like growth at both the anode and the cathode.

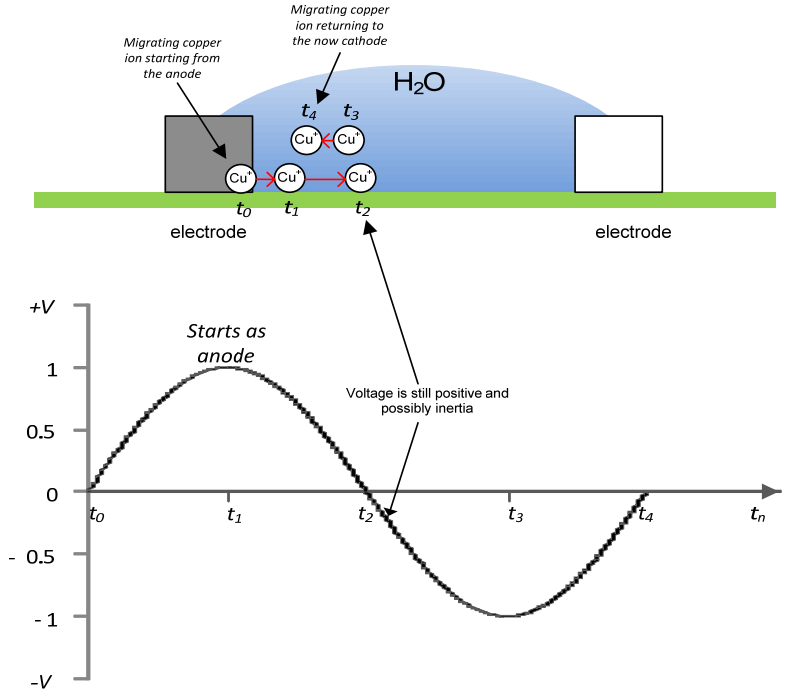

Figure 31 – AC Bias Cell: Idealised Relationship of a Copper Ion Migration path

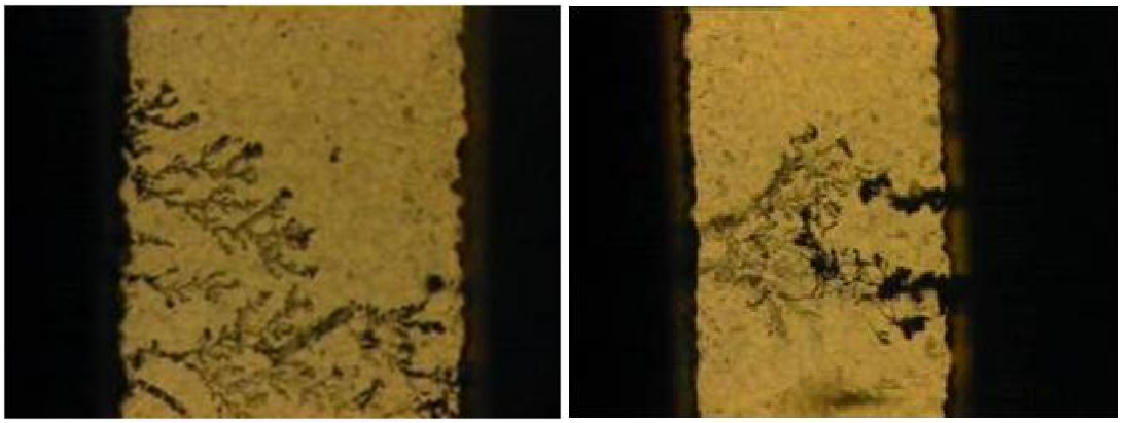

Figure 32 – AC Dendrite Growth (a: 0.001Hz, b: 0.1Hz)

This is further detailed by Hamann [72] where he explains the application of an AC potential to a cell. Due to the rapidly changing potentials, the various processes at the electrode surfaces are forced to oscillate with an applied frequency above 1Hz. The process of redox will also oscillate although the greater the distance from the electrode the more dampened the concentration changes. If there is no DC offset to the AC signal then the cell may not form growths such as dendrites. However, a DC offset will encourage a net current flow and thus increase the chance of dendrite formation.

Based on the theoretical explanation in Figure 31, the growth of metallic dendrites would be impossible to form in a purely AC circuit. In practice, as also demonstrated in Figure 32, if enough water is present to bridge the two electrodes while they are biased then there will be a diffused, white or blue-green residue formed (sometimes black or dark grey on the top of chip capacitors) as the metals dissolve into the moisture, as shown in Figure 33. These images are produced by biasing several water contaminated printed circuit boards with an AC potential across the tracks.

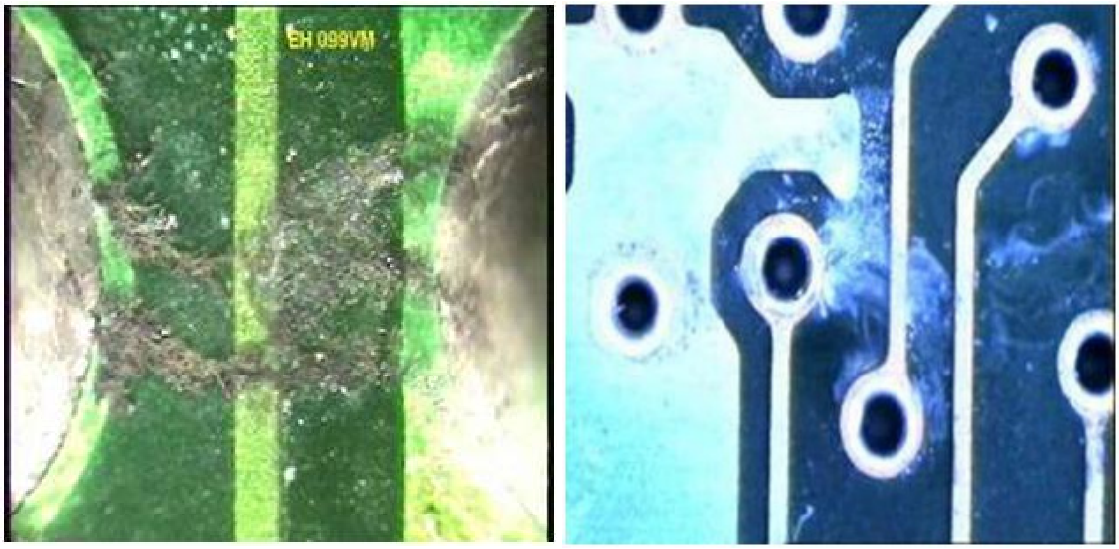

(a) (b)

Figure 33 – Diffuse, White or Blue-green Residue on AC Circuits

The image shown in Figure 32 seemingly demonstrates dendrite growths under AC conditions. However, the definition of AC needs to be considered in the case of electrochemical migration. The growth on Figure 32(a) is formed at a frequency of 0.0001 Hz, which is equivalent to 10,000 seconds for one complete cycle. The cell is exposed to a peak voltage of 2V twice per cycle, once at 2,500 seconds and again at 7,500 seconds. The growth of the dendrites probably occurred during these intervals, which is also suggested by Chan [84]. Thus, the dendrites effectively grew under DC conditions, i.e. above 1.23V demonstrated in Experiment 2 in this thesis.

Chan [84] suggests an AC SIR (Surface Insulation Resistance) approach which may pose several advantages as an alternative to DC SIR. Firstly, the disturbance to the ion distribution of the systems due to the measurement itself is minimised, i.e. under DC ions distribute evenly at the electrodes reducing the resistance. Secondly, voltage accelerated experiments may be possible, as in theory no net migration will occur.

Under an AC voltage, the mobile ions may merely oscillate back and forth hypothetically resulting in no net flow. However, Chan explains the process may produce a redox reaction that may not be reversible; as the voltage rises above the activation potential for decomposition of water then the redox process will begin. If this

is the case, each half cycle that is favourable for the reaction will still accelerate the ions toward the opposite electrode possibly due to the inertia. This can be considered as similar to the theoretical model shown in Figure 31, however, at the appropriate activation potential the anode loses hold on the ion and accelerates it towards the cathode, i.e. the AC field creates momentum and the hysteresis over shoots the field strength and accelerates the ion towards the cathode.

From the frequency tests Chan conducts, the AC current stays stable for several hours. However, over longer time periods the SIR decreases slowly, and steadily, to 2-3 times less than the initial value after 150 hours. A point worth noting in these results is that the SIR does not increase at all under the AC bias.

Compared to DC SIR, Chan's results demonstrate the potential advantages of AC measurements. On a DC system the electrodes are fixed and there is a known cathode and anode polarity. In this type of system the pH levels differ towards either an acid, H^+ migration, for the cathode or an alkaline, OH^-, migration, for the anode. With an AC system there could be various interactions and this could have implications for the residual salts left in the electrolyte and could explain the images in Figure 33.

In a paper by Yin[85] he demonstrates the effect of AC on two metals bismuth and nickel. Yin grew nickel and bismuth nano-wires using AC electrodeposition for applications of high density recording devices and sensors. Yin uses an anodised aluminium oxide film as the cathode and a graphite bar as the anode. He states electrodeposition of metal into porous alumina film directly following anodisation, can only take place under AC conditions. Producing either bismuth or nickel nano-wires requires different conditions. To produce nickel nano-wires, the electrodeposition can only take place under an AC potential, whilst the production of Bi nano-wires requires both an AC potential and a DC bias. Using common electrochemical deposition (DC alone) causes problems. He terms this the skyscraper effect, i.e. wires towering over others. This is interesting and could be indicative of whisker or dendrite formation seen in electrochemical migration of PCBs and should thus be further investigated.

Yin also finds the frequency range used affects the results. Another point for noting is that high quality deposition of nickel can be obtained with AC frequencies from 10 to 750 Hz and for bismuth the optimum frequency range is between 10 and 100 Hz.

The reason for the difference seen as the frequency changes is unclear. However, Yin compares this to a similar phenomenon seen in *pulse* electroplating, which the acceleration effect to the opposite electrode could therefore facilitate the growths. The effects of frequency on the deposition could also be explained by the difference in particle size, in that bismuth is a heavier metal than nickel; i.e. if the effect of simple harmonic motion on a molecule is considered, it can be concluded the rate of oscillation will be dependent on the mass. Thus a particle that has a larger mass will vibrate slower than a lighter particle.

The paper does highlight the difference could be associated with the double layer capacitance which is a function of the AC frequencies. However, if the electrodes are of the same size for both materials (bismuth and nickel) then why would the double layer capacitance have such a difference? Further investigation is needed to ascertain more data and a fuller understanding of the double layer and its effects with different metal and electrolytes.

Yin's paper is not unique and there have been several other papers published describing AC electrodeposition [86, 87], albeit most on the formation of nano-wires.

From the literature search it is evident that the effects of AC on the process of electrochemical migration are significant and it does show that some formations with AC may happen, under the right conditions, on PCBs.

The interesting point from Yin's work is that both nickel and bismuth are used in soldering in electronics, and tin/bismuth alloys may be the successor to the tin/lead alloys currently used in commercial soldering processes.

2.4 Methods for detecting ionic migration

The detection of electrochemical migration is traditionally conducted using a standard industrial technique termed Surface Insulation Resistance (SIR) and executed within a given standards, a number of which are shown in Table 6.

Standard	IEC 61189-5 (in draft)	IOS 9455-17 (latest)	J-STD-001C	IPC-TM-650 2.6.3	IPC-TM-650 2.6.3.3	Bellcore
Temperature/ Humidity	40°C/93%RH	85°C/85%RH	85°C/85% RH	Class 1:35/90°C at 98%RH for 4 days static. Class 2:50/90°C at 98%RH for 7 days static. Class 3:25/65°C at 90/98%RH for 7 days cycling.	85°C/85%RH	35°C/85% RH
Test Duration	72 hours	168 hours	168 hours	168 hours	168 hours	120 hours
Measurement Frequency	20 min intervals	Twice in 24 hour period	24 hrs, 94 hrs and 168 hrs	24 hr intervals	24 hrs, 94 hrs and 168 hrs	25 hrs and 120 hrs
Test Voltage	5v	50v	100v	100v	100v	100v
Bias	+5v	+50v	-50v	-50v	-50v	-50v
Test Coupon	Under Review	IPC-B-24	IPC-B-36	IPC-B-25A	IPC-B-24	IPC-B-25A

Table 6 – Summary of SIR Standards and Some Parameters

A number of factors can influence the phenomenon of electrochemical migration with some of these factors listed in Table 7.

Item	Factors
Conductors	-Nature of the metal or alloy -Surface condition/roughness -Conductor configuration -Conductor spacing
Substrate	-Composition and moisture absorptivity -Structure -Reinforcements and their nature
Atmosphere	-Temperature -Humidity -Corrosive elements and their concentration -Electrical conductivity of the medium -Air velocity
Operating Conditions	-Electrical potential -Temperature -Humidity

Table 7 – Factors that can Influence Electrochemical Migration

Three main factors are needed to be present for electrochemical failure to occur, they are electrical potential, moisture and an ionic contamination[88]. Electrochemical failure can be visualised as a Venn diagram, shown in Figure 34. Increasing and

decreasing these factors can be thought of as increasing and decreasing the diameter of the circles.

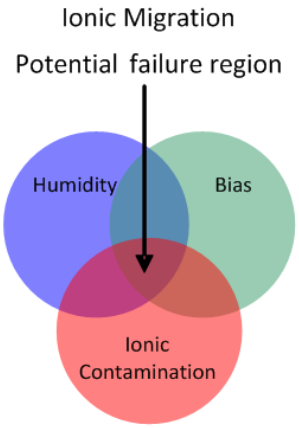

Figure 34 – Venn Diagram of Electrochemical Failure Modes

The following Sections describe current test methods for detecting the presence of electrochemical migration on printed circuit boards.

2.4.1 Surface Insulations Resistance (SIR)

Surface insulation resistance testing is a method used to assess the point that materials used in electronics degrade through electrochemical phenomena and is described in the IPC (Institute of Interconnecting and Packaging) standard IPC-9201[89] The testing usually involves biasing a test sample, Figure 35, with a DC potential between 50-100V and artificially elevating the temperature and humidity levels to one of the standards shown in Table 6, with the aimed effect of accelerating the aging of the product. The aging of the product is associated with the Arrhenius reaction rate[89] where every 10ºC rise doubles the aging rate. For example, a year of service at 35ºC/50% RH would be approximated by six months exposure to 45ºC/50% RH or three months 55ºC/50% RH.

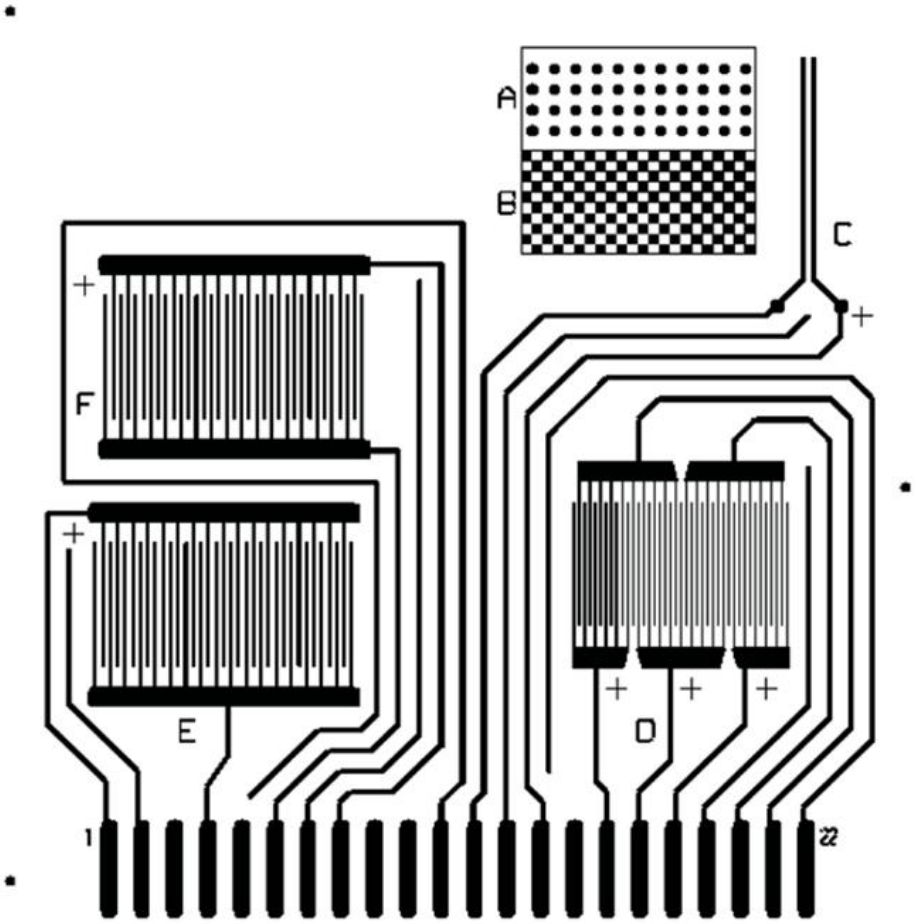

Figure 35 – IPC-B-25A Test Comb[89]

If the test sample contains a low ionic content then the measured SIR will remain in the acceptable region, within a given tolerance of the initial reading. However, if the ionic content is high, as may be experienced from improperly-cured solder resist or flux residues, then unacceptable leakage currents, corrosion and metal migration, or dendritic growth, can occur. The testing is conducted on a pass or fail criterion based mainly on SIR electrical values. Often the electrical measurement fails to reveal the presence of surface dendrites from contaminants related to processing chemicals. This is because the dendrite burns out between electrical readings when the circuit continues to be biased at 50 volts[22].

Misconceptions and poor understanding of the objectives of SIR testing are common. SIR testing, to date, is used primarily as a 'quality' test of single materials and processes such as the assessment of soldering fluxes. The difficulties with SIR testing

as a true tool for the reliability evaluation of printed circuit boards are brought about for several reasons[62]. These are predominantly:

- Lack of definitions of expressions used or inconsistent use of defined expressions.
- Insufficient knowledge of the failure mechanism.
- Poor understanding of what one is trying to achieve with SIR testing.
- Difficulties in testing true printed circuit boards.

One of the major misconceptions about SIR testing is that surface insulation resistance is a material property, whereas the purpose of SIR testing is to accelerate failure mechanisms that are only related to SIR[90]. In Tegehall's critical review on the SIR test method[62] he considers the purpose of normal SIR testing is to accelerate electrochemical migration. Thus if it becomes a test method for acceleration of a failure mechanism, primarily electrochemical migration, then the test should be named the electrochemical migration test.

According to the IPC, Surface Insulation Resistance is defined[89] as:

> *a property of the material and electrode system. It represents the electrical resistance between two electrical conductors separated by some dielectric material(s). This property is loosely based on the concept of sheet resistance, but also contains element of bulk conductivity, leakage through electrolytic contaminants, multiple dielectric and metallization materials and air.*

Thus, as SIR is measured during an electrochemical migration test, it gives the impression that the electrochemical migration can be quantitatively measured. Tegehall argues that this is not the case as there is no method to separate electric current due to migrating metal ions from current due to other migrating ions. The biased comb will eventually cause an increase of SIR (reduction in current leakage) due to electrochemical processes of corrosion, where oxides effectively partially insulate the cathode; thus indicating an improvement of reliability.

Tegehall explains that it is more complex to measure SIR than the present methods detail. SIR is determined using Ohm's law R=V/I. In humid conditions most of the

current flow on contaminated boards is generated through ion migration. This causes a depletion of ions in the area between the biased surfaces (free ions in the water will be attracted to the electrodes), which will result in a decrease of current, i.e. an increase in SIR. This is shown by Chan [84], who notes that initially the SIR rapidly increases then slows down over time. On a contaminated board of 10µg/in^2 table salt, there was an initial decrease of SIR from 1 x 10^{10} ohms to 5.3 x 10^6 ohms. However, when a bias of 100 volts was applied to the contaminated board the SIR increased to 3.7 x 10^7 ohms after 60 seconds, 1 x 10^9 after a few hours and 8 x 10^9 ohms after 100 hours, as in Figure 36.

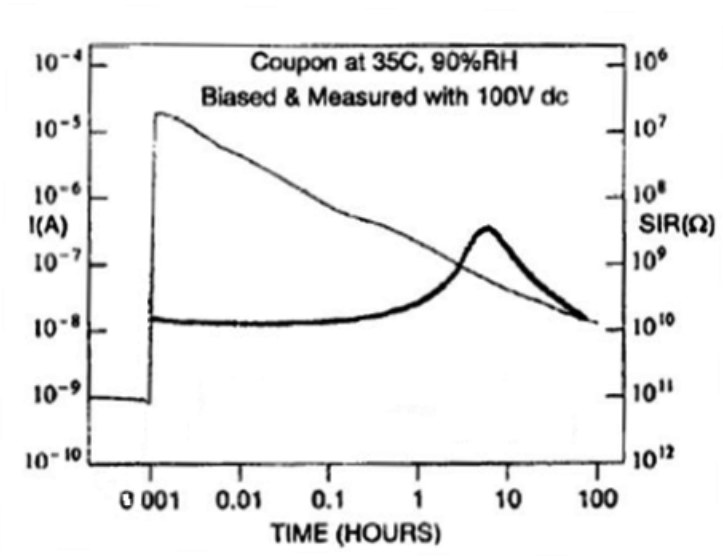

Figure 36 – Current and SIR for Coupon Contaminated with Salt Solution 10µg/in^2[84]

Chan also shows SIR increases continuously when a bias is applied to a specimen contaminated with table salt solution and approached the values of a clean board after a few days. This demonstrates the initial condition of the SIR test should be observed (not disregarded) and measured after a few days as some standards prescribe.

Some standards prescribe that measurements of SIR should be gathered using a voltage with reverse polarity after 60 seconds. By reversing the polarity, the SIR will start to drop as ions start to migrate in the opposite direction and then increase again later when the area between the conductors once more becomes depleted of ions[62].

EU-sponsored SIR research, conducted by NPL [40] has determined several important factors that should be implemented in any new testing programs. These are:

- The test pattern should have a pitch of 200um and a width of 400um.
- The test conditions should be 40°C, 93% relative humidity.
- The measurements should be taken at 20 minute intervals.
- The test voltage should be 5 volts, in line with most microprocessor circuitry operating voltage. This would results in a voltage gradient of 25V/mm (5V/0.2mm).
- When conducting process characterisation tests, the test patterns must be over-mounted with dummy components.

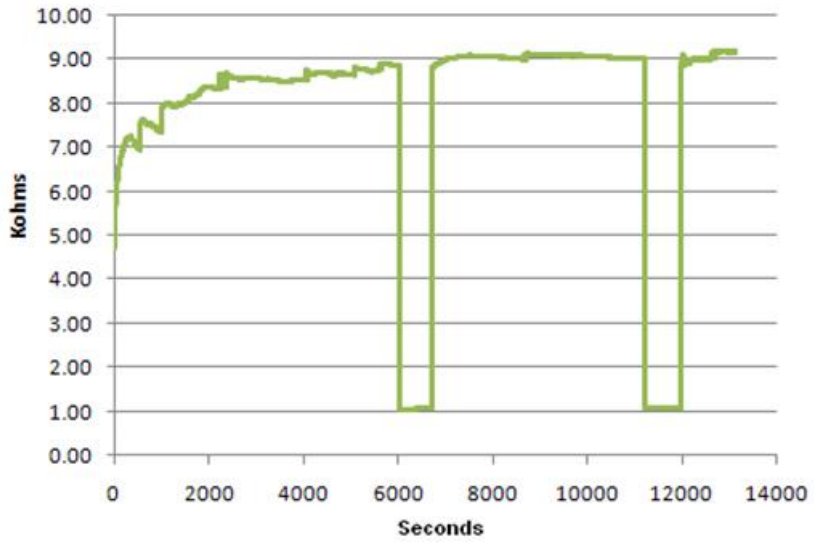

Figure 37 – Dendrites Fusing in Commercial Water

Figure 37 shows a continuous plot from a SIR test, in saturated conditions, over a 14,000 seconds period. This plot shows two sharp drops in resistance. This is due to dendritic growth fusing the path of the test comb. The formation of dendrites normally does not have any impact on SIR except for a few seconds when a short is formed and the dendrite is burned off [12]. However, this does depend on the magnitude of the current used. If a current is used that is within the current-carrying capacity of the dendrite then it may be hours before the dendrite either blows open the circuit or remains as a short circuit. This is shown in Figure 37 at around 6,000 seconds and approximately 11,000 seconds.

These results highlight the problem with taking infrequent measurements. For example; if a measurement is taken at the beginning of the test, t = 0s, and the next is

then taken, say, at t = 8,000s it may be incorrectly perceived that the material under test has a good resilience to forming dendrites. This situation could be termed Measurement Aliasing as the sampling time is too infrequent to represent the actual true signal which is the measured data. A measurement system that can supply a greater sampling rate would reduce the probability of missing a dendrite's fuse and provide a more accurate picture of the system under test.

Current methods of reliability validation of ionic migration all use some form of DC bias to augment the migration of metal ions in a controlled environment and their occurrence is detected by the measure of some DC characteristics such as resistances on a test coupon. Almost all suppliers and manufacturers of electronic equipment drive to minimise the occurrence of ionic growth by ensuring the materials used in soldering electronics, such as flux, solder pastes and laminates, comply with standards set by international bodies, although there are still reports of failures due to ionic migration, even after stringent validation testing.

2.4.2 A Novel Method for Analysing CAFs

The linear circuit, developed by Ready[22], is used as a method of analysing the growth of CAFs without damaging them once formed.

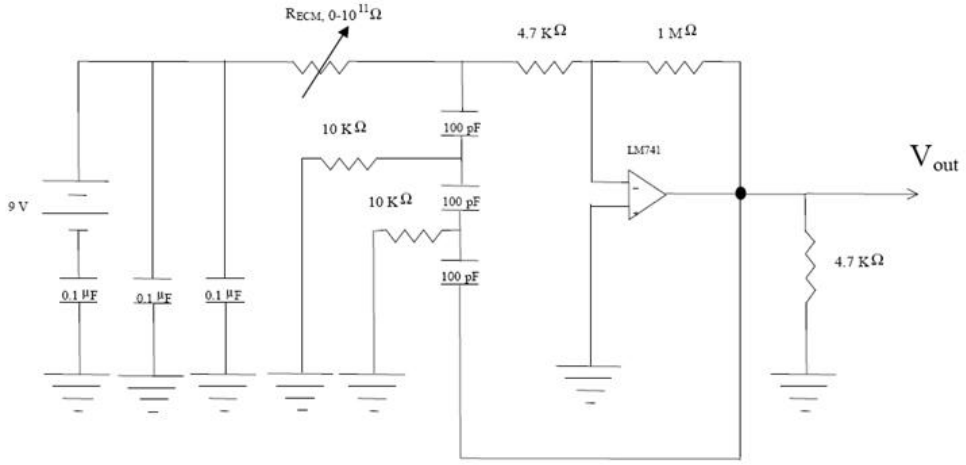

Figure 38 – Electrical Schematic of Ready's Linear Circuit[22]

This circuit serves to monitor the RC time constant formed by the banks of 0.1uF capacitors and the R_{ECM}(sample under test). The circuit operates by switching a bias on to R_{ECM} for a given period, measured by the linear circuit, where the energy from the 0.1uF capacitors discharges into the test sample, R_{ECM}. The exponential discharge response is plotted over time and any deviations from the initial discharge plot are considered a function of the surface insulation. The advantage of this method over the standard SIR testing technique is that it prevents excessive damage of CAF or dendrites, potentially caused by the constant current bias in a SIR test. However, the main drawback with this technique is that it is not a continuous monitoring method and potential signal aliasing may be a concern if electromigration activity is to be observed.

2.4.3 Saturated Condition Test

There are some techniques that can be used to simulate the effects of saturated conditions. The most common is the Water Drop (WD) test where a drop of water is placed between two biased electrodes, see Figure 39. However, the results from the WD test can vary significantly due to numerous factors, including variations in the drop size, the evaporation of the water droplet and water volume to contamination ratio; for example, 1 mole of contamination in the water drop test will have a lower

resistance than 1 mole in a large volume of water, thus affecting the conductivity and resulting in sample-to-sample measurement errors.

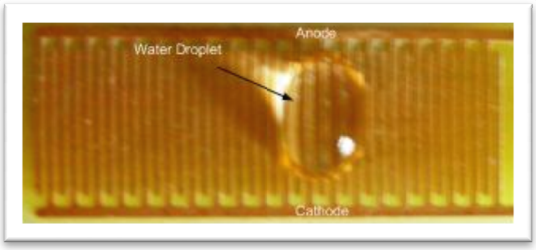

Figure 39 – Water drop Test on a Comb Pattern

A more repeatable method, termed water-filled cuvette test, would involve a larger volume of water that can be accurately measured and is of sufficient size to allow the test piece to be placed inside, although no methods or procedure describing such as method is currently available.

No literature cites or describes either procedures or standards available in the area of saturated SIR testing. Therefore, a new method is proposed in this thesis that addresses most of the weakness of the water drop test and has been termed the water-filled cuvette test.

2.5 Accelerated Life Testing of Electronic Products

Establishing the reliability of electronic products is conducted by testing assemblies to failure under accelerated conditions. This is done by artificially elevating the temperature, humidity and voltage levels of the electronic product. Then, using extrapolation techniques, the normal operating conditions can be estimated.

The effect of temperature on most chemical and electrochemical processes is usually some function of the Arrhenius relationship, as in Equation 11.

$$K = Ae^{(-\frac{E_a}{kT})} \qquad \textbf{Equation 11}$$

The acceleration factor or rate of reaction given by K (dimensionless), and A is an experimentally derived constant (depending on material characteristics and test).

Boltzmann's constant k is 8.617 x 10^{-5} eV/K, T is absolute temperature (Kelvin) and E_a is the value of the activation energy of the reaction (eV).

The Arrhenius equation is valid for a variety of mechanisms such as ionic drift, electrochemical migration and corrosion at fixed humidity[91]. The activation energy is found empirically and a value of 0.9eV encompasses most of the temperature-dependant failure mechanisms seen with printed circuit boards[91].

The effect of the relative humidity (RH) can be described by equation 12[26]:

$$k_H = k_O e^{(C.RH^2)} \qquad \textbf{Equation 12}$$

The acceleration factor is given by K_H (dimensionless), RH is the percent relative humidity and C is a calibration constant equal to 4.4 x10^{-4} for RH in percentage.

Equation 11 and Equation 12 indicate that at a higher temperature, or a higher humidity the acceleration factor or reaction rate is also higher. Sinnadurai[92] proposes a combined form of Equation 11 and Equation 12 to produce a single acceleration factor (A_f) for both temperature and humidity, which is shown in Equation 13. The actual conditions, or normal operating condition, and the accelerated conditions refers to the subscript *life* and *test*, respectively.

$$A_f = \exp\left[B\left(\frac{1}{T_{life}} - \frac{1}{T_{test}} \right) \bullet C\left(RH_{test}^2 - RH_{life}^2 \right) \right] \qquad \textbf{Equation 13}$$

The value of the constants B and C are determined experimentally, although estimated value proposed by Sinnadurai[93], are 8120 and 0.025, respectively.

The expected life (t_{life}) of the specimens under test can be calculated using the acceleration factor from Equation 13 and can be shown as the product of the total test time (t_{test}), as in Equation 14[93].

$$t_{life} = A_f t_{test} \qquad \textbf{Equation 14}$$

2.6 Preventative Measures and Dendrite Design Contingency

The intention of this section is firstly to outline current preventative techniques for reducing failures associated with dendrite formation on electronic products and the problems associated with these methods. Secondly, to propose new areas of investigation to minimise the growth of dendrites in the area of electronic design, termed dendrite design contingency.

There are four main factors required to cause an electrochemical migration failure: metal electrodes, the presence of water, voltage bias and mobile ions that act as catalysts for the initiation of dendrites to grow. The failure mechanisms associated with these factors include several forms of corrosion and resistance changes in the operation of the circuit due to ion migration. Both potentially causing catastrophic failures.

The methods used for preventing dendrites tend to depend on the application in which the product is used, with safety critical and durable systems requiring a high degree of preventative measures. However, applications such as standard home personal computers may include little or no electrochemical preventative measures.

Current preventative methods usually focus on printed circuit board protective coatings which are categorised mainly by thickness. A conformal coating [39] is usually less than 0.1mm thick, and is applied as a very low viscosity liquid that wets all of the surfaces leaving virtually no capillaries. Once thermal or UV curing has been applied, the coating tends to be free from air bubbles and other defects.

Non-conformal coatings [39] are used for more rugged applications and provides a more mechanically robust assembly. However, the application of this type of coating is difficult as the thickness tends to be greater than 0.1mm and as a result air can become trapped within gaps below 0.3mm, due to the coating's viscosity and surface tension. For this reason, when using such coatings the assemblies must be placed in a vacuum chamber to remove all air from beneath the coating.

These coatings are in the form of lacquers and epoxy, with the most commonly used being phenolic, acrylic and silicone lacquers and epoxy[94].

- The advantage of using phenolic lacquers is that they are extremely cheap although limited by their electrical characteristics at high voltages and frequencies. This type of coating is used in non-demanding applications in temperature range -55 to + 125ºC.
- Acrylic coatings are used for temperatures between -60 to +135ºC and provide vastly improved electrical characteristics over phenolic lacquers and are easy to rework, but sensitive to chemical attack.
- Silicone coatings can be used over a wide temperature range (-60 to +260ºC) and provide excellent dielectric characteristics. They also provide good thermal and mechanical shock resistance due to their flexibility.
- Epoxy coatings are used in temperature ranges between -60 to +200ºC and are used where excellent electrical and solvent resistance properties are required but are generally very difficult to remove for rework.

These preventative measures all add cost to the final product, as either materials or processing cost, and therefore methods that can be designed into the product to reduce the risk of dendrite growth provide both improved reliability and improved economics. These measures should ultimately aim to reduce water accessing the printed circuit board conductors by sealing the circuit from the atmosphere. However, if water does infiltrate the conductors on the printed circuit board it is highly likely that a failure will occur. The scale of these failures due to equipment operating parameters is currently poorly documented and therefore makes it difficult to develop contingencies to tolerate or manage these failures. The experimental work covered in the following sections aim to address these concerns by establishing design boundaries derived from a controlled series of experiments.

The implementation of further contingences could allow a product to manage or, at best, tolerate the risks associated with the growth of dendrites. To understand the meaning of dendrite tolerance would involve the parameter window of dendrite growth on a printed circuit board being expanded by exploring the limits of the factors associated with ion migration. There are many areas poorly documented on dendrite growth; three parameters that can be easily controlled are the operating temperature, the operating voltage and the track spacing. These three parameters are design related

and the understanding of the parametric limits with reference to dendrite growth may enable a failure contingency to be developed.

There is limited literature on the impact of dendrite growth at normal operating temperatures (5ºC – 50ºC), as the majority of reliability testing methods use higher temperatures as a method of aging the product, but the risk associated with the growth of dendrites at these operating temperatures is not fully understood.

The same is true for the impact of voltage on dendrite growth, as almost all surface insulation tests for assessing the risk of dendrite growth use voltages much higher than those experienced on typical microprocessor circuits. Higher voltages and currents can provide a self-healing effect by destroying the fused dendrite and many of these tests are not truly representative of normal operating conditions. Identifying the critical dendrite growth characteristics over the range of voltages that are used on a microprocessor circuits would allow for the addition of a failure contingency and thus reduce the impact of any dendrite growth.

Whilst it is understood that via and track spacing influence the risk of CAF formation there is very little literature on the impact of track spacing on dendrite growth. The mechanism that causes a CAF formation is usually associated with the large pH gradients experienced at the electrode interfaces and if these interfaces are sufficiently close the acid/base interfaces form metallic salts. Dendrites, on the other hand, are formed by the process of migrating metal ions and therefore track spacing may yield different results.

The following experimental work aims to provide both an understanding of electrochemical reliability impact on printed circuit boards and to develop a model and subsequently design guidelines for reducing dendrite susceptibility, called a dendrite design contingency.

Chapter Three: Experimental Approach

This Chapter describes the equipment, samples and configurations of experiments to develop the background to understanding the parameters involved in dendritic growth.

3.1 Sample Designs

Commercial non-plated copper Vero board shown in Figure 40 was used for the preliminary experiments. This board has a 2.54 mm spacing with copper thickness of 35um on fibreglass (FR4) substrate. The copper was cleaned with ammonia and rinsed in isopropanol and deionised water.

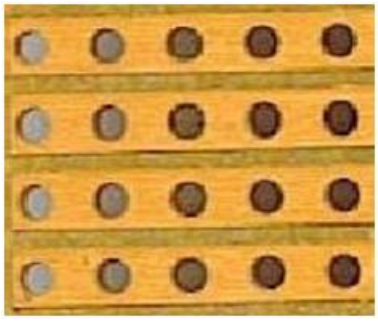

Figure 40 – Image of Vero Board Used

A custom printed circuit board (PCB) was required for the dendrite growth experiments and developed for this research. The PCB was designed with four different sample configurations, Figure 41 and Figure 42. The first three samples (Comb Samples) consist of a finger-comb style design, with distances between the fingers of 0.2 mm, 0.3 mm and 0.4 mm (8 mil, 12 mil, 16 mil) respectively. These are typical track spacing values used in the design of automotive engine controllers. The fourth sample (SMD Sample) was produced with a single surface mounted component pad. Each of the samples was separated with a score line used to break each sample

from the main PCB. The PCB was manufactured from one ounce copper[1] and the thickness of the copper surface features was 70µm.

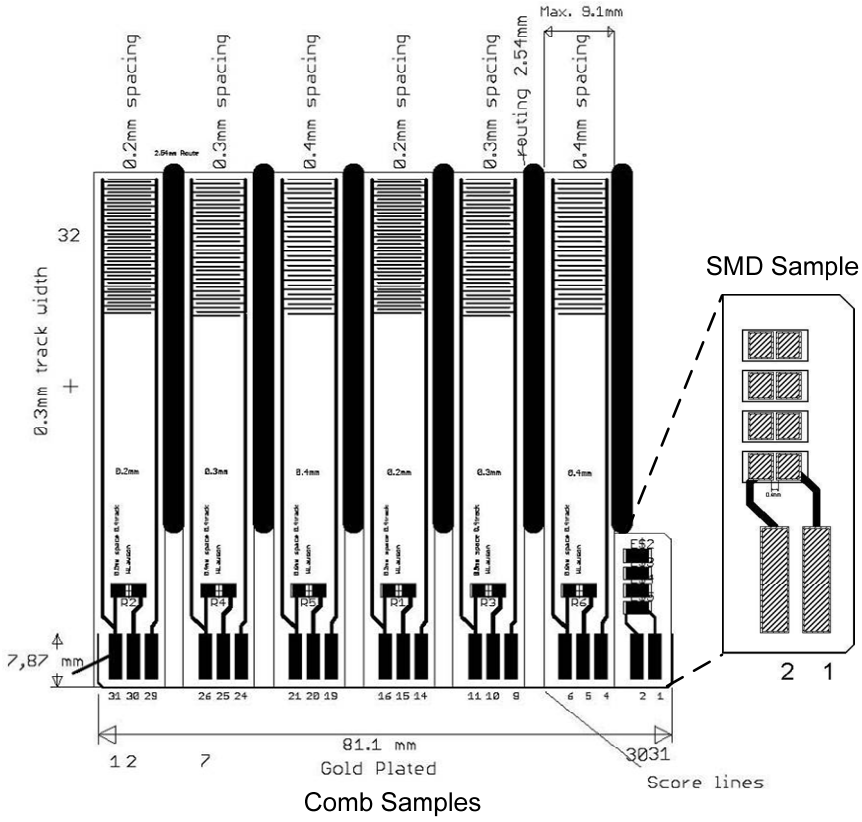

Figure 41 – Left, PCB Design. Right, Magnified View of SMD Sample

The combs were gold-plated with nickel barrier to preserve the copper track; as copper can easily oxidise and even corrode under the influence of atmospheric contaminants. Other protective barriers are HASL solder (Hot Air Solder Level), organic coatings and tin plating. However, these coatings can only provide a very short shelf-life, or may contaminate the copper with complex compounds or may leach into the copper.

[1] (1oz over $1ft^2$), the printed circuit board industry still uses imperial measurements and most of the standards are therefore shown in imperial measurements.

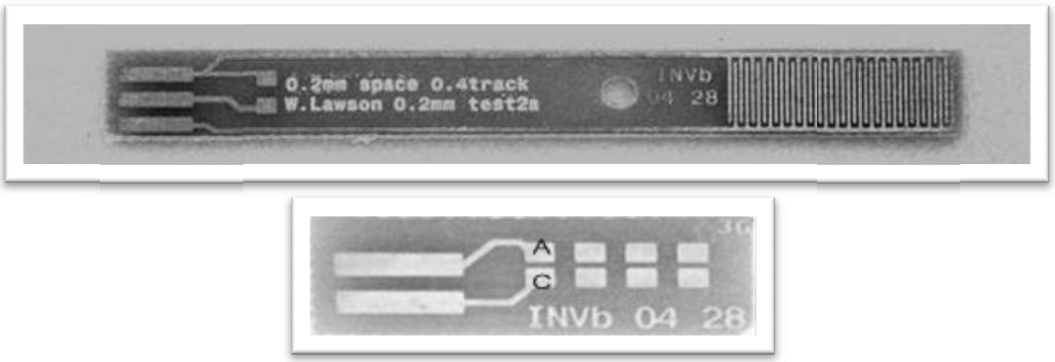

Figure 42 – Top, Single Comb Sample. Bottom, 0.4 mm spaced SMD Sample

3.1.1 Removing the Gold Plating

Before the combs were used in an experiment the gold was removed by ultrasonically agitating in a solution of 10 g potassium-iodide, 6 g iodine and 10 ml water, or until the potassium iodide solution became saturated. This process removed the gold although it did leave a non water-soluble brownish-white residue on the copper, shown in Figure 43.

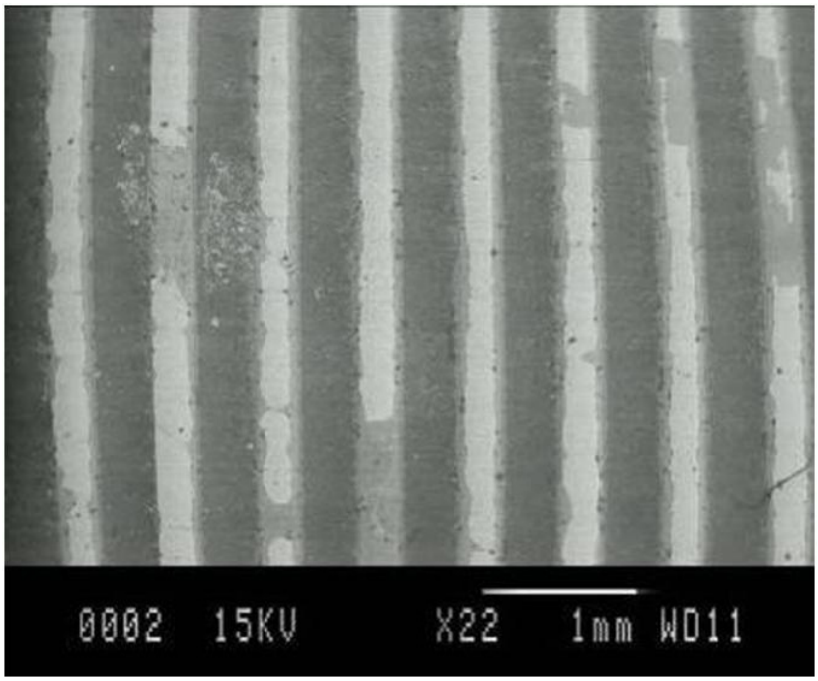

Figure 43 – After Gold has been Removed

As a method of establishing the residue's elements, an EDX analysis was conducted, shown in Figure 44. From the EDX analysis a large iodine peak can be seen. Reference literature[52] suggests a brownish-white compound formed from copper and iodine is likely to be copper iodide (CuI). Copper iodide has a poor solubility in water although it is soluble in liquid ammonia.

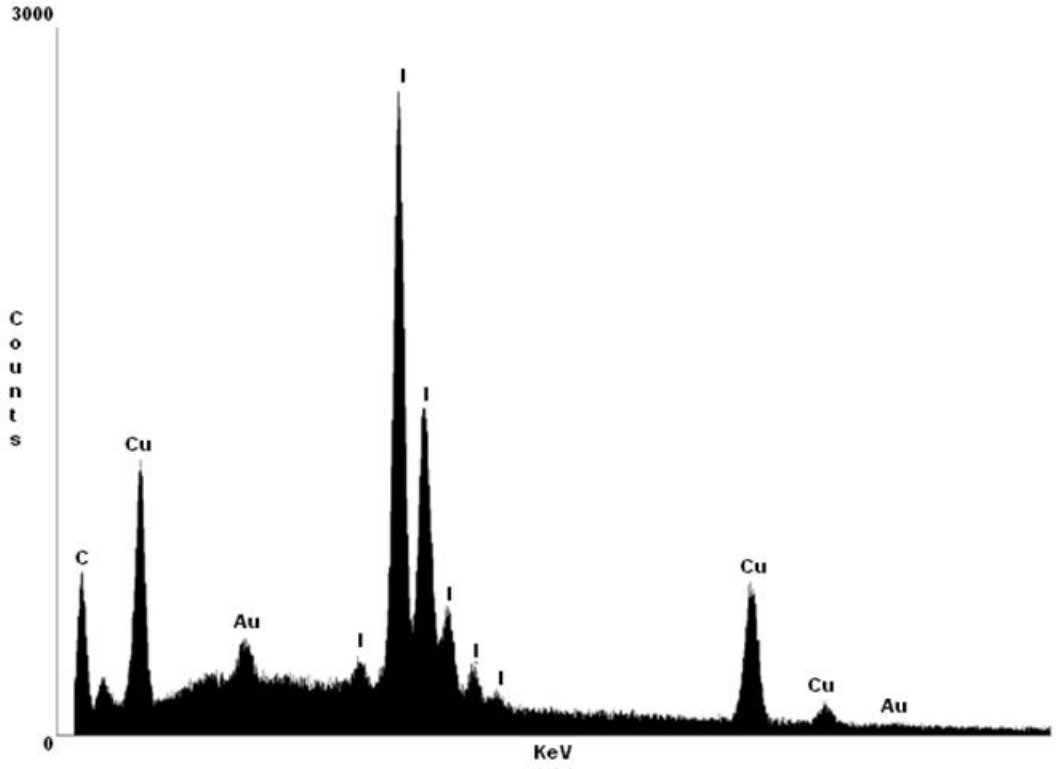

Figure 44 – EDX after Gold Removal, Note the high iodine content.

Agitating the combs in a dilute solution of ammonia served to remove the copper iodide and expose the copper. The EDX analysis in Figure 45, clearly shows the ammonia solution removed virtually all the iodide. The combs were finally rinsed in deionised water before use.

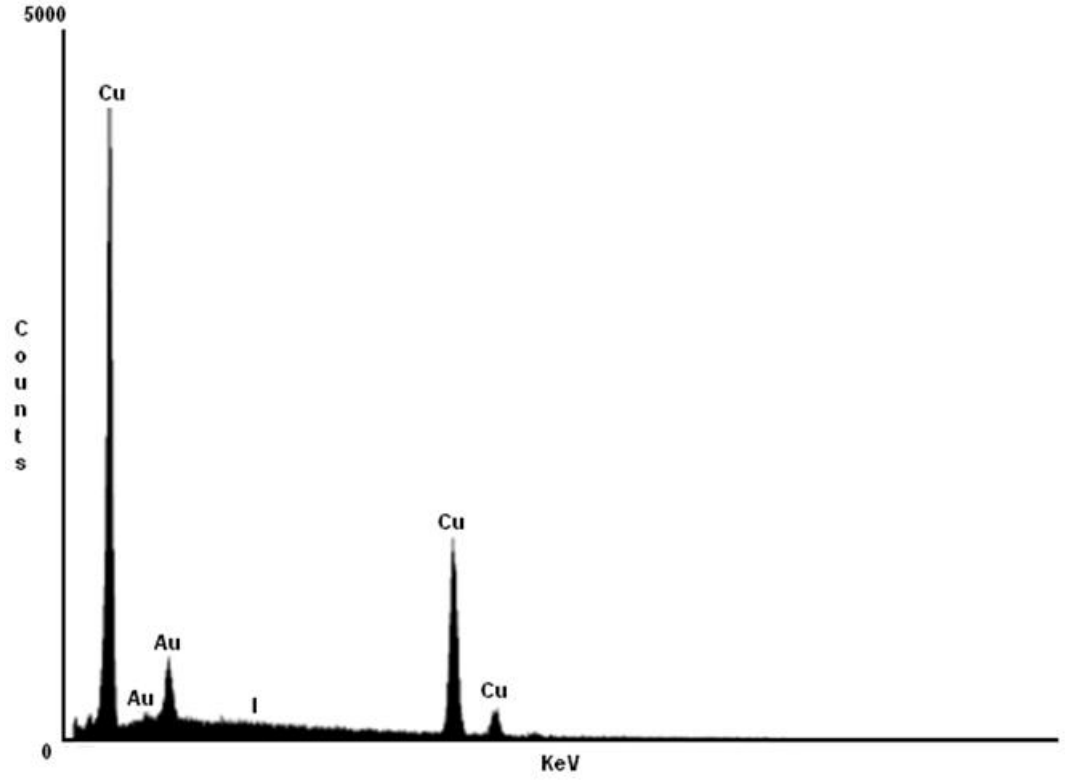

Figure 45 – EDX of Ammonia Cleaned Comb, Note the absence of iodine.

3.1.2 Sample Preparation

To ensure the samples were free from contaminants, such as oxides and grease, the copper iodide was left on the samples and removed with ammonia within a standard one hour preparation time of the experiments being conducted. The samples were then cleaned in isopropanol and finally rinsed in ultra-pure deionised water.[2] The samples were then allowed to dry at ambient temperature (< 25°C) to minimise growth of copper oxides. Samples left for more than 5 hours were re-cleaned using the aforesaid method.

The growth of copper oxide (Cu_2O) at room temperature proceeds at an exponential rate for approximately 100 hours, after which it proceeds to grow at a linear rate. After 90 days a layer of thickness 10 nm is formed. Heating copper to 105°C produces the same thickness of oxide [26].

[2] Water was purified using Elga PURELAB Option DV35 and Elga Ultra. These are coupled and produce 0.0666uS·m^{-1} and 0.055uS·m^{-1} water respectively.

3.2 Design of Experiment

To analyse the data efficiently for the saturated experiments, a method known as factorial design is used to reduce the number of test runs and obtain a deeper understanding of the results gathered. Factorial designs are part of a group of statistical analysis techniques called Design Of Experiments (DOEs) and there are several texts [95-98] that detail its theory.

DOE is a collection of statistical and mathematical techniques used to develop, design and formulate complex systems, and to improve existing product designs [97]. DOE techniques are effective in identifying factors that have the greatest influence on the measured response of 'black box' systems, i.e. complex systems. They are an efficient method for exploring trends in an unknown response space. DOE is the process of planning an experiment so the appropriate data will be collected and analysed by statistical methods, resulting in an objective conclusion from the data.

There are three basic principles of DOE used in this research: replication, randomisation and factorial design.

- Replication is the repetition of a given experiment. Replications allow the determination of the experimental error, used as the fundamental unit of measure for determining whether observed differences in the data are statistically significant.
- Randomising a design cancels the impact of many factors neglected in an experimental design. The correct randomisation of a design can ensure extraneous factors that may be present are applied equally to all test samples, in effect averaging over the experiment [96] and thus minimising any latent time-related factors that might bias the results [99].
- In a factorial design several factors are varied simultaneously according to the experimental configuration; the results are then logged as a response. For example, if k variables are being investigated and each variable has n levels (values) then a full factorial design requires k^n experiments to analyse all possible combinations of the experimental space. If an experiment has three variables that are of interest and each variable is to be studied at three levels then a total of 27

(3 x 3 x 3) experimental runs must be performed to investigate the parameter space fully. In the saturated experiments, three factors were studied but each factor had a different number of levels (3, 3 and 5), thus a total of 45 (3 x 3 x 5) runs. Using more than two levels allows the identification of non-linearity within the experiment; hence the term multilevel factorial.

3.3 Experiment Structure – Flowchart

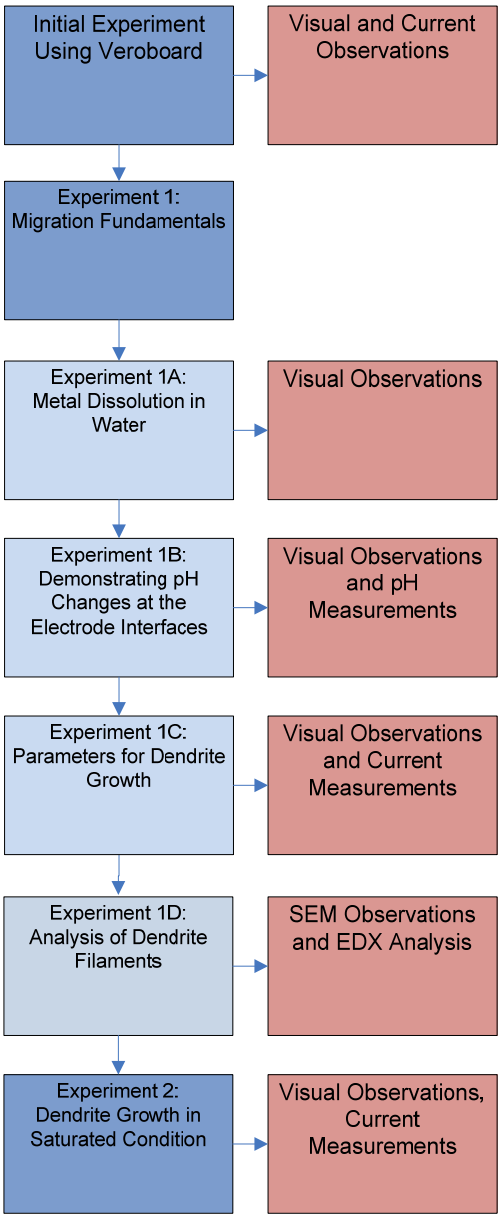

Figure 46 – Experiment Flow Chart

3.4 Experimental Setup

3.5 Fundamental Experiment – Observations of Dendrites

The initial work involved a number of simple experiments. These required a number of small pieces of Veroboard™ (used for circuit prototyping), a video microscope, a signal generator and tap water (pH 7). The outline setup is shown in Figure 47.

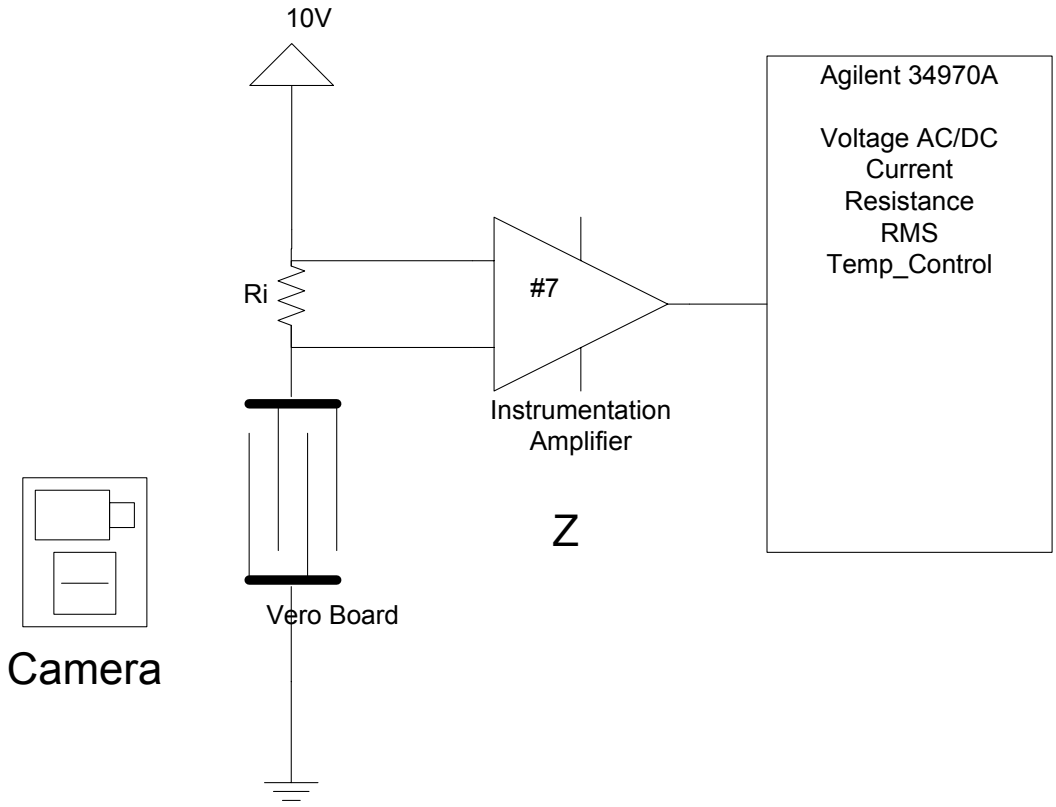

Figure 47 – Setup of Biased Piece of Vero Board

The test samples consist of a section of standard Vero board. A wire is soldered to each strip (electrode), and a DC power supply and a signal generator are used as the bias power sources. The bias is applied across the copper strips with a small amount of distilled water ($0.1 uS \cdot m^{-1}$) used. These samples are placed under a microscope and filmed using time-lapse photography.

The first test involves a specimen of 10 mm length Vero board with a drop of tap water with a bias of 10 volts DC applied. Observations reveal initial gas evolution before the first signs of a dendrite tip. After tip formation, dendrite growth is not

observed until 10-30 seconds have elapsed. Not all tips develop into dendrites. This seems unusual because, from the literature [71], the growth of a dendrite starts from a point source and emanates at an exponential rate, due to the increase of energy as it moves closer to the opposing electrode.

3.5.1 Configuration of Experiment 1A: Metal Dissolution in Water

The dissolution of metal ions is demonstrated in several experiments that involve the use of standard commercial grade copper and platinum leaf. To conduct these tests a metal leaf test fixture is made from a glass slide and two graphite electrodes. This fixture allows the metal leaf to be placed onto the graphite electrodes and suspended in deionised water ($0.055 uS \cdot m^{-1}$), shown in Figure 48. The water is kept in place by bonding two glass tubes at either side of the graphite to produce a water-tight seal. Each of the graphite electrodes is electrically connected to an adjustable-voltage power supply. To minimise the effects of depth-of-field on the microscope, the metal leaf is suspended on top of the water's meniscus.

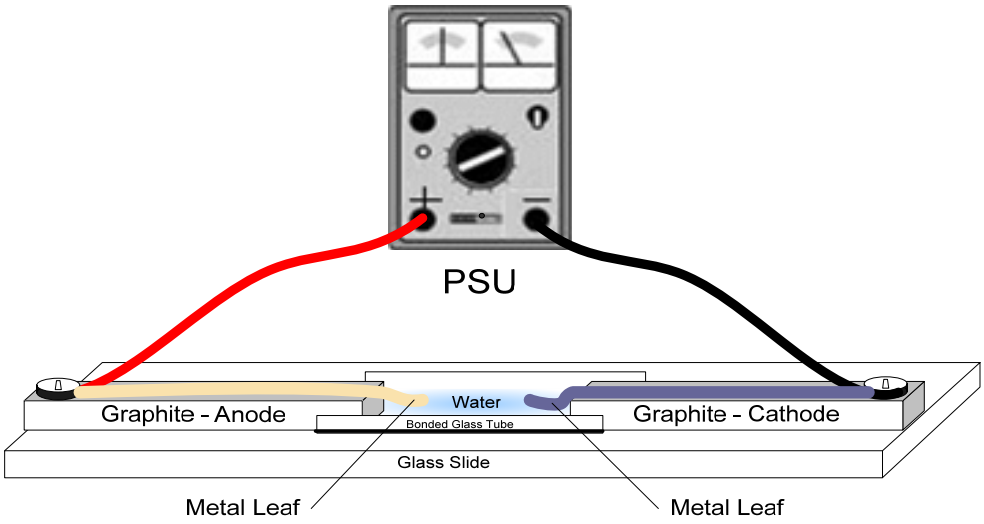

Figure 48 – Equipment Configuration for Metal Leaf Test

3.5.2 Configuration of Experiment 1B: Demonstrating pH Changes at Electrodes

The changes in pH at the electrodes' interfaces were demonstrated by two experiments, both biased by a 15 volt power supply. The first experimental setup involved a custom-built electrochemical cell shown in Figure 49. The cell was built on a glass slide with two graphite electrodes bonded on each side of the slide, using an automotive grade silicone sealant (Dow Corning SE 738 Clear). The Dow Corning sealer was used because of its inert and non-corrosive properties towards electronic products. Along the side of the two electrodes, two pieces of fine glass tube were also bonded producing a water tight reservoir. The reservoir was used to hold the deionised water and universal indicator solution.

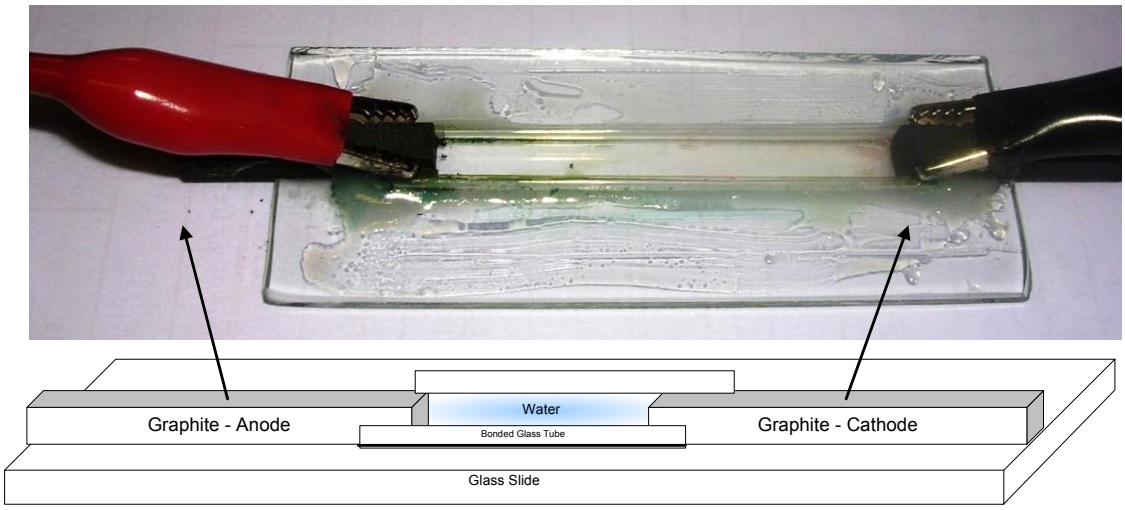

Figure 49 – Custom Electrochemical Cell

The second experimental setup involved applying a 15V bias to a typical printed circuit board contaminated with deionised water and universal indicator solution. The printed circuit board consisted of soldered copper tracks coated with a green solder resist, shown in Figure 50. The electrodes were tinned copper leads soldered to the pads.

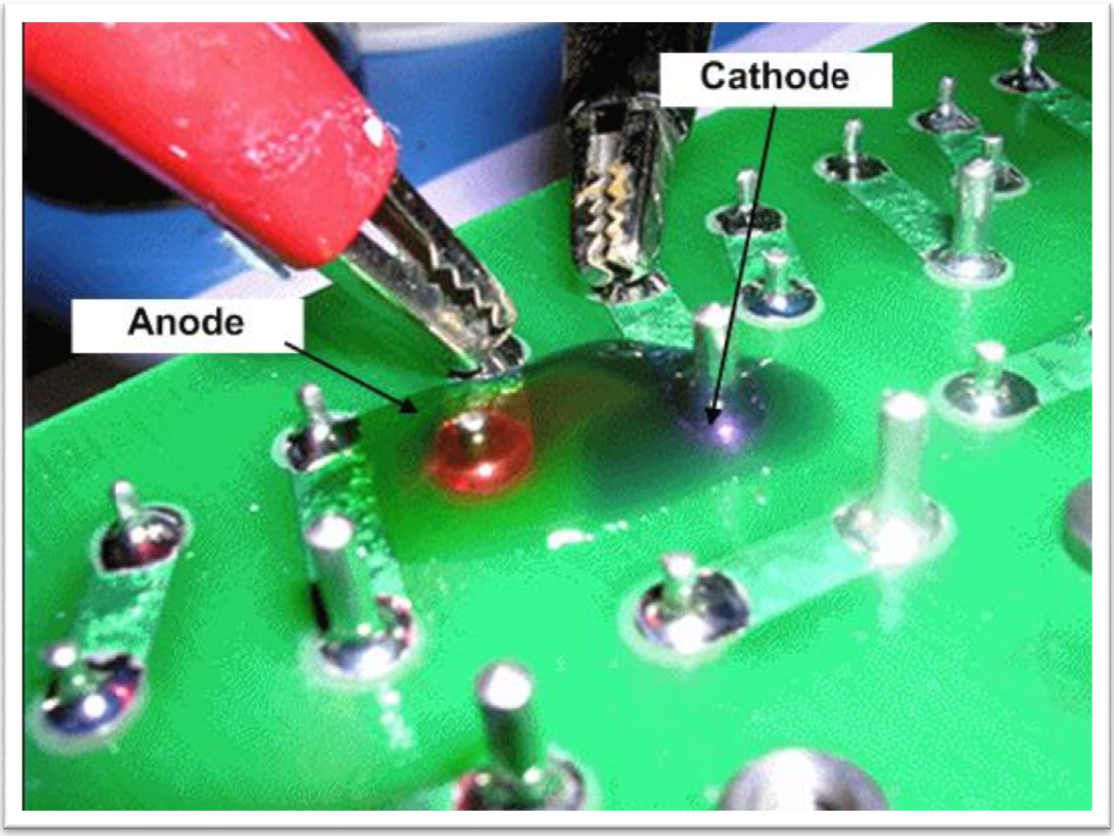

Figure 50 – Printed Circuit Board pH Sample

3.5.3 Configuration of Experiment 1C: Parameters for Dendrite Growth

As a method of controlling and identifying conditions required for the growth of copper dendrites a number of water drop tests were conducted on equipment built to control the temperature and both stabilise and sweep the voltage. Schematic and photograph of the equipment configuration are shown in Figure 51 and Figure 52.

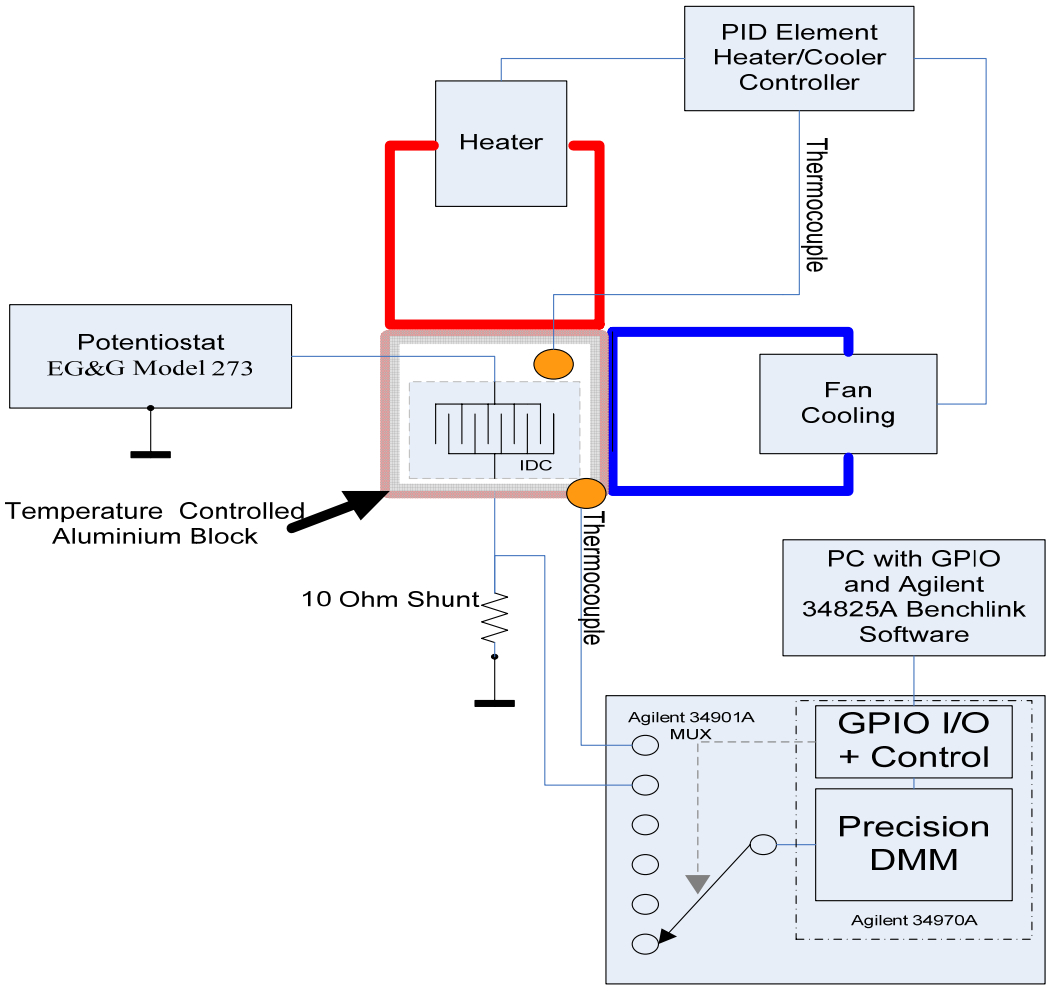

Figure 51 – Schematic of Conditional Dendrite Growth Equipment

A constant temperature was applied to the sample using a PID controller, using both heating and cooling to ensure the sample was not exposed to excessive thermal hysteresis. The voltage bias was provided by an EG&G Model 273 potentiostat, which could provide step and sweeping voltages at a constant current. The current flowing through the sample was measured from a shunt resistor with the potential drop being read by an Agilent 34901A precision data logger.

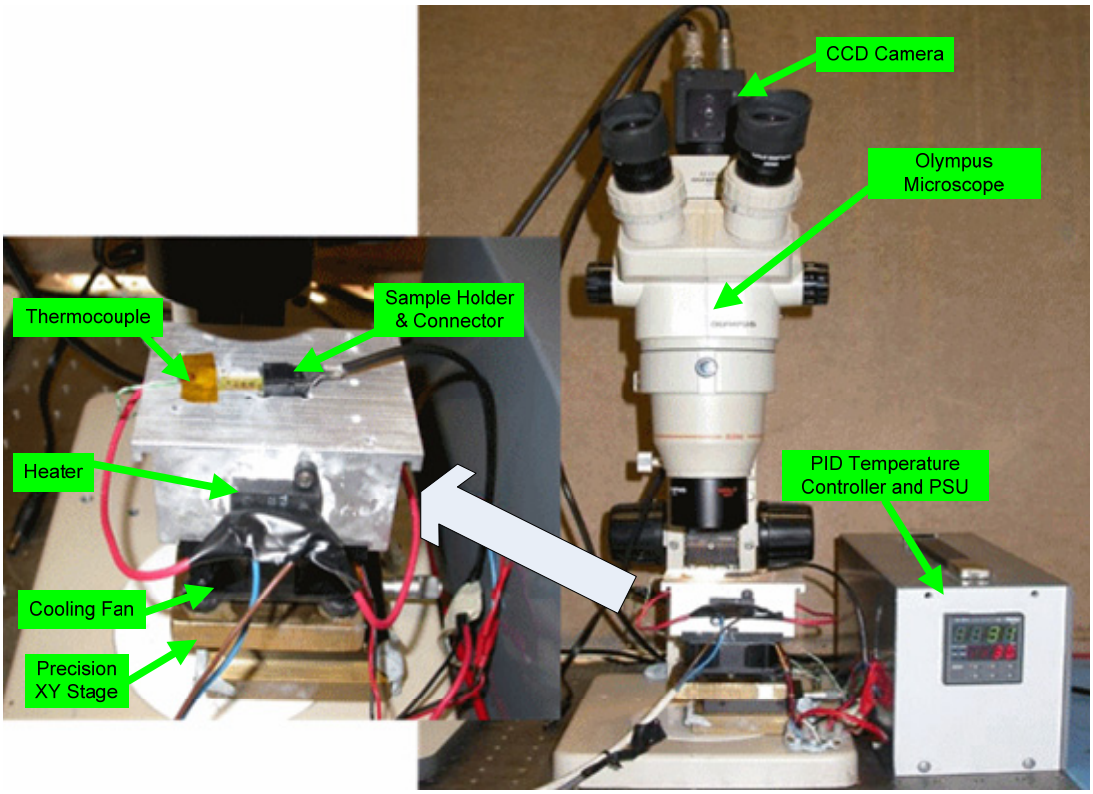

Figure 52 – Photograph of Conditional Controlled Dendrite Growth Equipment

The experiments used the SMD sample boards. The SMD sample was connected to the equipment by a moulded edge connector, which fitted into the countersunk aluminium heat block. The sample was then secured with the thermocouple and a piece of thermal tape. Both the anode and cathode pads were completely covered with a single drop of deionised water using a pipette.

3.5.4 Configuration of Experiment 2 – Dendrite Growth in Saturated Conditions

The analysis of dendritic growth under saturated condition was undertaken using the water filled cuvette method and the equipment setup shown in Figure 54.

The water filled cuvette method involves using transparent scientific grade cuvettes with a volume of 1.2 ml. The cuvette is filled with deionised water, and the electrodes and comb samples are placed into the opening. Any dendritic growth can be observed from the front by a microscope or a macro-lens after the test have been run, which prevents disturbance of any growth from the film of the water, Figure 53.

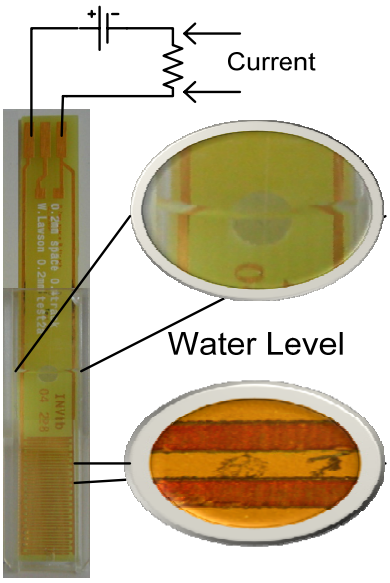

Figure 53 – Water Filled Cuvette Test

Constant voltage sources were used to bias five test combs placed into cuvettes. The cuvettes were held in a machined brass block and temperature was regulated *via* a PID controller, which adjusted the temperature of the brass block. The brass block was also cooled to 0°C; allowing for lower temperature stabilisation, i.e. 5°C and 25°C.

The current through the combs was measured *via* the volt drop across the 10K ohm resistors and recorded on the Agilent data logger. The results of each of the experiment were transferred to Excel for analysis.

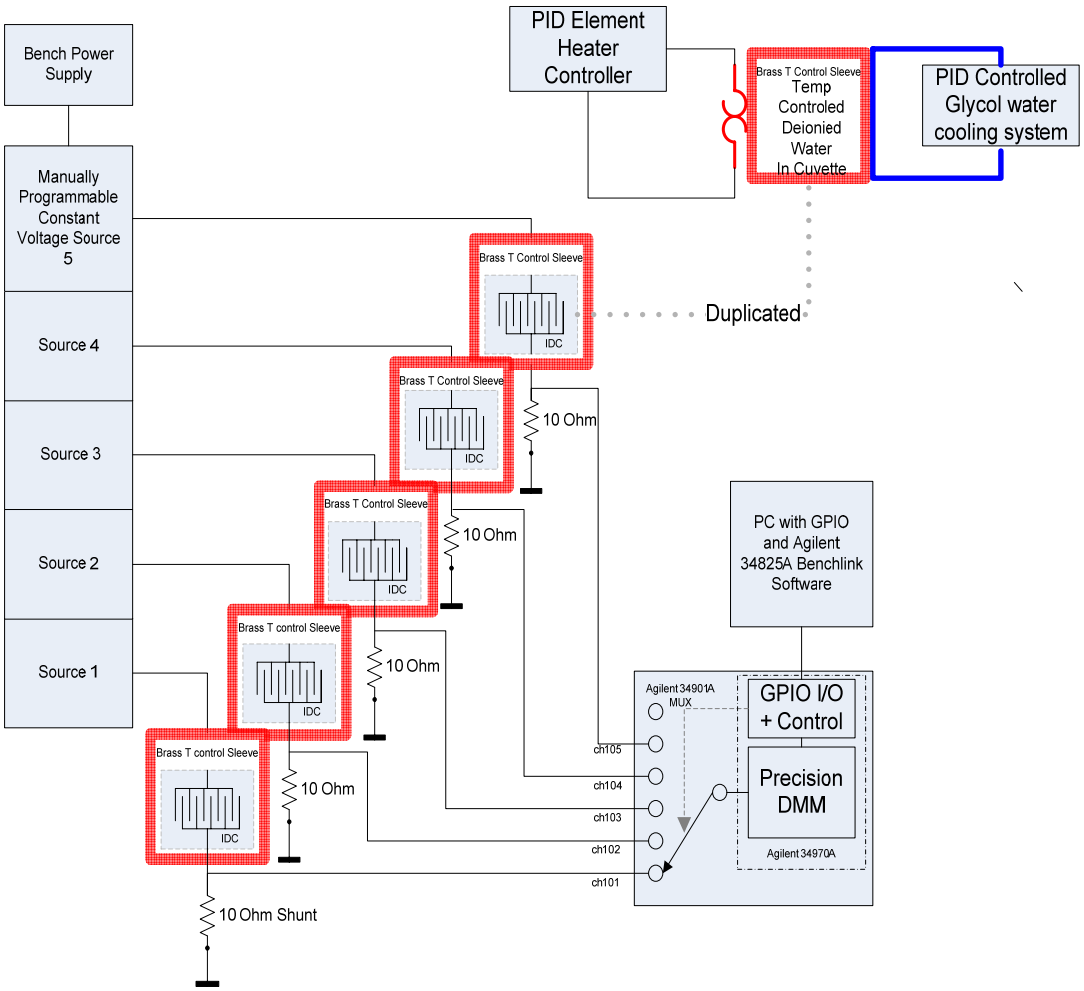

Figure 54 – Schematic: Dendrite Growth under Saturated Condition Equipment

Chapter Four: Fundamental Experimental Observations of Dendrites

The first experiments using Vero board were video observations of dendrite growth using an optical microscope. Tests were conducted on copper Vero board samples with a 10 V DC bias. The first experiment was the observation of the effect of DC on the sample. Before the bias was applied a drop of deionised water was placed between the two electrodes. Once the bias was applied, the time-lapse camera was activated. The time-lapse was set to 2 seconds per frame. When the current was first applied to the copper sample, shown in Figure 55, the generation of gas bubbles was very rapid and took place on the cathode, Figure 56.

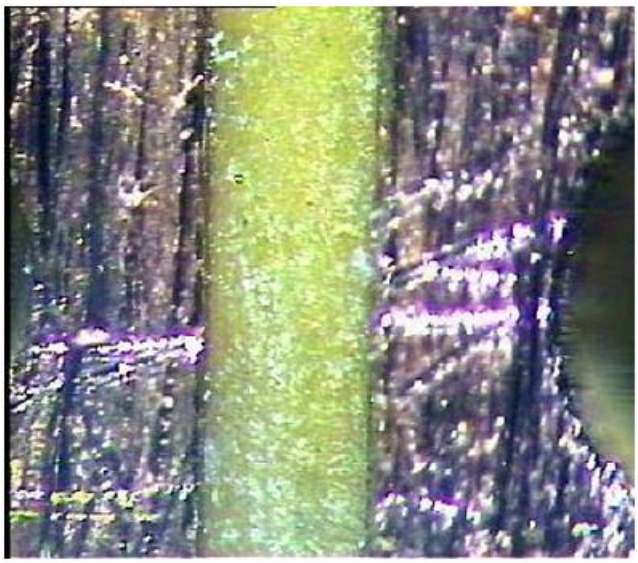

Figure 55 – DC bias on copper initial state

Figure 56 – DC bias on copper just after bias applied

Within 10 seconds the bubbling slowed down and small formations started to grow from the cathode electrode. These formations started growing towards the anode electrode with a tree-like structure – commonly known as a dendrite; images in Figure 57, Figure 58, Figure 59 and Figure 60), with cathode shown on the right and the anode on the left.

Four phenomena were apparent from the observations:

- Firstly, the starting time for a dendrite to initiate seemed to be random in nature.
- Secondly, the fractal nature of the dendrites differed from sample to sample.
- Thirdly, the fusing effect when a dendrite shorted the electrodes, and
- Finally the creation of gas bubbles.

Both initiation times and fractal nature of the dendrites are associated with contamination levels [38, 39, 66] and indicate that the sample preparation procedure may improve these characteristics.

Figure 60 shows the dendrite has stopped growing and a slight blow-out can be seen, circled, resulting in small black fragments and a break in the dendrite.

Figure 57 – First Phase of the Growth of Dendrites

Figure 58 – A Dendrite Dominates the Current Path.

Figure 59 – Moment the Dendrite made Contact with the Anode, before it 'fused'.

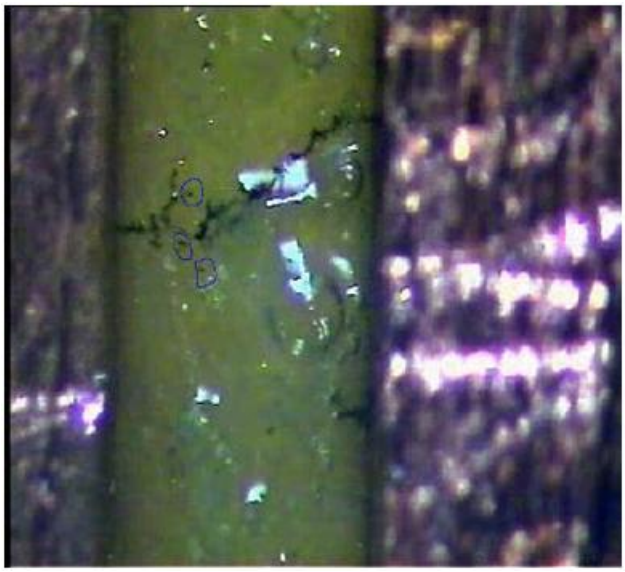

Figure 60 – The Fused Dendrite, the blue circles shows the break.

Figure 61 shows the final phase of the experiment where no further dendritic growth was initiated or continued. The electrolyte (water) has been replaced by a blue-crystallised material. It is noted a dendrite tends to be produced close to the point where hydrogen is being formed, at the cathode. Areas with no gas formation yielded no dendrites. It is not certain why this happened but this phenomenon needs to be further investigated.

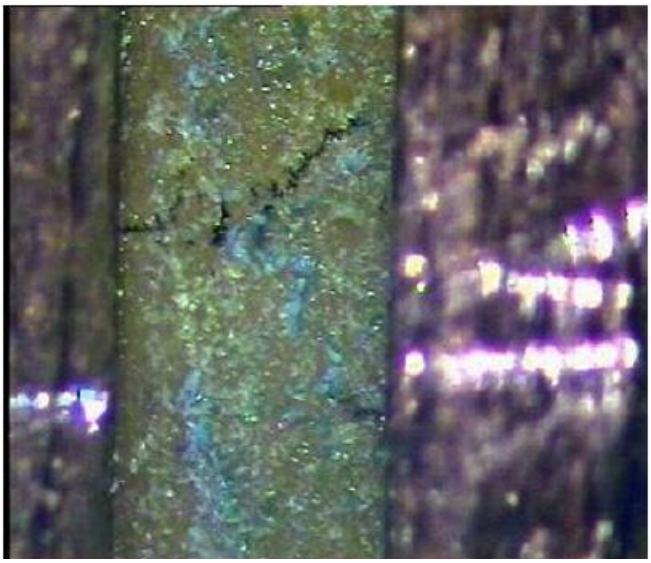

Figure 61 – Final Stages of Experiment: Blue-crystallised Finish

The electrodes used are both copper, and their activity in terms of electrochemical half-potentials may be irrelevant; the sample will not operate like a galvanic cell. The voltage and current generated by a galvanic cell are directly related to the types of dissimilar materials used in the electrodes and electrolyte.

The selection of the anode or the cathode biasing polarity is based on the polarity of the bias applied, and not offset by any additional electrode potential. For example, if a metal with a different electrochemical potential was used this could change the cell potential. However, if one of the electrodes oxidises then this would change the net potential required to start migration, i.e. (Ec-Ea) – Vsupply.

Initially, as the bias was applied to the sample, fierce bubbling occurred at the cathode. This could be explained by examining the reactions that occur at both the anode and the cathode. The anode produces hydrogen until the copper has oxidised and slowly reduces surface energy, therefore inhibiting the migration potential. In the presence of aqueous contamination, the electrochemical reactions that can occur at the anode and cathode are given in Table 8 [100].

Equations	Anode	Cathode
1	$H_2O \rightarrow \frac{1}{2}O_2 + 2H^+ + 2e^-$	$O_2 + 2H_2O + 4e^- \rightarrow 4OH^-$
2	$Cu \rightarrow Cu^{+1} + e^-$	$2H_2O + 2e^- \rightarrow 2OH^- + H_2$
3	$Cu \rightarrow Cu^{+2} + 2e^-$	$Cu^{2+} + 2e^- \rightarrow Cu$
4		$Cu^+ + e^- \rightarrow Cu$

Table 8 – Reaction at Both Electrodes

The stepped growth of a dendrite is shown in the images of Figure 57 to Figure 61. The two electrodes are made of the same material and placed into an electrolyte. When the bias is applied, a current flows through the electrolyte, initiated by any free ion in the fluid. Close to the cathode, ions are reduced by electron transfer from the electrode and form a growing deposit. The inverse takes place at the anode; metal is dissolved and new ions are formed. For liquid electrolytes, as used in this experiment, the non-uniformities in the ion concentrations and the heat produced at the electrodes as a result of redox leads to strong convective flows. If the electrolyte (or contaminate) had a higher viscosity (gel-like) then convection is restricted and ion transport can only be caused by diffusion and migration of the ions [101]. Convection flow of small contaminants, such as debris, was observed on the sample when the volume of water was at its greatest.

A single needle-like point on the surface of the cathode would give rise to high current densities, thus the cathode would pose the most likely platform for the birth of a dendrite because a large current density would propagate at this point. This could be tested by creating a needle-like point on the cathode although the point would need to be in the order of 1um diameter [71].

Chapter Five: Results and Discussions of Experiment 1 – Parameter Space of Dendritic Growth

The main aim of this work is to investigate the parameters required for a suitable model to reflect the characteristics of dendrite initiation time, relative to temperature, voltage and track spacing. Conclusions drawn from these fundamental experiments were used to refine the parameter window for the factorial design used in Experiment 2, in Chapter Six:. Whilst the known working region has been defined for temperatures 5ºC to 50ºC, the critical ranges for voltage and land distances for optimum, (i.e. minimum growth), dendritic growth requires further refinement.

The aim of the first set of experiments is to visually demonstrate the foundations associated with electrochemical failure modes in electronic products. The impact of contaminants, dendrite fusing, metal dissolution, pH gradients and the impact of biased voltage levels is investigated. The flow of the experimental order is shown in Figure 46.

5.1 Experiment 1A: Metal Dissolution in Water

As in the Chapter 2 literature review, when metals ionise they become cations and migrate from the anode to the cathode when biased in an electrochemical cell. However, not all metals readily ionise in water, for example platinum and palladium.

5.1.1 Copper Dissolution in Water

In an aqueous solution copper can migrate with ease in both electroless and electrodeposition systems. In an electroless (or corrosion) system, copper dissolution can occur via the potential differences in the standard reduction potentials from the half-reactions in Equation 15 and Equation 16, respectively [102]. Copper dissolution in an electrodeposition (or electrochemical) system occurs via the biased electrodes that form the electrochemical cell.

$Cu \rightleftarrows Cu^{2+} + e^{-}$ standard electrode potentials = 0.37 V **Equation 15**

$HO_2^{-} + H_2O + 2e^{-} \rightleftarrows 3OH^{-}$ standard electrode potentials = 0.87 V **Equation 16**

Copper migration and dissolution in an electrodeposition system was demonstrated by placing two copper leaf strips on each of the fixture's graphite electrodes and suspending them on the meniscus of ultra pure water. After biasing the fixture at 15V, the copper leaf on the anode started to 'dissolve' very quickly thus demonstrating the transportation of copper ions, $Cu \rightarrow Cu^{+} + e^{-}$, towards the cathode as shown in Figure 62. The gas bubbles observed are oxygen as shown by $2H_2O \Rightarrow O_2(gas) + 4H^{+} + 4e^{-}$

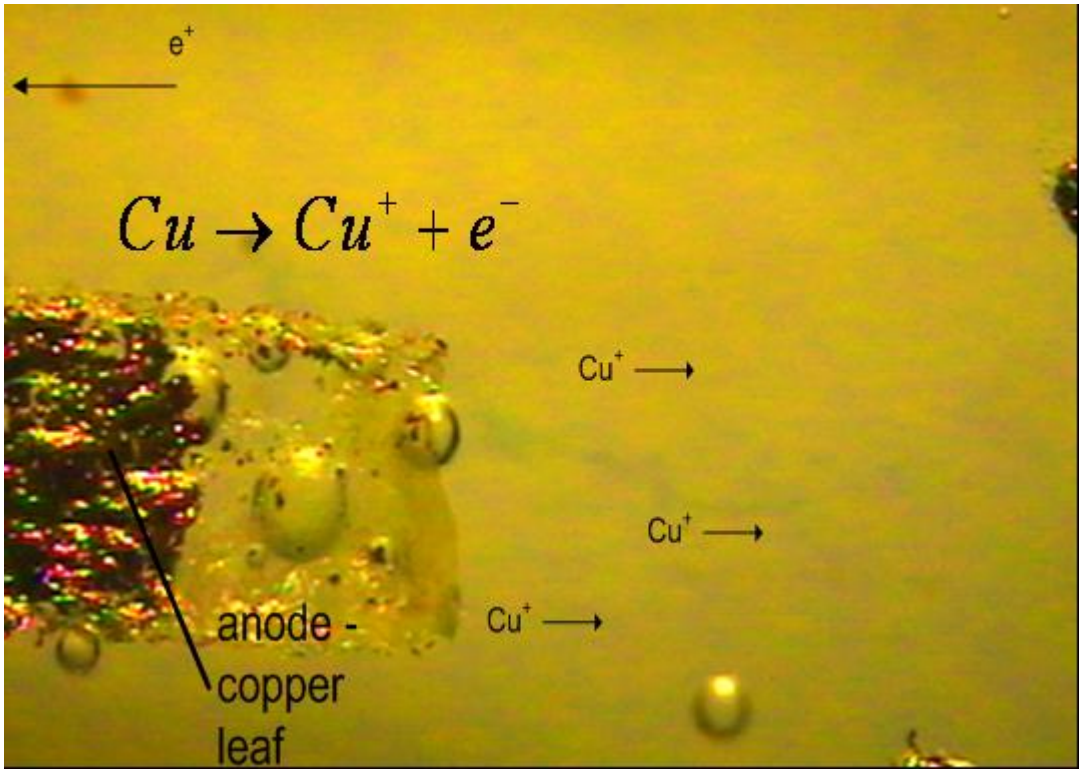

Figure 62 – Copper Dissolution in Water at the Anode: Cu+Cu Electrodes

On the cathode side there was no sign of metal dissolution, although there were visible signs of hydrogen gas production ($2H^{+} + 2e^{-} \Rightarrow H_2$) and a single dendrite. Copper ions formed from the dissolution of the copper migrating towards the cathode and form a dendrite if a nucleation point is sourced. To confirm the cathode acts as a charge carrier for the process of dendrite growth, the cathode metal was changed to an inert material, namely platinum, and re-biased with 15V. After a few seconds a

dendrite was evident on the platinum cathode, as in Figure 63. The dendrite was thus grown from a process of positively charged deposits on the cathode and therefore it is possible dendrites could be formed on any conducting material.

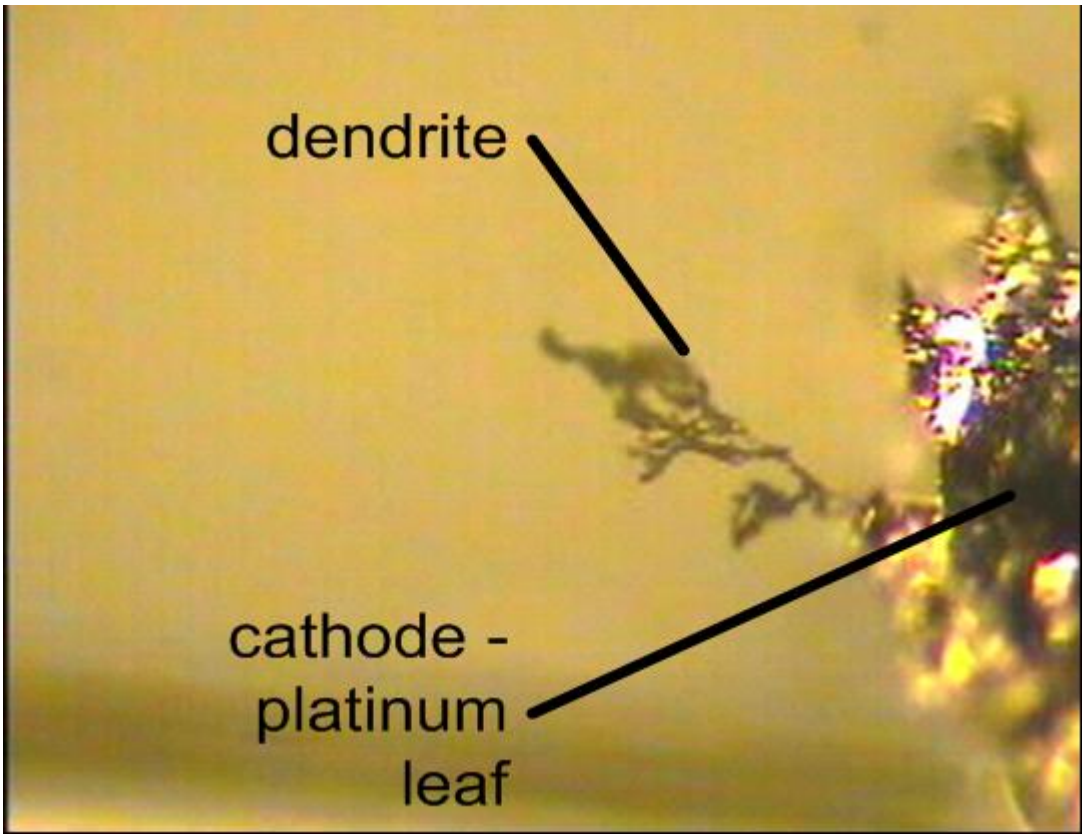

Figure 63 – Dendrites Forming at Platinum Electrode

If the copper leaf anode is replaced by platinum leaf and the copper cathode leaf is again biased with 15V then it is seen that the platinum anode does not dissolve and therefore no dissolution or dendrite growths are visible, as shown in Figure 64.

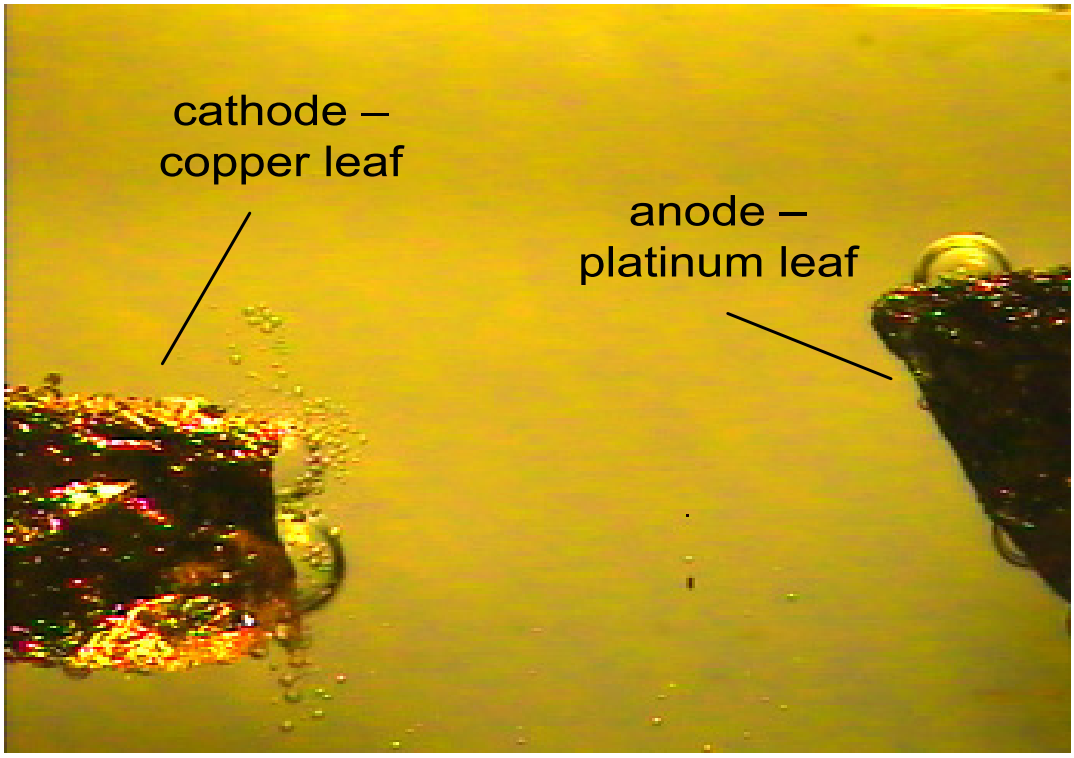

Figure 64 – Electrolysis with Copper Cathode and Platinum Anode

These tests show the copper anode dissolving in the water and forming copper ions, which migrate towards the cathode. These copper ions deposited on the cathodic electrode formed dendrites on both copper and platinum cathodes. Switching the cathode material to an inert metal also allowed the growth of a dendrite. Thus the influence the cathode has on the growth is in the form of a conductor, providing a path for the flow of electrons, rather than a species contributor.

5.1.2 Discussion

The dissolution of metal under electrolysis, Experiment 1A, was the first test in a series of experiments (Experiment 1) to visually demonstrate a number of the mechanisms associated with electrochemical migration failures. This experiment shows the dissolution of copper at the anode using commercial grade copper leaf when biased. The copper leaf was initially used as both the anode and the cathode. When the bias was applied it was observed the anode copper leaf rapidly dissolved into the water whilst on the copper cathode a dendrite began to form. The effect of the cathode material has no effect on its ability to grow or act as a charge carrier as demonstrated

by changing the copper cathode to platinum leaf, a known electrochemically inert material. In this configuration a dendrite still grew on the cathode. However, the metal used at the anode does affect both the growth and the dissolution rate. Replacing the copper anode with platinum leaf yielded no dendritic growth on the cathode nor was there any dissolution at the anode.

Therefore, on a printed circuit board the electrochemical failure mode on a particular land such as track, pad or via would depend on the polarity and the metal used. For a positively biased land, metal erosion is likely to occur. Erosion would be dependent on the metal used and the contamination available, with the electrochemical migration potential of some common metal used in the electronics industry shown in Table 4, demonstrating clearly that copper only requires water to migrate.

For negatively biased lands dendritic growth is likely to occur, and although this would be independent of its own cathodic metal the probability of dendritic growth would differ dependent on the anodic metal used and the pH at the cathode interface. The Pourbaix diagram for copper, Figure 19, shows the cathode stays mainly immune over all pH ranges, with signs of passivation caused by copper oxidisation at pH levels greater than approximately pH 8 and voltage level below approximately 0.5V. At these parameters the cathode would oxidise and potentially become immune from further dendritic growth due to the resistivity of copper oxide formed around the negative land. If, however, the polarity of the land changes, due to a function of the circuit, then these conditions would change to that seen on the positive land and the effects of pH would change, as also shown in Figure 19.

5.2 Experiment 1B: pH Changes at the Electrode Interfaces

Two experiments were used to demonstrate the change of pH at the electrode interfaces of a simple cell and between two printed circuit pads.

The first test used a simple cell constructed from a glass slide and two graphite electrodes, chosen for their inertness. Deionised water was used for the electrolyte and a bias of 15v applied. After 1 minute the pH at each of the electrodes was measured using litmus paper. At the anode the litmus paper's colour changed to a dark red corresponding to full-scale pH 2 (acid). At the cathode the litmus paper's colour changed to dark purple corresponding to full-scale pH 12 (basic). However, in the middle of the electrode the litmus paper did not change colour implying the solution was a neutral pH 7, see Figure 65.

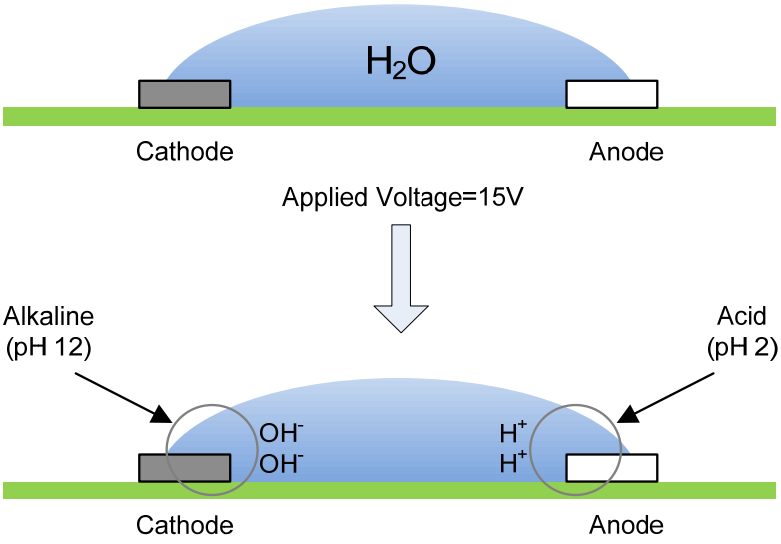

Figure 65 – pH Change in vicinity of Electrodes

The same experiment was again conducted but rather than use litmus paper a solution of universal indicator (range pH.4 –pH.10) and deionised water was used. When biasing the cell the pH differs at each electrode, three distinct colours became visible: red at the anode, purple at the cathode and green in between the electrodes, as in Figure 66. At the anode it is more acidic and at the cathode more basic. The anode is the source of H^+ and therefore by definition of Equation 17 the acid pH decreases

towards pH.1 as the production of H^+ ions increases. Conversely the cathode is the source of OH^-. Thus the pH increases toward pH.14 becoming more basic as the number of H^+ ions reduces due to OH- production and diffusion toward the anode.

$$pH = -\log_{10}(H^+) \qquad \textbf{Equation 17}$$

From similar observations of these OH- and H+ concentrations Kohman [3] proposed Equation 18 and Equation 19 to explain the reaction occurring at both the cathode and anode.

$$Cathode: \quad 4H_2O + 4e^- \rightarrow 2H_2 + 4OH^- \quad (alkaline) \qquad \textbf{Equation 18}$$

$$Anode: \quad 2H_2O \rightarrow 2H^+ + O_2 + 4e^- \quad (acid) \qquad \textbf{Equation 19}$$

This experiment was repeated three times with different voltage biases; 5V, 10V and 15V. The only difference noted over the voltage levels was the speeds at which the red and purple boundaries reduced the green neutral region over time, this is probably indicative of increased ion diffusion.

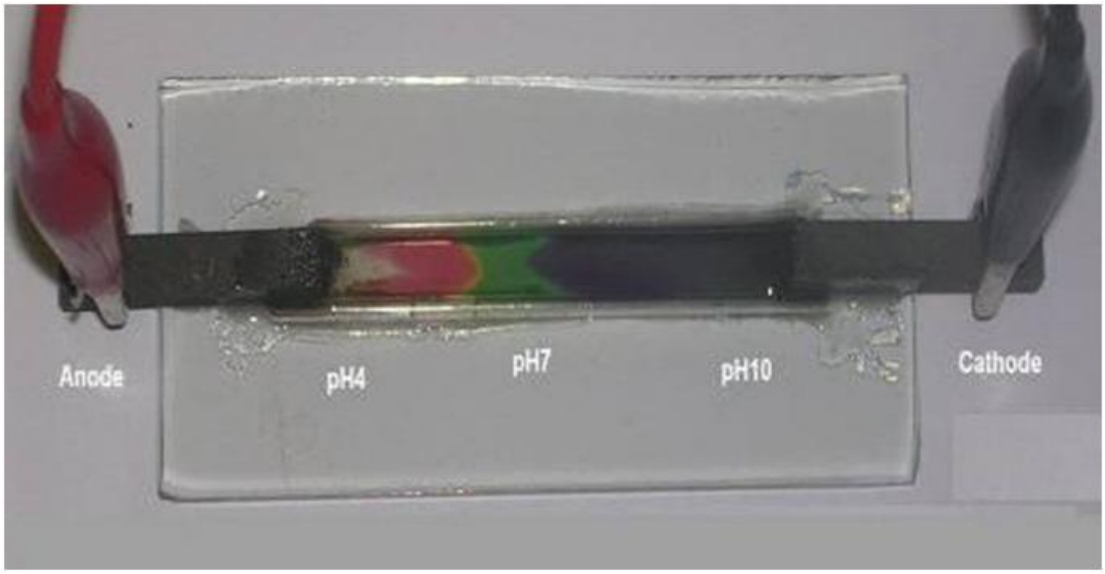

Figure 66 – Demonstration of pH at both Anode and Cathode

The second experiment attempted to simulate printed circuit board contamination by applying a quantity of universal indicator between two pads and then biasing with a

15V potential. As seen in Figure 67 similar colour gradients to those of the graphite experiments were experienced.

From both experiments a pH gradient was created at each electrode with the generation of acidic H^+ ions at the anode and basic OH^- ions at the cathode. At the anode a high concentration of H^+ ions forms and oxygen gas is produced. At the cathode a high concentration of OH^- ions forms and hydrogen gas is produced [103].

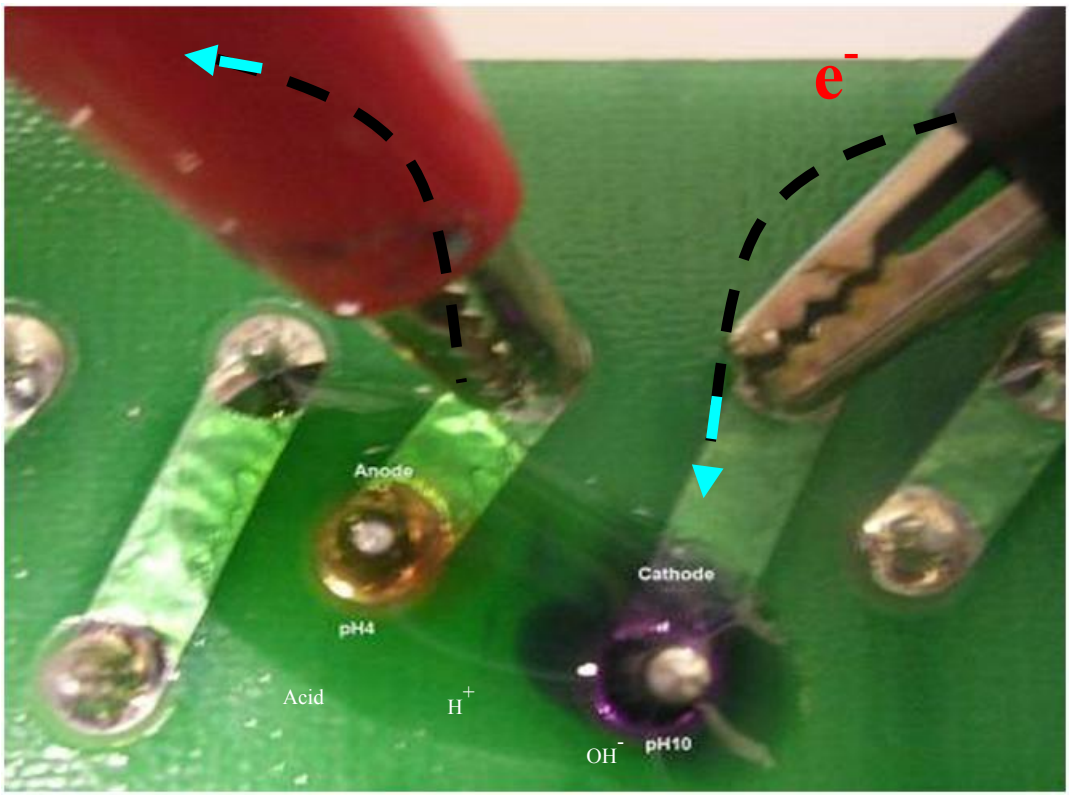

Figure 67 – High pH Gradient on Two Pads of Printed Circuit Board

The effect pH gradients have on the reliability of circuit board electrodes depends on the electrode polarity, as seen from the simplified Pourbaix diagram in Figure 30. Using the Pourbaix [50] diagram as an indicative tool for viewing the inter-relation between pH and voltage can provide information about the degree of corrosive severity for different metals. The diagram shows between the regions of pH.7 – 11 the copper is passivated at the anode and corrosion will therefore not occur. Below pH 7, corrosion will occur at the anode whilst the cathode maintains immunity.

5.2.1 Discussion

Whilst extreme pH level chemical exposure in the operation of the printed circuit board is unlikely, the exposure to extreme pH levels due to electrochemical activity is a certainty if the circuit is contaminated with water. This is demonstrated by Experiment 1B with the use of biased electrodes and two pH indication mediums: litmus paper and universal indicator.

This experiment simulates a powered printed circuit board when it is contaminated with water, demonstrating the extreme pH levels experienced at the conductor interfaces. As the two biased solder joints show in Figure 67 when universal indicator is added to the water contamination, the anode or the positive joint becomes highly acidic and likewise the cathode or the negative solder joint becomes highly basic (or alkaline), due to the level of H^+ formation. Even if no dendrites form between water contaminated lands the risk of corrosion is quite feasible, again demonstrated by the copper Pourbaix diagrams, Figure 19. The diagram shows corrosion can occur on the most positive electrode, anode, at the extreme end of the pH scale, i.e. pH>1. Whilst dendritic growth may be restricted to a number of metals, such as copper, tin and lead, corrosion can occur with most metals, if not in the presence of water alone, then with the addition of halides.

The effect of pH on dendrite growth is not fully understood although experimental studies in saturated conditions have been conducted, indicating critical pH thresholds [64] that may aid or hinder the formation of dendrites. It is noted that the pH concentrations can affect the overall shape of growth [66]. However, the pH gradient between the anode and the cathode with glass-laminate circuit boards produces metal-salts internally resulting in CAF formation. The main catalysts for CAF formation are high temperatures, greater than 60ºC, and increased voltage gradients.

The effect of voltage increases the pH diffusion region at the electrode interfaces, thus reducing the neutral pH region. If the voltage level increases sufficiently close to the acid-basic diffusion regions then there is a possibility that salts will form. This is the critical point for CAF formation, when the land distances and voltage level are large

enough for the pH diffusion zones to merge between the glass-fibre layers and form copper salts.

5.3 Experiment 1C: Parameters for Dendrite Growth

The aim of these tests (DC bias voltage test) is to empirically set the factorial design levels for the voltage factors. This involves applying manual biasing with six voltages (1V, 2V, 4V, 6V, 10V and 15V) to the SMD samples with temperature set to 30°C and observing signs of dendrite growth after 300 seconds.

Figure 68 shows the images of the six different SMD samples for voltages levels between 1V to 15V, with the cathode shown at the bottom of each image. In the 1V and 2V images no signs of redox or dendrite growth are evident. At 4V redox is initiated with slight signs of dendrite 'spores' on the cathode. At 6V a dendrite successfully bridged the electrodes within 100 seconds, this was also the case at voltage levels of both 10V and 15V. Between 6V and 15V the bias was removed after 100 seconds to prevent the dendrite from fusing. Evidently there is a critical voltage threshold where dendrites will readily form and bridge.

Dendrite Thresholds	Low Threshold (V)	High Threshold (V)
Initiation Critical Voltage	2	4
Growth Plateau	4	6

Table 9 – Summary of Dendrite Thresholds

From these experiments the critical voltage levels off at some point between 4V and 6V. The dendrites initiated at some point between 2V and 4V, demonstrating a second critical voltage threshold. Table 9 summarises these thresholds.

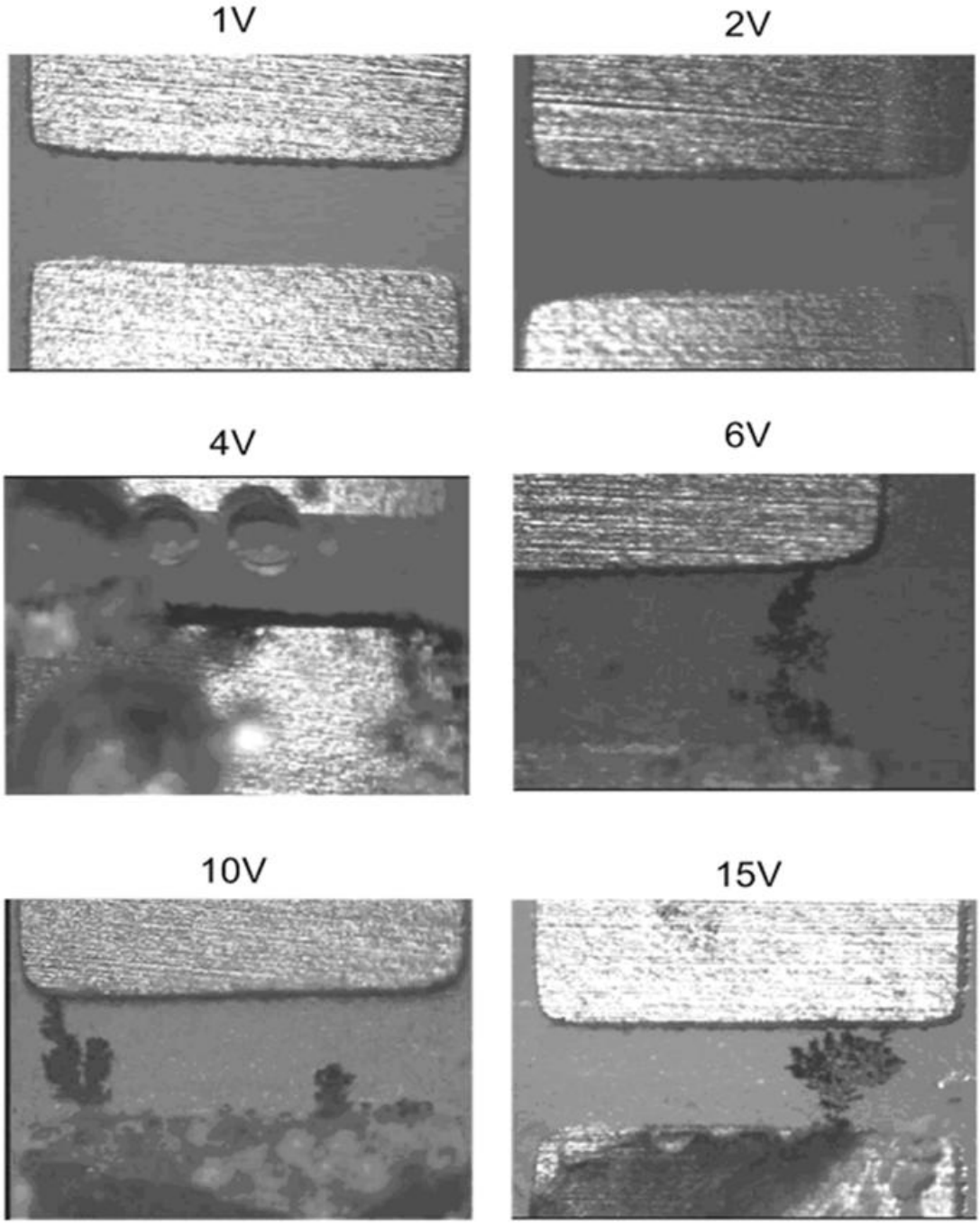

Figure 68 – Voltage Level Observations at 30°C

5.3.1 Potential Sweep

To determine the voltage dependence of copper mass migration for initiating dendrite growth a potential sweep experiment was conducted, using the equipment shown in Figure 51 and Figure 52. A voltage sweep from 0V to 4V, Figure 69, over 400 seconds was applied to SMD Samples at four temperatures of 30, 35, 40 and 60°C.

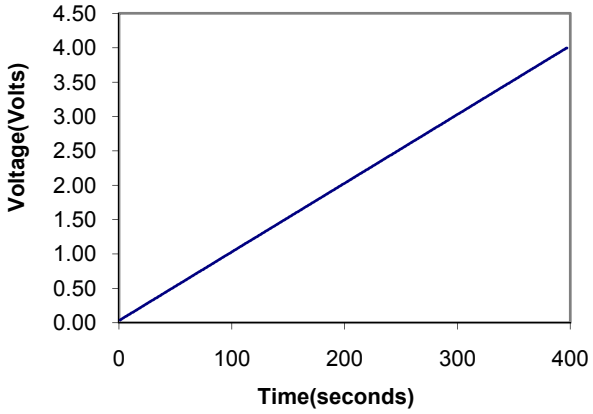

Figure 69 – Voltage Sweep from 0V to 4V over 400 Seconds

Figure 70 shows a plot of the voltage against current, with the bottom graph showing the current on a log scale. The first noticeable difference is the effect of temperature. As the temperature increases it can be seen that the onset voltage for the initial flow of current also increases, whilst maintaining a similar gradient, although similar onset voltages were produced for 35°C and 40°C. The voltage range between 30°C and 60°C is 2.2V and 2.8V, respectively, giving a rate for dendrite initiation of 0.02V/°C. The current required to initiate the dendrites can be seen more clearly from the bottom graph of Figure 70. From this graph, the average current for all temperatures and dendrite onset voltages is constant at approximately 20uA, implying that the voltage has a greater significance on the dendrite onset time. At voltages greater than 2.8V the current gradient begins to level at approximately 2mA rising to a maximum current of 5mA, demonstrating a dendrite 'holding' current.

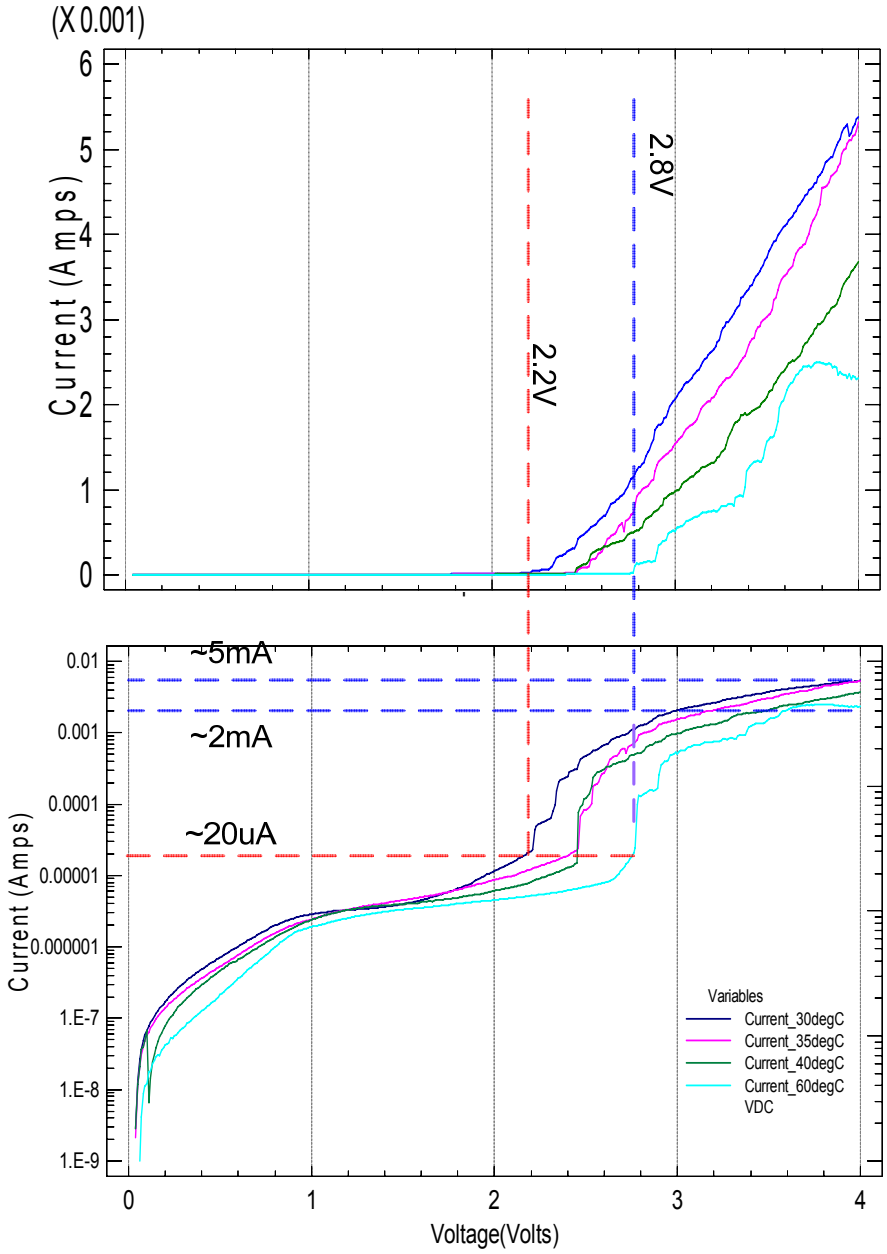

Figure 70 – Voltage and Temperature Effect on Migration, Current in linear [top] and log scales [bottom]

$$I_{fuse} = kD^{\frac{3}{2}}$$ **Equation 20**

Using the Preece [104] equation, Equation 20, and transposing to gain the diameter of the copper dendrite, Equation 21, can provide an indicator of the dendrite range. Where I_{fuse} is the current required to fuse the metal, k is the Preece coefficient factor (which is 80 for copper) and D is the diameter (mm).

$$D = \left(\frac{I_{fuse}}{k} \right)^{\frac{2}{3}}$$ **Equation 21**

Note that the Preece equation was developed in air and therefore some error may be incurred due to thermal dissipation through the water. Evaluating Equation 21 from 1-10mA for copper produced the results shown in Table 10. For 'fusing' currents between 2mA and 5mA the diameter of the hypothetical dendrite could be between 0.855um and 1.575µm. Note the values are fusible currents and currents shown in Figure 70 have not demonstrated a fuse-like condition, i.e. a sharp current drop.

Current(A)	Diameter(m)
1.000E-03	538.609E-09
2.000E-03	854.988E-09
3.000E-03	1.120E-06
4.000E-03	1.357E-06
5.000E-03	1.575E-06
6.000E-03	1.778E-06
7.000E-03	1.971E-06
8.000E-03	2.154E-06
9.000E-03	2.330E-06
10.000E-03	2.500E-06

Table 10 – Evaluation of the Preece Equation

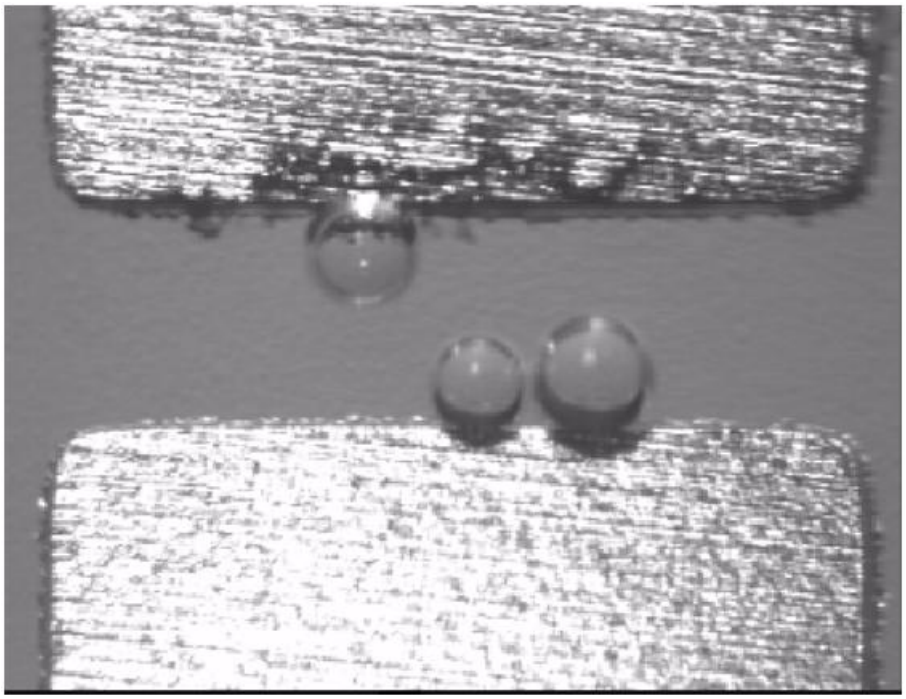

Figure 71 – At 30°C Sweep captured at 2.8V

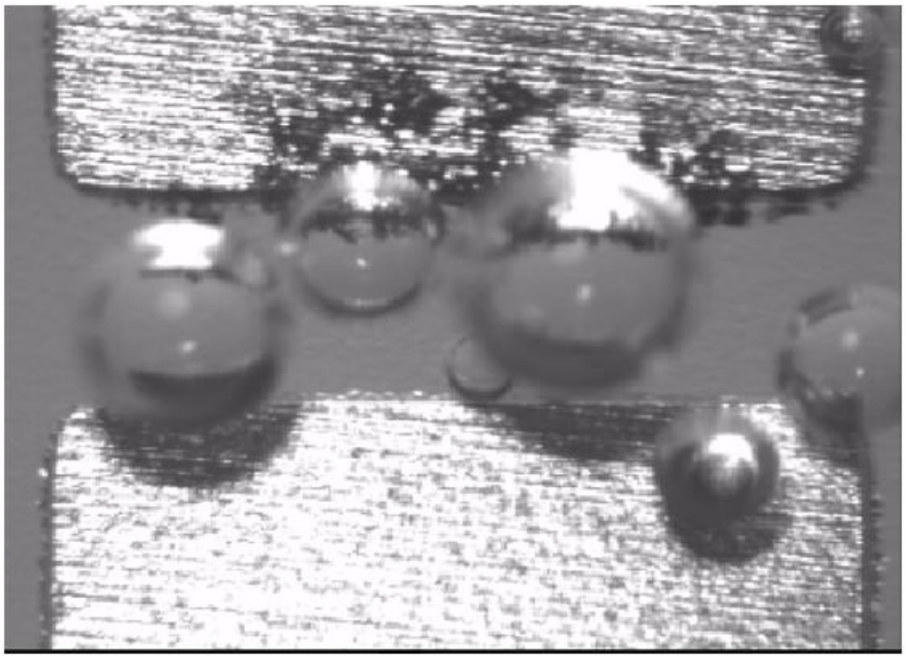

Figure 72 – At 30°C Sweep captured at 3.25V

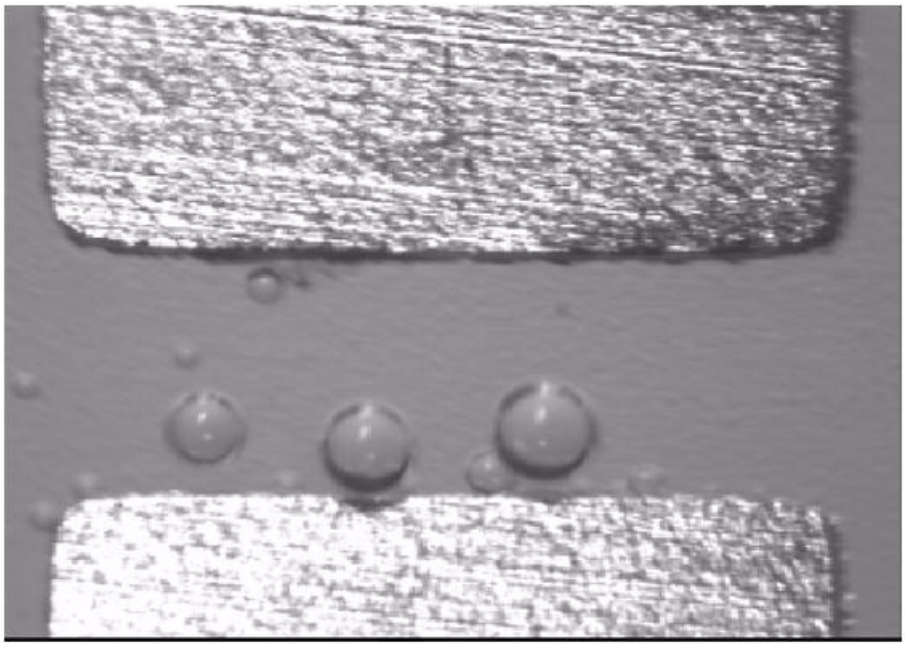

Figure 73 – At 35°C Sweep captured at 2.5V

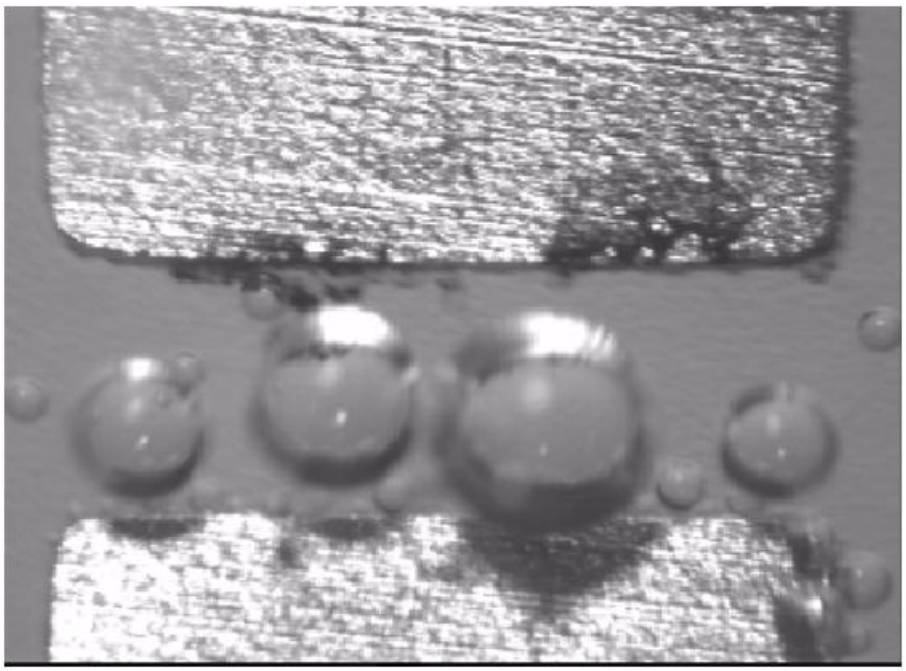

Figure 74 – At 35°C Sweep captured at 3.55V

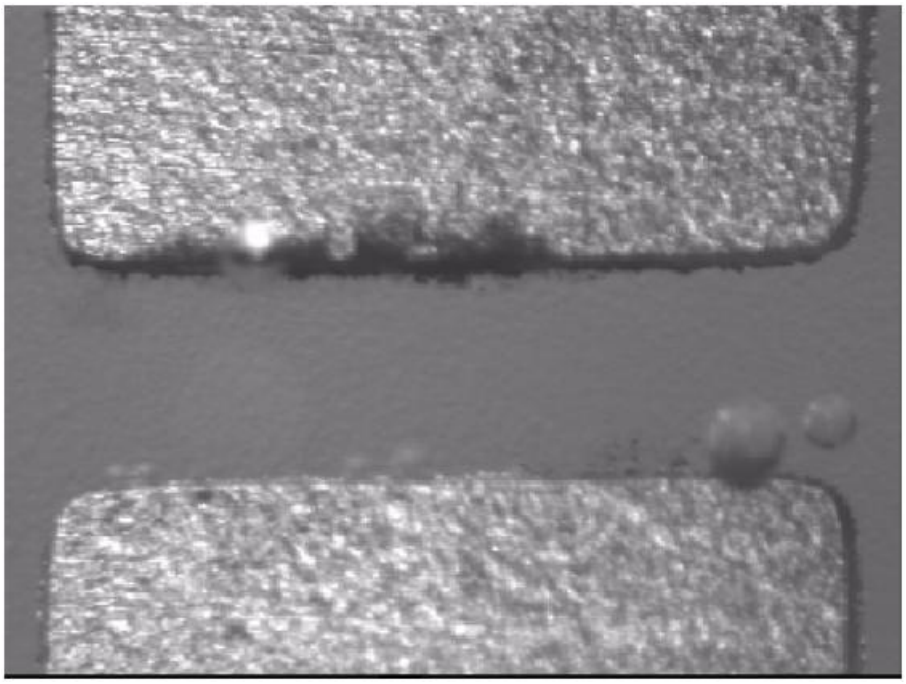

Figure 75 – At 40°C Sweep captured at 2.45V

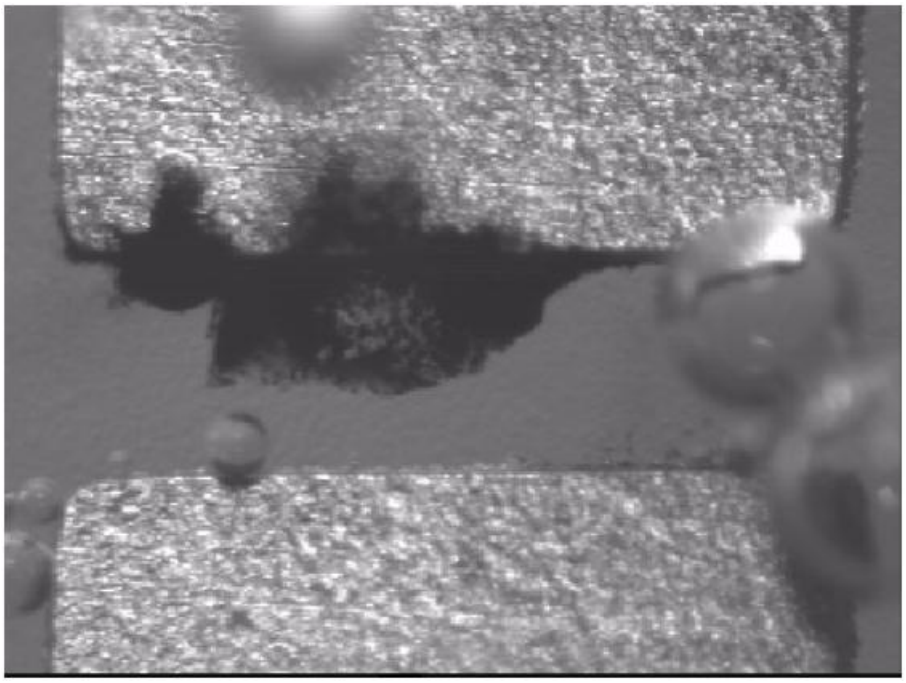

Figure 76 – At 40°C Sweep captured at 2.8V

5.3.2 Discussion

Experiment 1C, demonstrates the impact various voltage levels have on dendritic growth over a period of 100 second and the definition of the voltage factor level for the factorial design in Experiment 2 in Chapter 6.

A typical SMD pad was contaminated with deionised water and electrically biased. Tests were conducted at six voltage levels from 1V to 15V with the temperature set to 30ºC. Visual observations were made at the different voltage levels and signs of dendrite formation over a 300 second period noted. Figure 68 shows the images of the six different SMD samples for voltages levels between 1V to 15V, with the cathode shown at the bottom of each image.

At voltage levels 1V and 2V no signs of dendrites were observed, however, growths of dendrites were observed from 4V. At voltage levels higher that 4V the growth of dendrites was accelerated with dendrite fusing occurring at 6V after 100 seconds. From these test the initial critical voltage points is established at 2-4V for the dendrite initiation period and 4-6V as the growth rate plateau period.

To establish a more accurate measurement of the voltage level of the initiation periods at different temperatures, a potential sweep experiment was conducted between 0-4V over 400 seconds and at temperatures of 30, 35, 40 and 60ºC.

The results of this experiment demonstrates that the initiation voltage is affected by temperature at a rate of 0.02V/ºC with the first sign of a potential dendrite at 2.2V shown at the lower temperatures.

At voltage level greater that 2.8V dendrite fusing was evident with a holding current averaging 2mA. Using Preece's equation the average diameter range of the dendrite was estimated at between 0.855um and 1.575µm giving an indication of the short circuit potential and that electronic systems with current less that 5mA may be more susceptible to dendrite shorting, as oppose to systems with higher current, i.e. greater than 5mA, which will fuse the dendrite and thus eliminate the failure mode.

5.4 Experiment 1D – Analysis of Dendrite Filaments

The following experiment involved imaging the filaments of a dendrite using an Olympus microscope with CCD camera, a Jeol JSM 840 SEM and analysing the atomic compositions using a SuperDry II EDX system. The aim of this experiment is to provide insight into the mechanics of dendrite growth and formation. The dendrites were grown on a 10V biased 0.2 mm copper comb sample at 25°C with the tracks covered by deionised water. The samples were prepared by cleaning with ammonia and rinsing in isopropanol, followed by a final rinse in deionised water.

Dendrites are formed by the deposits of metal ions, specifically copper ions, on point sources located on the cathode. If the filament grows from metal ions then the dendrites' atomic composition will consist mainly of the donor metal; in these experiments copper. If, however, additional reactions occur *in situ* of dendritic growth then the composition may be formulated with other atomic elements.

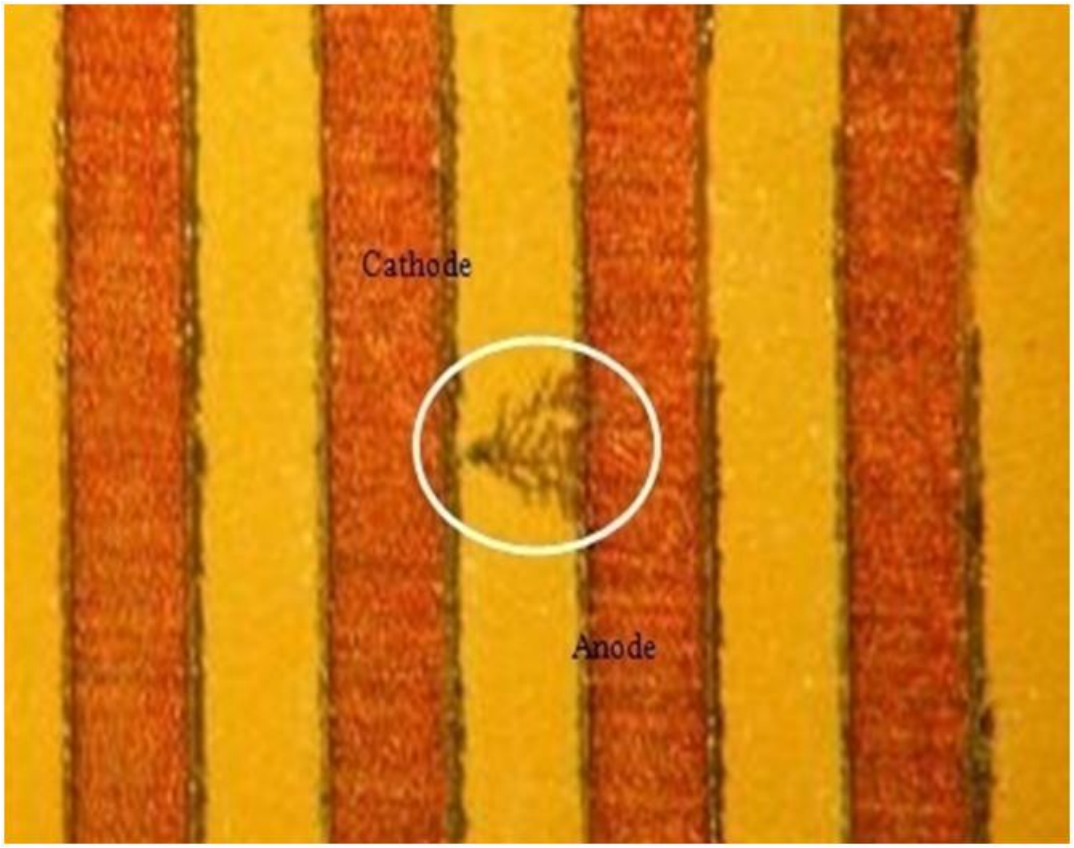

Figure 77 – 50x Magnification of a Comb with Dendrite

The first stage of the experiment was to grow a number of typical copper formed dendrites and allow the water to naturally dry at room temperature. Figure 77 shows part of the sample comb with obvious signs of dendritic growth, in particular the formation of a classic tree-like dendrite growth.

A 200x magnification can be seen in Figure 78. The images clearly show a dendrite emanating from the cathode portraying the classic fractal branching usually associated with dendritic growth.

The image in Figure 79 shows branching towards the right-hand cathode rather than focused towards the anode, which has probably occurred due to stray copper ions in the water attracted to the point source of the filaments, produced whilst the dendrite was emanating towards the anode, thus splintering off towards the second cathode. The images clearly show a dendrite emanating from the cathode portraying the classic fractal branching usually associated with dendritic growth.

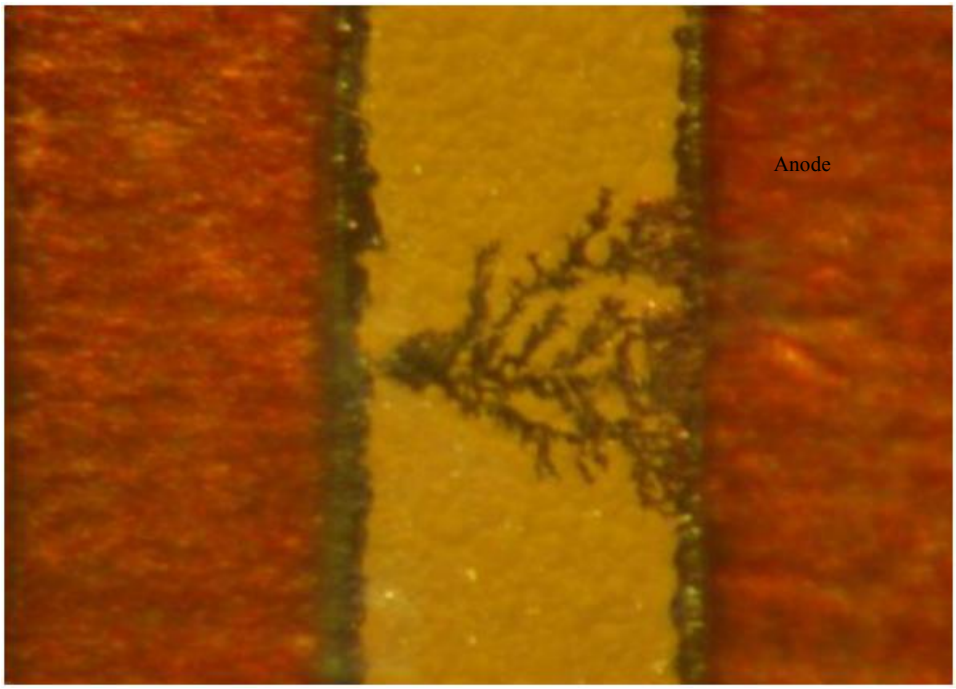

Figure 78 – 200x Magnification of the Dendrite Shown in Figure 77

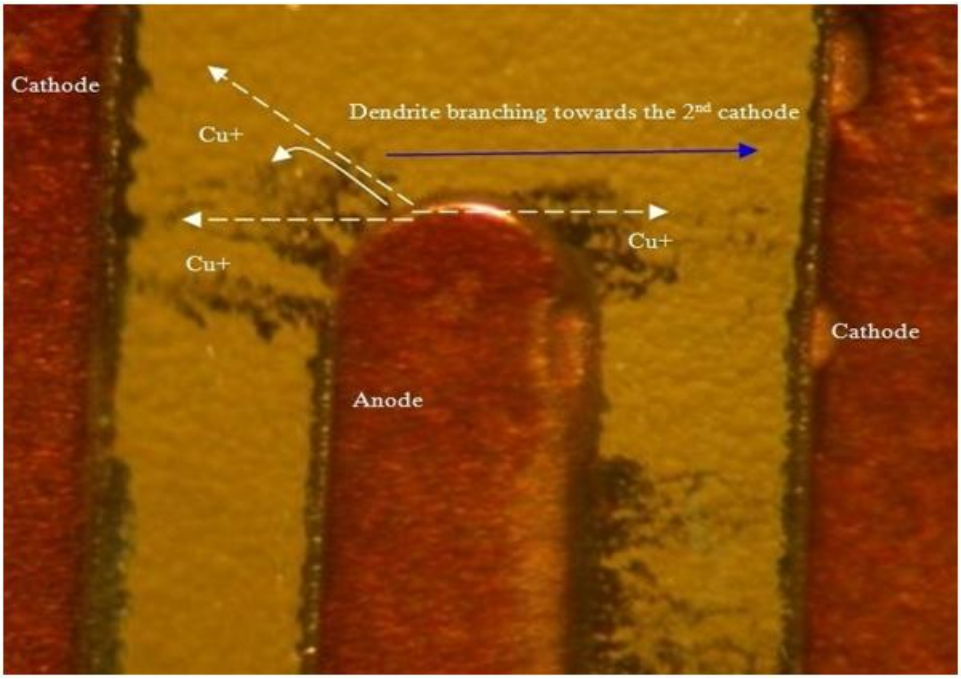

Figure 79 – 200x Magnification of a Dendrite Branching Toward 2nd Cathode

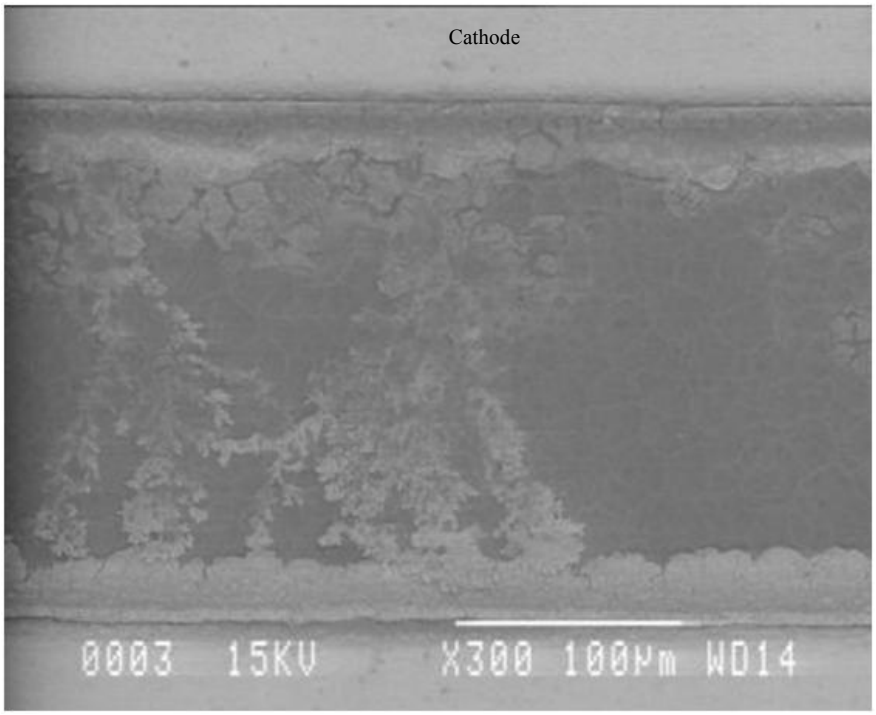

Figure 80 – 300x SEM Image of Two Dendrites

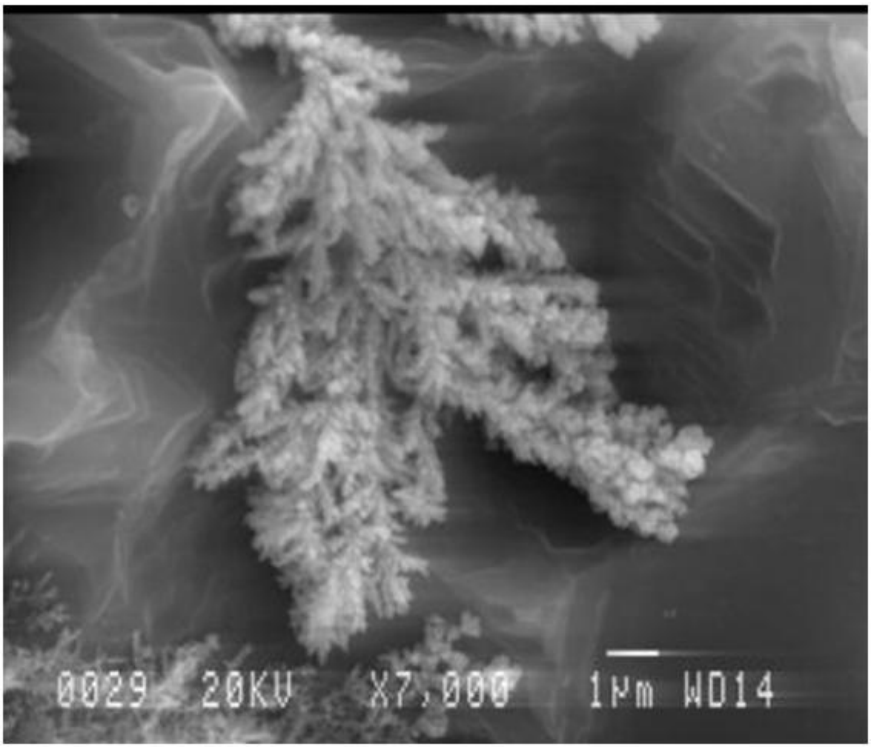

Figure 81 – 7Kx Magnification of a Dense Dendrite Tip

Figure 82 shows the EDX analysis of the dendrite whisker illustrated in Figure 81. This demonstrates dendrites grown between copper tracks are primarily formed from copper.

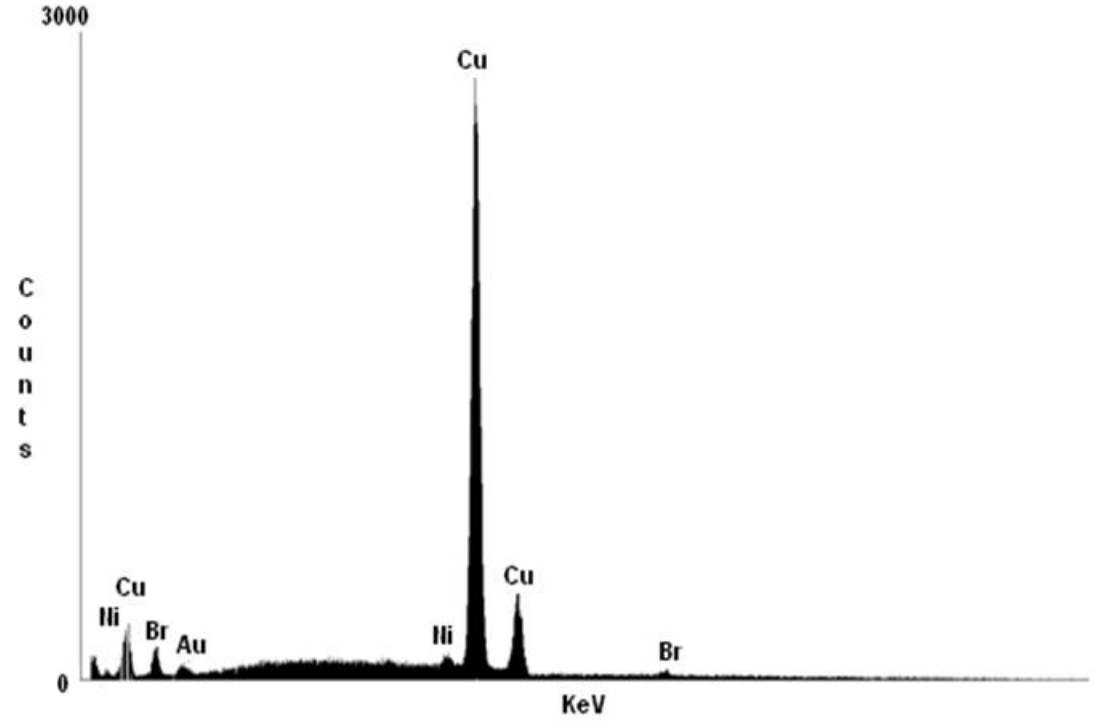

Figure 82 – EDX Analysis of Dense Dendrite Tip in Figure 81

5.4.1 Discussion

The EDX analysis, Figure 82 of the dendrite tip, Figure 80 and Figure 81, shows the dendrites consist primarily of copper. Traces of bromide and nickel were also found. Whilst copper can form various compounds with bromine, the bromine counts on the EDX did not show significant ratios with the copper, i.e. CuBr and $CuBr_2$ would produce 1:1 and 1:2 ratios respectively, and the largest peak of bromine is approximately 10% of the largest copper peak. The nickel trace is probably from the gold plating process, as nickel is use as a barrier to prevent the gold leaching into the copper.

5.5 Conclusion

The results of the tests provide the basis for the main experimentation and led to the improvement of both sample design and sample preparation. In the initial experiments it was observed that initiation times and fractal nature of the dendrites could have been affected by stray contaminants from either the samples or consumables such as water. Consequently, for the main experimentation, custom gold plated samples were produced, Figure 41, to reduce the impact of oxidisation and other contaminants. The gold was removed and the EDX results demonstrated the cleanliness of the samples showing only the presence of copper on the tracks, Figure 45. Due to the complex nature of contamination, i.e. knowing what contaminants are on any given sample at any given time and the effect contaminants may have on dendritic growth, this sample preparation process enables experimental continuity and provides the basis for consistent results. Furthermore, deionised water was used with conductivity less than $0.1uS/m^{-1}$ for all experiments.

Dendrite bridging and the self-healing nature of dendritic growth were demonstrated when a bridged dendrite fused. This provides evidence that dendritic growth may not be a permanent failure on a printed circuit board although both the current leakage leading up to the short and the high transitional currents produced by the short could prove to be problematic. In industrial SIR testing measurements are made at various time periods and therefore it is possible that the formation of dendrite growth is missed due to acquisition aliasing, again providing further support for continuous measurement systems to detect dendrite fusing. If more dendrites form and then short, not only will the increase in current leakage be problematic, but the high current surge oscillations from the shorting dendrites are likely to become an issue with most microprocessor circuitry.

The formation of hydrogen and oxygen gas bubbles at the cathode and anode, respectively, is demonstrated. This phenomenon could aid in the evaporation of the water and eventually remove the water-based problem. However, two areas of concern are noted, namely the splashing effect and the residual compound formed after dehydration. The splashing effect produced by the bubbles could contaminate other

regions of the printed circuit board and initiate further electrochemical failure modes. It is uncertain the impact residual contaminates may have on a printed circuit board's overall reliability due to the lack of information on the contaminate type at the time of rehydration. The Pourbaix diagram indicates corrosion may occur with more acidic (pH < 7) compounds on the anode of a copper track or pad.

Chapter Six: Results and Discussions of Experiment 2 – Dendrite Growth in Saturated Conditions

Tracks, pads and vias on printed circuit boards can suffer from a variety of problems if the surfaces are contaminated with electrical conducting substances. The aim of this experiment is to produce a model multilevel full-factorial design to study the effects of temperature, voltage and electrode gap on dendritic growth under saturated conditions, i.e. water droplet contamination.

6.1 Modeling Growth of Copper Dendrites in Saturated Conditions

Potential step voltammetry (PSV) experiments were carried out using a precision voltage source, potentiostat, and high input impedance data-logger (Agilent 34970A), with the transition from E1 to E2 controlled manually whilst the data-logger was running in continuous mode. The PSV experiments were conducted from zero volts with a step of 1.25V and i_{cut} = 100mA. The technique used involves controlling the temperature of a small cuvette filled with 1.2ml of deionised water.

Figure 83 – 1.2ml Cuvette

A number of interdigitated printed circuit boards (IPCB) were designed with gap spacings of 0.2, 0.3 and 0.4mm on nickel-barrier gold plated 0.07 mm copper FR4 fibreglass circuit board, Figure 84. Using gold plated copper ensured the IPCB stays

free from copper oxide contamination over time,[3] as copper will not produce dendrites when contaminated with copper oxides, due to the oxide's insolubility in water [19].

Figure 84 – Copper Interdigitated Printed Circuit Boards

A voltage biased IPCB was then placed into the cuvette and the current was measured over a period of 300 seconds; this was repeated according to the experimental design permutations. A sharp rise in current signified a dendrite short and the time was noted as the first evidence of dendritic growth under the given conditions; the value was then logged, see Figure 85**.** A multilevel factorial design was used to control the experimental execution and minimise experimental error. The experiment was designed using a randomised 3 factor multilevel factorial design using 'Statgraphics Centurion XV'[105] and consisted of two (replicated) 3 x 5 x 3 runs. Table 11 displays parameters used for the design with their respective levels.

[3] The gold was removed before experimentation with KI + I_2, rinsed in deionised water and the cupreous iodide residue was removed with ammonia, finally rinsing in deionised water, see section 3.1.1..

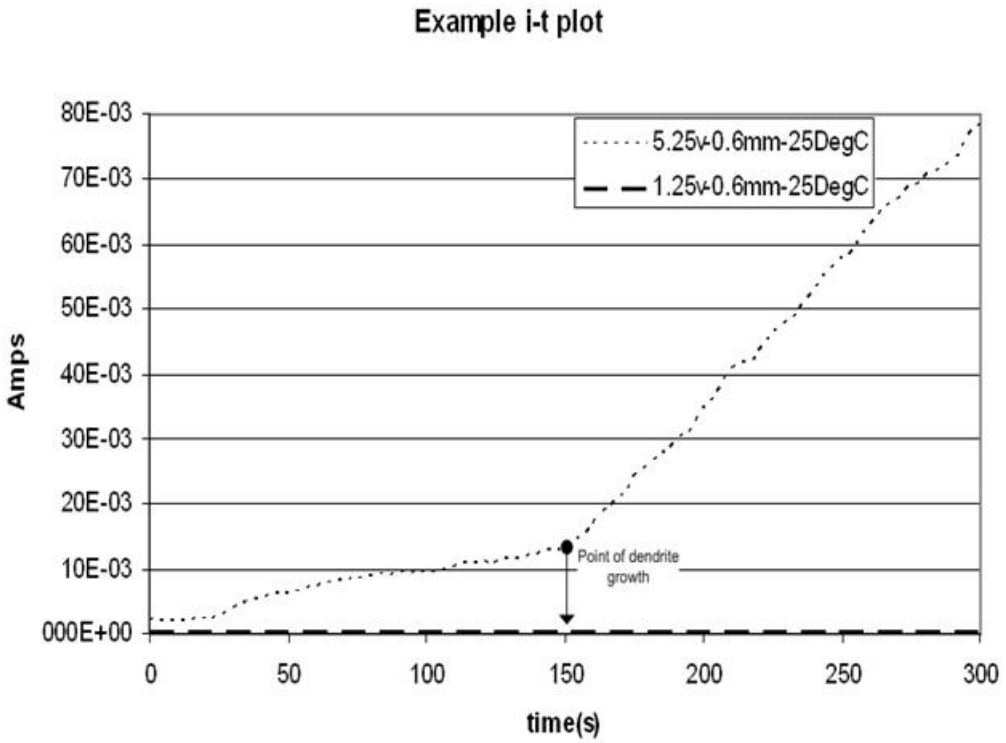

Figure 85 – Example i-t Plot for 5.25v and 1.25v at 25°C and Gap Spacing on 0.2 mm

The gap distances, 0.2-0.4 mm, originated from the typical spacing used on a microprocessor based printed circuit boards. The temperature range, 5 to 45°C, is typical of the normal operating temperature of most electronics products. The voltage range, 1.25-5.25V, originates from typical operating voltages of modern microprocessor circuits.

Factors	Low	High	Levels	Units
Temp	5.0	45.0	3	'C
Voltage	1.25	5.25	5	V
Gap	0.2	0.4	3	mm
Responses	Units			
D_init_time_sec	Seconds			

Base Design	
Number of experimental factors	3
Number of responses	1
Number of runs	90
Error degrees of freedom	79
Randomized	Yes

Table 11 – Factors Included in Design of Experiments

6.2 Discussion of Results

When measuring the dendrite initiation point from the i-t curves, Figure 85, none of the 1.25V charts demonstrates any signs of rapid current surges, implicit of dendrite shorts, nor was there any significant movement in current. This voltage threshold coincides with the voltage required to electrolyse water. Equation 22 to Equation 24 shows the reaction for the electrolysis of water [106], note that E_a is close to 1.25v.

Anode:	$H_20 \rightarrow ½O_2 + 2H^+ + 2e^-$	E_a = 1.229V with reference to the standard hydrogen electrode (SHE)	**Equation 22**
Cathode:	$2H^+ + 2e^- \rightarrow H_2$	E_c = 0V with reference to SHE	**Equation 23**
Overall:	$H_20 \rightarrow ½O_2 + H_2$	E_c- E_a=-1.229V	**Equation 24**

The cathode for all the experiments was held at 0V and therefore E_c= 0; with the anode held at greater than, or equal to, 1.25V. Voltage required to start the electrolysis of water, shown in Equation 22 to Equation 24, is calculated using the Nernst equation, Equation 25, with the Gibbs free energy (ΔG) sourced from standard tables [52, 53].

$$\Delta G = -nFE^{\theta} \qquad \textbf{Equation 25}$$

Where n is the number of electrons transferred for one step of the overall reaction, F is the Faraday Constant (96,487 C mol^{-1}) and E^{θ} is the electrode potential.

Thus from Equation 25, n = 2 and for $H_2O_{(liquid)}$ ΔG = -237,100 J/mol at 25ºC, this gives the electrode potential of 1.229V.

Species	ΔG (J/mol)	E_a (V)
H_2O	-237,100	1.229
Cu(s)	0	0
Cu^+(aq)	50,000	0.518
Cu^{2+}(aq)	65,000	0.337
CuO	-129,700	0.672
Cu_2O	-146,000	0.757
$OH^-_{(aq)}$	-157,000	1.627
$Cu(OH)_2$	-373,000	1.939

Table 12 – ΔG [52, 53, 53] and Calculated Ea Values of Typical Ionic Species, when copper is electrolysed in water.

Table 12 illustrates the activation energies and the calculated theoretical voltages for a number of typical species that may be present when electrolysing copper in pure water. The electrolysis of H_2O (1.229V), Equation 25, closely matches the empirical voltage below which dendrites did not grow, i.e. 1.25V. The highest activation voltage (1.939V) of copper (II) hydroxide is unlikely to have an impact as it has poor solubility in water. When biasing 0.4 mm combs at 25°C, with 1.5V, 1.4V and 1.3V dendrites were visible after 900 seconds, but at 1.2V there were no signs of dendrites.

From the experimental data there is a certain degree of probability that a dendrite will not grow at 1.25V within 300 seconds. However, this degree of certainty can not be demonstrated above 300 seconds as this was the maximum duration of the experimental run. Therefore, in all the 1.25V cases, for dendrite initiation time, a figure of 301 seconds was given to the model as this demonstrated that no dendrites grew within the experimental time, shown in Table 13.

			Block 1	Block 2
Temp ('C)	Voltage (V)	Gap (mm)	D_init_time_sec (sec)	D_init_time_sec (sec)
5	1.25	0.2	301	301
5	1.25	0.3	301	301
5	1.25	0.4	301	301
5	2.25	0.2	110	190
5	2.25	0.3	193	110
5	2.25	0.4	185	255
5	3.25	0.2	30	50
5	3.25	0.3	100	100
5	3.25	0.4	275	125
5	4.25	0.2	100	40
5	4.25	0.3	150	25
5	4.25	0.4	130	50
5	5.25	0.2	90	40
5	5.25	0.3	85	30
5	5.25	0.4	50	30
25	1.25	0.2	301	301
25	1.25	0.3	301	301
25	1.25	0.4	301	301
25	2.25	0.2	50	53
25	2.25	0.3	62	51
25	2.25	0.4	150	100
25	3.25	0.2	33	11
25	3.25	0.3	80	20
25	3.25	0.4	55	65
25	4.25	0.2	12	5
25	4.25	0.3	40	92
25	4.25	0.4	125	15
25	5.25	0.2	20	10
25	5.25	0.3	45	12
25	5.25	0.4	25	25
45	1.25	0.2	301	301
45	1.25	0.3	301	301
45	1.25	0.4	301	301
45	2.25	0.2	35	25
45	2.25	0.3	60	40
45	2.25	0.4	65	70
45	3.25	0.2	15	12
45	3.25	0.3	15	30
45	3.25	0.4	40	33
45	4.25	0.2	21	27
45	4.25	0.3	20	13
45	4.25	0.4	32	18
45	5.25	0.2	9	6
45	5.25	0.3	11	14
45	5.25	0.4	35	50

Table 13 – Multifactoral Runs and Experiment Results of D_init_time_sec, sorted by temperature.

Figure 86 illustrates the factors that have the greatest effect on D_init_time_sec, clearly indicating that voltage has a significant negative effect on dendrite initiation time. As the voltage increases so the D_init_time_sec reduces, implying that dendrites

initiate faster as the voltage is increased. Note the standard error is significantly less than the effect yielding a large signal-noise ratio.

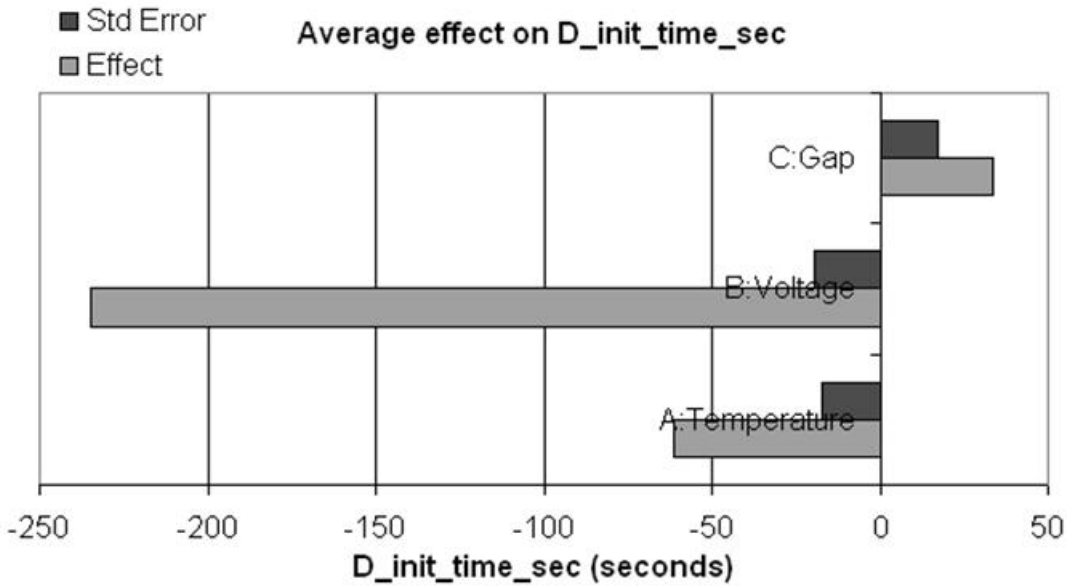

Figure 86 – Pareto of Response D_init_time_sec

Table 14 shows the ANOVA (analysis of variance) table of the response D_init_time_sec. The ANOVA tests the statistical significance of each effect by comparing the mean square against an estimate of the experimental error. The F-Ratio is the ratio between signal and noise and the P-Value is the significance of the F-Ratio at 80% confidence i.e. a P-Value less than 0.2 is significant. Temperature, voltage and gap all have P-values less than 0.2 and can therefore be considered in further analysis. When initially analysing the experiment all the effects were considered and those with P-Values less than 0.2 were removed (Note 20% was the product of the measurement equipment tolerances).

Source	Sum of Squares	Df	Mean Square	F-Ratio	P-Value
A:Temperature	66798.6	1	66798.6	63.11	0.0000
B:Voltage	2223.49	1	2223.49	2.10	0.1511
C:Gap	26356.2	1	26356.2	24.90	0.0000
AA	4774.05	1	4774.05	4.51	0.0367
BB	200773.	1	200773.	189.70	0.0000
ABB	18901.9	1	18901.9	17.86	0.0001
BBB	51782.3	1	51782.3	48.93	0.0000
BBC	10545.0	1	10545.0	9.96	0.0022
Total error	85727.5	81	1058.36		
Total (corr.)	1.06479E6	89			<=0.2

Table 14 – ANOVA Table of Responses D_init_time_sec

6.2.1 Model of Dendrite Initiation Time

After completing the experiments a best fit third order polynomial regression model was created, Equation 26. This model was from the calculated regression coefficients, in Table 15.

Coefficient	Estimate
Constant	858.27
T:Temperature	-1.54
V:Voltage	-641.91
G:Gap	168.17
V^2	166.04
V^3	-14.13

Table 15 – Regression Coefficients Values from D_init_time_sec

Coefficient values less than 0.1 had little effect on the final model results and were therefore removed from the final model to reduce the overall complexity. For example, removing all the coefficient values below 0.1 affected the R-Square value by 2 percentage points. The results from the model demonstrate a good fit between the model and data for each of the different factors, shown by the adjusted R-squared value of 90%. The R-Squared statistic indicates the fraction of the total squared error that is explained by the model, thus values approaching 100% are more desirable.

$$D\_init\_time\_\sec = 858.27 - 1.54T - 641.91V + 168.17G + 166.04V^2 - 14.13V^3$$ **Equation 26**

Figure 87 to Figure 89 illustrate the time for a dendrite to initiate (D_init_time_sec) for temperature, voltage and gap produced from the polynomial shown in Equation 26.

Figure 87 and Figure 88 both show a plateau between 3V and 4V. This is likely to be associated with the increase of gas bubbles at the electrodes causing:

i) a reduction in the current flow due to the gas resistance as it appears as a cloud of insulators obstructing the electrical path between the electrodes, and/or
ii) the increased movement of gas bubbles at the electrode as this can damage the dendrites before they can 'jump' across the gap. As the gas bubbles adhere to the surface of the electrodes and grow, buoyancy could eventually force them free. If a bubble happens to be close to a dendrite's nucleation point, i.e. the point at which the dendrite starts to grow, then it may obstruct, stop or damage the dendrite.

Gas formation was observed from 2V with the bubble growth noticed at increasing voltages on the electrode interfaces, whilst at 1.25V the production of gas was not evident. When the power was switched off the gas bubbles eventually escaped to the surface and resistance returned closely to its original lower value.

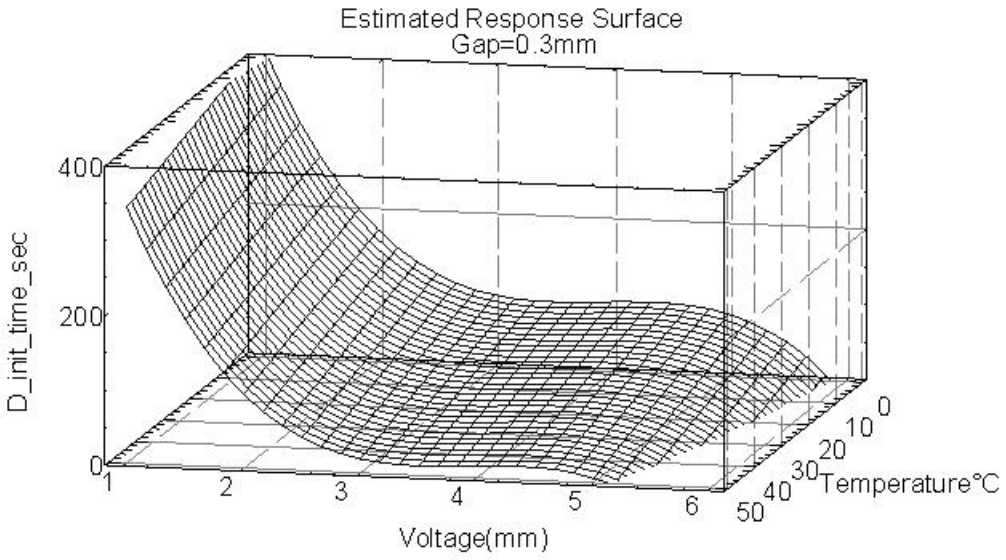

Figure 87 – D_init_time_sec as a Function of Voltage and Temperature, with Gap held at 0.3 mm.

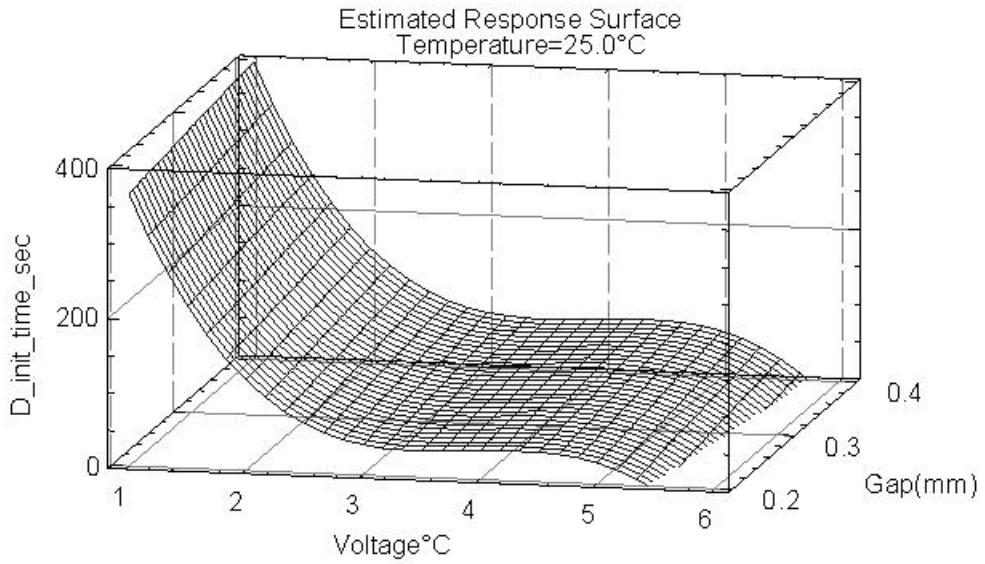

Figure 88 – D_init_time_sec as a Function of Voltage and Gap, with Temperature held at 25°C.

Figure 89 illustrates the effect of Gap and Temperature relative to dendrite initiation, which is linear on both axes.

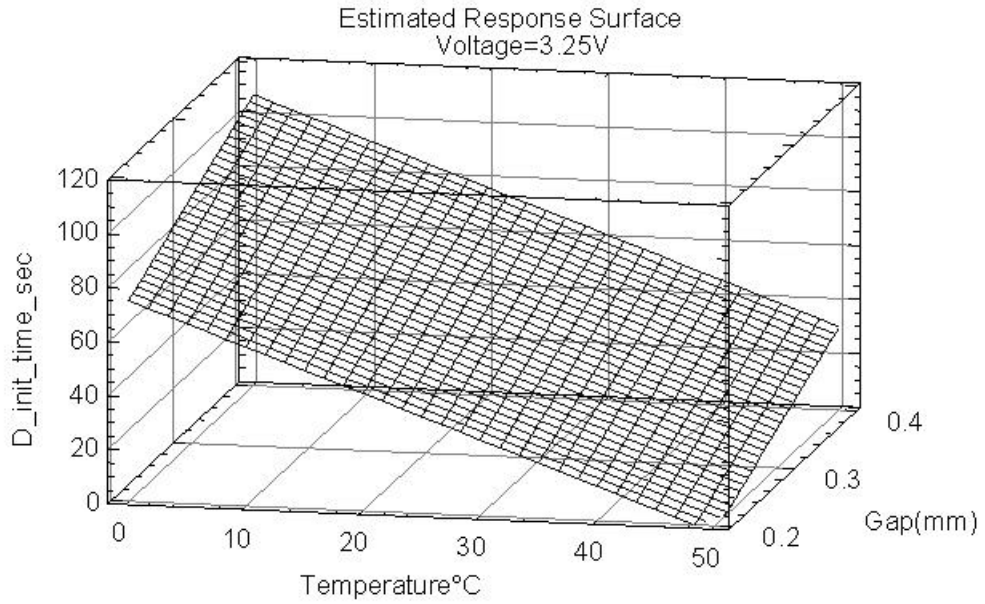

Figure 89 – D_init_time_sec as a Function of Temperature and Gap, with Voltage held at 3.25V.

This result coincides with experimental observations made by Krumbein [34] who notes the average initiation time of the first dendrite appearing, shown in Table 16.

Voltage	Time Interval			
(V)	0.64 mm Spacing		1.24 mm Spacing	
	Mean	Stdev	Mean	Stdev
6.00	0.92	0.14	2.40	1.00
5.00	1.00	0.34	3.30	2.50
4.00	0.93	0.55	-	-
3.00	1.75	0.35	4.70	1.00
2.00	1.81	0.59	-	-

Table 16 – Krumbein's Data on Average Time between Initiations of a Dendrite

Krumbein explains that '*the turbulence produced by bubble formation at the interface between the conductor and the water-covered insulator appears to play a major role in the apparent saturation of the failure rate when a certain level of applied voltage has been reached*'. His expression 'saturation' is the point where his average time data levels off between 4-6V. He went on to say the gas bubbles tended to interfere with the nucleation of the first dendrite towards the anode.

6.3 Summary

When a track, pad or via is contaminated by a water drop or splash this saturated condition could, at lower voltages (between 3 and 5V), produce a constant rate of dendrite growth eventually leading to a short circuit. However, whilst higher voltages do show significant signs of dendrite growth, this is counteracted by the buoyancy effects of gas formation; as the voltage increases to a point where the gas production and the dendrite formation have a cancelling effect. Increasing the gap of the circuit lands did show some reduction in dendrite short circuit time. However, increased voltages and reduced temperatures yield the best scenario for reduced probability of dendritic growth. Below 1.25V, dendrites did not grow and this could be associated with the onset voltage required for the electrolysis of H_2O, although the impact of other contaminants may increase this threshold.

Chapter Seven: Conclusions and Suggestions for Further Work

7.1 Conclusions

The objective of this thesis is to increase understanding of the phenomenon of electrochemical dendritic growth; to minimise field failures and develop a model that reflects the impact of conductor track spacing, temperature and operating voltage on such growths.

In the process of sample preparation a simple and less aggressive method was used to remove the gold from the printed circuit board combs. A solution of potassium-iodide and iodine was used to remove the gold and the remaining compound (copper-iodide) was removed with a further solution of ammonia. Alternative methods, such as *aqua regia* (concentrated nitric acid and hydrochloric acid), remove all metals and is less controllable. The effectiveness of this method is demonstrated by an EDX analysis that shows predominant copper peaks.

The formation of dendrites on the cathode, independent of the electrode material, is visually demonstrated using an electrochemically inert metal, platinum, commonly used in the electronics industry. Depletion of the anode metal is also demonstrated using copper. As a copper anode is depleted it is demonstrated an electrochemically inert platinum cathode can also develop dendrite formations, implying that the formation of the dendrite's main constituent is copper. This is confirmed by an EDX analysis of a dendrite filament with the identification of predominant copper peaks.

The effect of pH is demonstrated on a printed circuit board, highlighting extremely large pH gradients at each of the electrodes; strongly acidic at the anode and strongly alkaline at the cathode, as noted in Figure 90 . Pourbaix diagrams are an indicative method of predicting potential risks and show various states of corrosion can occur depending on the metal used and the polarity of the electrode. The Pourbaix diagram for copper indicates the cathode, whilst becoming extremely basic, remains relatively stable. The anode is likely to corrode.

Using the Preece equation the diameter of a dendrite filament was in the area of 0.855um and 1.575 µm. However, it must be noted the Preece equation is based on the assumption that the fusing material is in air.

Using a temperature controlled system for analysing dendrites, by continuously monitoring the current flow through a combed circuit that simulated a number of printed circuit board track distances, it is found all three parameters, track distance, temperature and voltage, affect the dendrite growth rate. Increasing the gap of the circuit lands did show some reduction in dendrite short circuit susceptibility, however, increased voltages and reduced temperatures yielded the best scenario for reduced probability of dendritic growth.

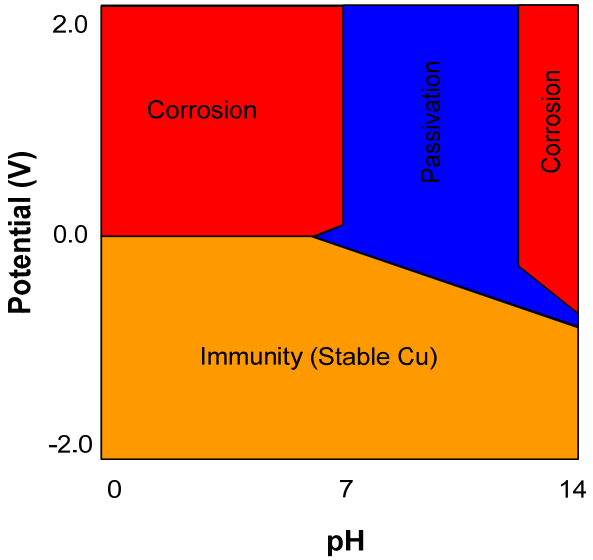

Figure 90 – Summarised Pourbiax Diagram for Copper

However, whilst higher voltages did induce significant signs of dendrite growth this is counteracted by the buoyancy effects of gas formation as the voltage increased, to a point where the gas production and the dendrite formation had a cancelling effect. Below 1.25V dendrites did not grow and it is shown this could be associated with the onset voltage required for the electrolysis of water, although the impact of other contaminants may increase this threshold.

The effect of reducing track distances produced an increased chance of dendrites forming if they were contaminated with water. As noted in the literature, reducing track

distance also increases the chance of CAF formation and it can be concluded that any form of electrochemical migration can be affected by electrode proximity, although the mechanisms by which the failure modes are created are not the same.

It is demonstrated that implementing larger track spacing and lower operating voltages within a design can significantly reduce the probability of dendrite growth. However, whilst reducing operating voltages is in line with current trends of reduced microprocessor core voltages, the increasing track spacing does not accord with the current design trends of reduced product size.

Reducing operating temperature may be a difficult target to achieve for products that are specified for operation in hostile conditions. However, this project does identify the significance of temperature at normal operating conditions, i.e. the temperature at which consumer products operate, and demonstrates applications that are expected to operate at higher temperatures are more likely to experience dendrite growth if contaminated by water.

7.2 Design Guidelines

The following summary provides design guidelines for industrial use to develop design parameters, and Figure 91 provides a quick reference for design parameters of both printed circuit board layout restrictions and environmental conditions.

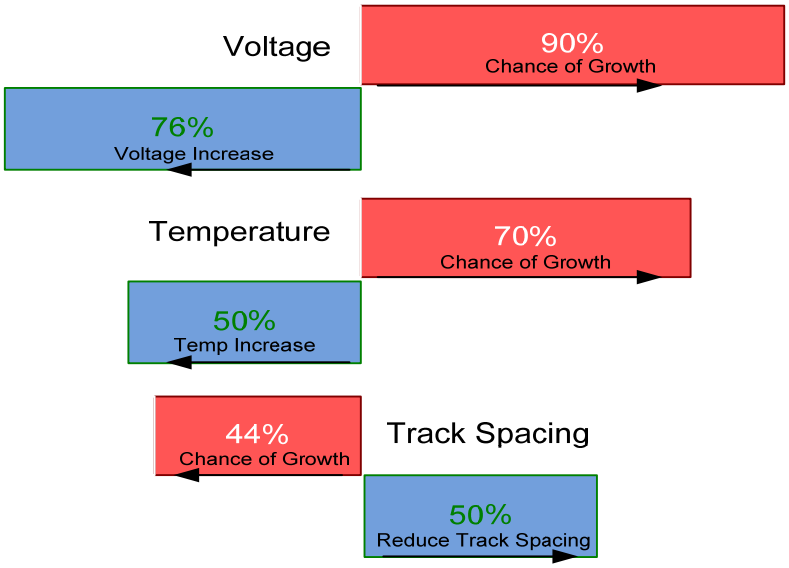

Figure 91 – Quick Reference Design Guideline for Reducing Dendrite Growth

A multilevel factorial design is used to analyse the effects conductor track spacing, temperature and operating voltage have on dendrite initiation times. It is shown individually plotted dendrite initiation times follow a linear response over temperature. The impact of gap spacing from 0.2 mm to 0.4 mm shows dendrite initiation time is increased by 44 %, as summarised in Figure 92. Increasing the gap spacing between printed circuit board tracks, pads and vias thus reduces the probability of a dendrite forming.

The effect of temperature on the likelihood of dendrite growth reduces as the temperature increases, i.e. the reduction of the dendrite initiation time is not linear with temperature but reduces almost exponentially as the temperature increases. A temperature rise of 40ºC (5ºC to 45ºC) affects the initiation time by more than 70 % or, assuming a linear response from 5ºC to 45ºC, then 1.5 sec/ºC or 0.66 ºC/sec, as summarised in Figure 93.

Voltage is the parameter that affects dendrite initiation time by the greatest measure and produces a parabolic curve, summarised in Figure 94. The effect of increasing the voltage from 1.25V to 5.25V reduces dendrite initiation time by 90 %. However, at 4.25V the initiation time reaches a minimum and then starts to again increase. This may imply there is a secondary process acting on the dendrite growth. It is thought this secondary process is probably caused by the formation of gas bubbles at the electrode interfaces which damages the dendrites and prevents them from short-circuiting as they continue to grow.

In summary, reducing track spacing by 50% effectively reduces the dendrite initiation time by 44 %. Likewise, increasing the temperature, by 40ºC, effectively reduces the dendrite initiation time by 70 %. As the dendrites form much quicker whilst these two parameters change it is noted that reducing track spacing and increasing temperature increases the chance of a dendrite growth.

The rate of change of dendrite initiation at voltages between 2.25V to 4.25V is much less than experienced at lower voltages. The effect of increasing the voltage by 76 % reduces the dendrite initiation time by 90 %, again implying an increased chance of dendrite growth as the parameter value increases.

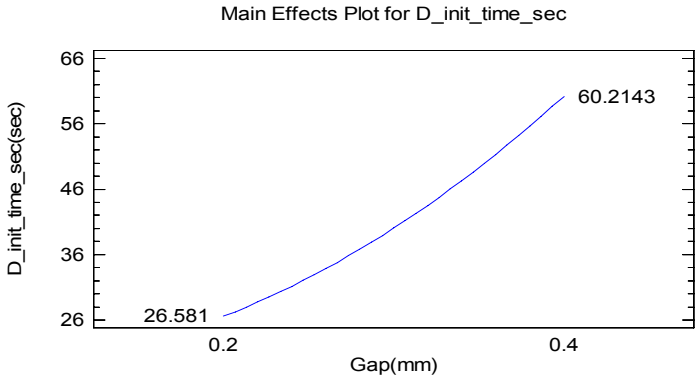

Figure 92 – Effect of Track Spacing on Dendrite Growth

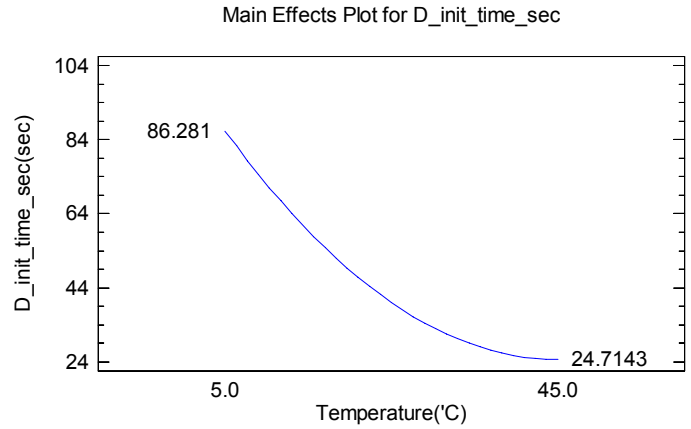

Figure 93 – Effect of Temperature on Dendrite Growth

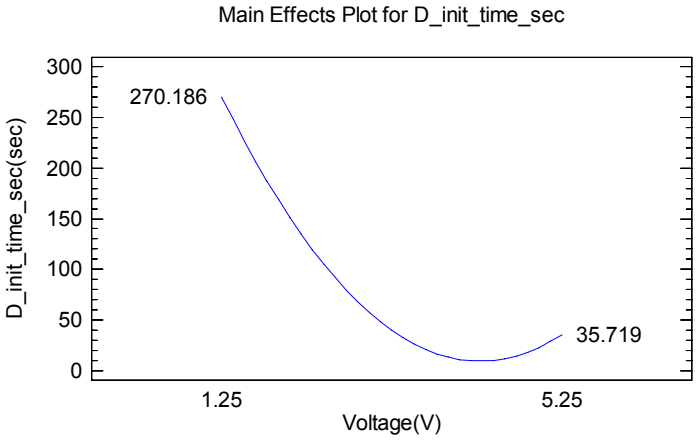

Figure 94 – Effect of Voltage on Dendrite Growth

7.3 Further Work

As this thesis focuses on DC dendrite formation it may be beneficial to further understanding of the impact of AC on the growth of dendrites, which could lead to the establishment of a growth threshold with reference to frequency. A combination of DC+AC (offset AC) could also be considered for further research.

A dendrite tended to be produced close to the point where hydrogen was being formed, at the cathode. Areas where there was no gas formation yielded no dendrites. It is not certain why this happened but this phenomenon needs to be further investigated. When the bias was removed and re-applied to a partially grown dendrite it was observed the dendrite did not continue to grow, whereas other dendrites grew from new nucleation points. It is unclear why this occurs although oxidisation of the dendrite tip may account for the phenomena. However, this is only speculation and this should be further examined.

Whilst the occurrence of electrochemical reliability failure modes, namely dendrite growth and CAF formation, are well reported there seems to be no literature published on the failure effects of large capacitances caused by the double-layer, of the metal-liquid interfaces, on printed circuit board contamination. Large capacitances caused by water contamination across two tracks would cause problems at lower voltages. As the core voltages of microprocessors reduce these phenomena may become an issue for electronic reliability.

As a late addition to this thesis work was conducted that raises questions about the capacity of various water types to form classic dendrite structures. Observations were made of various dendritic failures within a validation test; whilst attempting to re-grow dendrites, under very similar conditions, using water from the test, (standard tap water), it was obvious dendrite growth did not occur. When the same test was run using deionised water dendrites were produced. Possibly this may occur because standard tap water contains either, or both, chloride and fluoride, which will participate with copper ions to form a neutral copper complex. As the copper ions combine with halogens to form a neutral complex then copper ions are not available to form dendrites. Whilst this

answer is speculative it is suggested dendrite growth as a function of water type should be further investigated.

REFERENCES

1. Landis, G. A., Bailey, S. G., and Tischler, R., "Causes of Power-Related Satellite Failures," *Photovoltaic Energy Conversion, Conference Record of the 2006 IEEE 4th World Conference on*, 2006, pp. 1943-1945.

2. David Usborne. Satellite's failure leaves millions speechless in US. Independent, The (London) . 21-5-1998.
   Ref Type: Newspaper

3. Kohman, G. T., Hermance, H. W., and Downes, G. H., "Silver Migration in Electrical Insulation," *Bell System Technical Journal*, Vol. 34, No. 6, 1955, pp. 1115-1147.

4. Ready J.W.. Reliability Investigation of Printed Wiring Boards Processed with Water Soluble Flux Constituents. 2000. Georgia Institute of Technology.
   Ref Type: Thesis/Dissertation

5. ERA Technology, "Contamination and moisture effects on printed circuit board reliability," 2003.

6. Yost, D. E., "Silver migration in printed circuits," Proc. Symp. on Printed Circuits, Philadelphia, PA 1955.

7. Kohman G., T. e. a., "Silver Migration in Electrical Insulation," *The Bell System Technical Journal*, Vol. XXXIV, No. 6, 1955, pp. 1115-1147.

8. Chaiken S., e. a., "Silver Migration and Printed Wiring," *Industrial and Engineering Chemistry*, Vol. 51, No. 3, 1959, pp. 299-304.

9. Cavasin J., "The Silver Migration Problem," *Machine Design*, 1970, pp. 173-175.

10. Marderosian A.D. and Murphy C., "Humidity Threshold Variations for Dendrite Growth on Hybrid Substrates," *15th Annual Proceedings Reliability Physics*, 1977, pp. 92-100.

11. Boddy, P. J., "Accelerated life testing of flexible printed circuits: Part I: test program and typical results," IEEE Reliability Physics Symposium Proceedings, 1976, pp. 108-113.

12. IPC, "IPC-TR-476A Electrochemical Migration: Electrically Induced Failures in Printed Printed Wiring Assemblies," 1997.

13. Brewin A., Zou Ling, and Hunt C, "Susceptibility of Glass- Reinforced Epoxy Laminates to Conductive Anodic Filamentation," NPL, 2005.

14. Lawson, W.. Investigation into a modified area-of-spread method to monitor the effect of oxygen levels in a reflow oven. 1999. University Of Salford. 1999.
Ref Type: Thesis/Dissertation

15. Lawson, W. and Ekere, N. N., "Use of The Area-of-Spread Method for Monitoring The Stability of Reflow Furnaces
International electronics manufacturing technology symposium 24th IEEE/CPMT international electronics manufacturing technology symposium," IEEE Service Center; 1999, 1999, pp. 115-447.

16. Lawson, W.. The effects of hydrogen/nitrogen mixtures on Soldering in Electronics of copper and tin/lead surfaces for PCB assemblies. 1996. University Of Salford. 1996.
Ref Type: Thesis/Dissertation

17. Krumbein J.S. and Reed H.A., "New Studies of Silver Electromigration," 1978, pp. 145.

18. der Marderosian A.D., "The Electrochemical Migration of Metals, proceedings," International Hybrid Microelectronics Symposium: 134, 1987.

19. DiGiacomo, G., "Electrochemical Migration," *Electrochemistry of Semiconductors and Electronics - Processes and Devices*, edited by McHardy J and Ludwig F Noyles, 1992, pp. 258-259.

20. DiGiacomo, G., *Reliability of Electronic Packages and Semiconductor Devices*, McGraw-Hill Professional 1996., ISBN 007017024X

21. Viswanadham, P. and Singh, P., "Measurement of Migration Propensity," *Failure Modes and Mechanisms in Electronic Packages* ITP, 1997, pp. 226-228.

22. Ready J.W. and Turbini J.L., "A Novel Test Circuit For Detecting Electrochemical Migration," The 128th TMS Annual Meeting & Exhibition, 1999.

23. "Electrolytic Electromigration," *Electromigration and Electronic Device Degradation*, edited by Christou A 2006, pp. 142-155.

24. der Marderosian A.D. and Murphy C., "Humidity Threshold Variations for Dendrite Growth on Hybrid Substrates," *15th Annual Proceedings Reliability Physics*, 1977, pp. 92-100.

25. Link A.N., "Early Stage Impacts of the Printed Wiring Board Joint Venture, Assessed at Project End," 1997, http://www.atp.nist.gov/eao/pwbrpt.htm.

26. Wassink Klein R.J., *Soldering in Electronics, A Comprehensive Treatise on Soldering Technology for Surface Mounting and Through-hole Techniques*, 2 ed., Electrochemical Publications 1989., ISBN 090115024X

27. Fontana M.G. and Greene N.D., *Corrosion Engineering*, New York: McGraw-Hill 1978., ISBN 0071003606

28. Bumiller E., Pecht M., and Hillman C., "Electrochemical Migration on HASL Plated FR-4 Printed Circuit Boards," 2004.

29. Pauls D., "Residues in Printed Wiring Boards and Assemblies," *Circuit World*, Vol. 27, No. 1, 2000, pp. 32-41.

30. Ready, W. J. and Turbini, L. J., "The effect of flux chemistry, applied voltage, conductor spacing, and temperature on conductive anodic filament formation," *Journal of Electronic Materials*, Vol. 31, No. 11, 2002, pp. 1208-1224.

31. Murarka Shyam P., Verner Igor V., and Gutmann Ronald J., *Copper—Fundamental Mechanisms for Microelectronic Applications* 2000., ISBN 0471252565

32. Harsanyi, G., "Copper may destroy chip-level reliability: Handle with care - Mechanism and conditions for copper migrated resistive short formation," *Ieee Electron Device Letters*, Vol. 20, No. 1, 1999, pp. 5-8.

33. Shitamoto, H. and Nagatani, T., "The effect of migration in electrochemical deposition on a horizontal plate," *Journal of Physics D-Applied Physics*, Vol. 31, No. 10, 1998, pp. 1137-1143.

34. Krumbein J.S., "Metallic Electromigration Phenomena," AMP Incorporated, Harrisburg, PA 17105 - now Tyco., 33rd Meeting of the IEEE Holm Conference on Electrical Contacts, Chicago, Illinois 1987.

35. Harsanyi, G., "Electrochemical Processes Resulting in Migrated Short Failures in Microcircuits," *Ieee Transactions on Components Packaging and Manufacturing Technology Part A*, Vol. 18, No. 3, 1995, pp. 602-610.

36. Hwang, S. J., *Solder Paste in Electronics Packaging: Technology and Applications in Surface Mount, Hybrid Circuits, and Component Assembly* 1992., ISBN 044201353-1

37. Muren D., "Atmosphere Influence on Reflow Soldering," AGA, 1994.

38. Hunt , C. and Zou Ling, "The impact of temperature and humidity conditions on surface insulation resistance (SIR) values for various fluxes.," NPL, NPL Report CMMT(A)119, 1998.

39. Ellis.N.B, *Cleaning and Contamination of Electronics Components and Assemblies* 1986., ISBN 0901150207

40. Zou, Z. and Hunt , C., "Surface Insulation Resistance (SIR) Response to Various Processing Parameters," NPL, NPL Report CMMT(A)120, 1998.

41. Lea, C., *After CFCs? Options for Cleaning Electronic Assemblies.*, Electrochemical Publications 1992., ISBN 0901150258

42. Shangguan, D., Achari, A., and Green, W., "Application of lead-free eutectic Sn-Ag solder in no-clean thick film electronic modules," *Components, Packaging, and Manufacturing Technology, Part B: Advanced Packaging, IEEE Transactions on [see also Components, Hybrids, and Manufacturing Technology, IEEE Transactions on]*, Vol. 17, No. 4, 1994, pp. 603-611.

43. Barkey, D., Oberholtzer, F., and Wu, Q., "Kinetic Anisotropy and Dendritic Growth in Electrochemical Deposition," *Physical Review Letters*, Vol. 75, No. 16, 1995, pp. 2980-2983.

44. Uhlig, H. H., *Corrosion and corrosion control:an introduction to corrosion science and engineering*, 2nd ed., Wiley, New York, 1971., ISBN 0471895636

45. Parsons, R., "Electrochemical Nomenclature," *Pure and Applied Chemistry*, Vol. 37, No. 4, 1974, pp. 499-516.

46. Mills, I., International Union of Pure and Applied Chemistry, International Union of Pure and Applied Chemistry, and Commission on Physicochemical Symbols, T. a. U., *The Green Book: Quantities, units, and symbols in physical chemistry*, 2nd ed ed., Blackwell Scientific Publications, Oxford, 1993., ISBN 0632035722

47. Bard A J and Faulkner L R, *Electrochemical Methods: Fundamentals and Applications*, 2 ed. 2001., ISBN 0471043729

48. Atkins P., *The Elements of Physical Chemistry*, 3rd ed., Oxford University Press 2003., ISBN 0198792905

49. Osenbach J.W., "Corrosion-induced Degradation of Microelectronic Devices," *Semiconductor Sci.Technology*, Vol. 11, 1996, pp. 155-162.

50. Pourbaix M., *Atlas of electrochemical equilibria in aqueous solutions*, NACE International (National Association of Corros (Dec 1974) 1966., ISBN 0915567989

51. Groves P.D, *Electrochemistry*, John Murray 1974., ISBN 0719529352

52. Lide R.D., *CRC Handbook of Chemistry and Physics*, 75 ed., CRC Press 1994., ISBN 084930475X

53. Aylward H.G. and Tristan F.V.F., *SI Chemical Data*, John Wiley & Sons Inc 2002., ISBN 0470800445

54. Laidler K.J., Meiser H.J., and Sanctuary C.B., *Physical Chemistry*, 4 ed., Houghton Mifflin 2003., ISBN 0618123415

55. Lassner, E., Schubert, W. D., and Knovel (Firm), *Tungsten- properties, chemistry, technology of the element, alloys, and chemical compounds*, Kluwer Academic/Plenum Publishers, New York, 1999., ISBN 1591246768 (electronic bk.)

56. Popp, F. D. and Schultz, H. P., "Electrolytic Reduction of Organic Compounds," *Chemical Reviews*, Vol. 62, No. 1, 1962, pp. 19-&.

57. Bagotsky V.S., *Fundamentals of electrochemistry*, 2nd ed ed., Wiley-Interscience, Hoboken, N.J, 2006., ISBN 0471700584

58. Hamann C.H, Hamnett A., and Vielstich W., *Electrochemistry*, Wiley-VCH 1998., ISBN 3-527-29096-6

59. Roberge, P. R., *Handbook of corrosion engineering*, McGraw-Hill, New York, 2000., ISBN 0070765162 (alk. paper)

60. CRCT. FactSage (Fact-Web). 2006. CRCT, École Polytechnique de Montréal, Génie chimique / Chemical Eng.
Ref Type: Computer Program

61. Marderosian A.D., "The Electrochemical Migration of Metals, proceedings," International Hybrid Microelectronics Symposium: 134, 1987.

62. Tegehall P-E., "Reliability Verification of Printed Board Assemblies: A Critical Review of Test Methods and Future Strategy," www.smta.org, SMI 98 San Jose 1998, pp. 359-382.

63. Bockris J., R. K. N. A. G.-A. M., *Modern Electrochemistry: Fundamentals of Electrodics*, 2nd ed., Vol. 7, Kluwer Academic/Plenum Publishers 2000, pp. 1035-1400., ISBN 0306461668

64. Warren, G. W., Wynblatt, P., and Zamanzadeh, M., "The Role of Electrochemical Migration and Moisture Adsorption on the Reliability of Metallized Ceramic Substrates," *Journal of Electronic Materials*, Vol. 18, No. 2, 1989, pp. 339-353.

65. Siddhaye S. and Sheng, P., "Integration of environmental factors in process modelling forprinted circuit board manufacturing, Part II: Fabrication," San Francisco, CA 1997, pp. 226-233.

66. Schweigart, H., "Humidity and Polution effects on electronic equipment," Zestron Europe, Ingolstadt, Germany, http://www.zestron.com/us/news/fachv/pdf/humidity and pollution effects on electronic equipment.pdf, 2006.

67. Bjorndahl, W. D. and Lau, J. C., "Current carrying capacity of dendrites," IEEE, Vail, CO, USA 1994, pp. 399-405.

68. Lambert D, Gannamani R, and Blish R C, "Dendrite Fuse Re-growth Kinetics on Organic Substrates for Microprocessors," Phoenix, USA 2004.

69. Kawanobe T and Otsuka K, "Metal Migration in Electronic Components," 1982, pp. 220-228.

70. DiGiacomo, G., "Failure Distributions," *Reliability of Electronic Packages and Semiconductor Devices (Electronic Packaging & Interconnection S.)* 1996, pp. 16-17.

71. Bockris J., R. K. N. A. G.-A. M., *Electrodics*, 2nd ed., Vol. 7, Kluwer Academic/Plenum Publishers 2000, pp. 1035-1400., ISBN 0306461668

72. Hamann C.H, H. A. V. W., *Electrochemistry*, Wiley-VCH 1998., ISBN 3-527-29096-6

73. DiGiacomo, G., "Metal Migration (Ag, Cu, Pb) in encapsulated modules and time-to-fail model as a function of the environment and package properties," Proceedings Reliably Physics Symposium, 1982.

74. Elissa Bumiller et al, "Electrochemical Migration on HASL Plated FR-4 Printed Circuit Boards," IEEE Pan Pacific Symposium, 2004.

75. Elissa Bumiller et al, "Electrochemical Migration on HASL Plated FR-4 Printed Circuit Boards," IEEE Pan Pacific Symposium, 2004.

76. Lando, D. J., Mitchell, J. P., and Welsher, T. L., "Conductive Anodic Filaments in Reinforced Polymeric Dielectrics: Formation and Prevention," *Reliability Physics Symposium, 1979. 17th Annual*, 1979, pp. 51-63.

77. Lahti, J. N., Delaney, R. H., and Hines, J. N., "The Characteristic Wearout Process in Epoxy-Glass Printed Circuits for High Density Electronic Packaging," *Reliability Physics Symposium, 1979. 17th Annual*, 1979, pp. 39-43.

78. Boddy, P. J., Delaney, R. H., Lahti, J. N., Landry, E. F., and Restrick, R. C., "Accelerated Life Testing of Flexible Printed Circuits," *Reliability Physics Symposium, 1976. 14th Annual*, 1976, pp. 108-117.

79. Turbini L.J. and Ready W.J., "Conductive Anodic Filament Failure: A Materials Perspective," 1998.

80. Neves, B.. ECM Test Methods using AC. Lawson, Wayne. 12-8-2003. Ref Type: Internet Communication

81. Neves, B., "Setup, Procedures, and Patterns for CAF and ECM Testing.," *PC FAB*, 2002, pp. 40-46.

82. IEC, "IEC 61189 Test methods for electrical materials, printed boards and other interconnection structures and assemblies.," *IEC*, 2006.

83. Neves, B.. New Research in the Area of ECM testing. 15-8-2003.
Ref Type: Internet Communication

84. Chan , H. A., "Is the current surface insulation resistance (SIR) methodology appropriate to today's manufacturing technology?," Electronic Components and Technology Conference Proceedings., 46th, 1996, pp. 234-241.

85. Yin, A. J., Li, J., Jian, W., Bennett, A. J., and , X. M. J., "Fabrication of highly ordered metallic nanowire arrays by electrodeposition," *Applied Physics*, Vol. 79, No. 7, 2001, pp. 1039-1041.

86. Mikhaylova, M., Toprak, M., Kim, D. K., Zhang, Y., and Muhammed, M., "Nanowire formation by electrodeposition in modifed nanoporous polycrystalline anodic alumina templates," *Material Reseach Society*, Vol. 704, 2003.

87. Mikhaylova, M., Toprak, M., Kim, D. K., Zhang, Y., and Muhammed, M., "Fabrication of sequestial nanostripes by controlled electrodeposition," *Material Reseach Society*, Vol. 750, 2003.

88. Xiao N.Q., Grunwald F., and Carlson K., "Surface Leakage Current (SLC) Methodology for Electrochemical," *Circuit World*, Vol. 23, No. 4, 1997, pp. 6-10.

89. IPC-9201, "IPC-9201 Surface Insulation Resistance Handbook," 1996.

90. Ellis.N.B, "On Insulation Resistance," *Circuit World*, Vol. 21, No. 2, 1995, pp. 5-11.

91. Sinnaduria N., *Handbook of Microelectronics Packaging and Interconnections Technology*, Electrochemical Publications 1985., ISBN 0901150193

92. Sinnadurai N., Kuppuswamy T.S., Chandramouli R., and Rao B.K.N. Environmental testing component reliability observations of telecommunications equipment operated in tropical climatic conditions. Quality Reliab.Eng.Int. [8], 189. 1992.
Ref Type: Magazine Article

93. Sinnadurai N. and Wilson, K., "The Aging Behavior of Commercial Thick-Film Resistors," *Components, Hybrids, and Manufacturing Technology, IEEE Transactions on [see also IEEE Trans.on Components, Packaging, and Manufacturing Technology, Part A, B, C]*, Vol. 5, No. 3, 1982, pp. 308-317.

94. Lea, C., *A Scientific Guide to Surface Mount Technology*, Electrochemical Publications 1988., ISBN 0901150223

95. Cobb, G. W., *Introduction to design and analysis of experiments*, Springer, New York, 1998., ISBN 0387946071 (alk. paper)

96. Montgomery D, *Design and Analysis of Experiments*, 5 ed. 2000., ISBN 0471316490

97. Myers, R. H. and Montgomery, D. C., *Response surface methodology process and product optimization using designed experiments*, 2nd ed ed., J. Wiley, New York, 2002., ISBN 0471412554 (cloth : alk. paper)

98. Clements B.R., *The experimenter's companion*, Amer Society for Quality 1991., ISBN 0873891147

99. Box G, "Must We Randomize Our Experiment?," *Quality Engineering*, Vol. 2, No. 4, 1990, pp. 497-502.

100. Ready, W. J.. Reliability Investigation Of Printed Wiring Boards Process with Water Soluble Flux Constituents. 2000. 2-8-2003.
Ref Type: Thesis/Dissertation

101. M.-O.Bernard, M. P. J. F. G., "Mean-field kinetic lattice gas model of electrochemical cells," *Physics Review*, Vol. 68, 2003.

102. Suni, I. I., "Kinetic limitations on metal dissolution during aqueous silicon wafer processing," *Electrochemical and Solid State Letters*, Vol. 1, No. 2, 1998, pp. 94-96.

103. The Royal Society of Chemistry, "The electrolysis of water - classic chemical demonstrations," 2006.

104. Chung-Seog C., Kil-Mok S., Dong-Ook K., Dong-Woo K., and Young-Seok K., "Analysis of Dispersive Characteristics and Structures of Copper Wire Melted by Overcurrent," *IEEJ Transactions on Power and Energy*, Vol. 125, No. 12, 2005, pp. 1327-1331.

105. StatGraphics. StatGraphics Centurion Statistics Software. 2006.
Ref Type: Computer Program

106. Suzanne S.Fenton, Vijay Ramani, and James M.Fenton, "Active Learning of Chemical Engineering Principles Using a Solar Panel / Water Electrolyzer / Fuel Cell System," American Society for Engineering Education Annual Conference & Exposition, 2004.

Appendix 1a

Published Paper, Lawson, W and Pilkington, RD and Hill, AE, 2007, 'Modeling and analysis of the growth of copper dendrites in saturated conditions using a multilevel factorial design analysis' , Microelectronics International, 24 (2) , pp. 28-34.

Appendix 1b

Internal White Paper: Lawson, W, Brief Introduction to Dendrites and CAFs on Printed Circuit Boards, Delphi Electronics Group, August 2007.

Appendix 1c

Conference Poster, Lawson, W and Pilkington, RD, and Boag, N, Novel methods for assessing the presence of ionic migration on printed circuit boards', Materials Congress London UK 5-7 April 2006.